Aus dem Institut der Prophylaxe und Epidemiologie der Kreislauferkrankungen (IPEK)

Klinikum der Ludwig-Maximilians-Universität München

Vorstand: Univ.-Prof. Dr. med. Christian Weber

The role of adipocyte Nfe2l1 in cholesterol homeostasis and atherogenesis

Dissertation
zum Erwerb des Doktorgrades der Naturwissenschaften
an der Medizinischen Fakultät der
Ludwig-Maximilians-Universität zu München

vorgelegt von Carolin Jethwa (geb. Muley)

aus Heidelberg

Jahr

2024

Mit Genehmigung der Medizinischen Fakultät

der Universität München

Betreuer:	Prof. Dr. rer. nat. Alexander Bartelt
Zweitgutachter:	Prof. Dr. rer. nat. Jürgen Bernhagen
Dekan:	Prof. Dr. med. Thomas Gudermann
Tag der mündlichen Prüfung:	11.02.2025

Table of contents

Zusammenfassung

Adipositas und damit verbundene kardiometabolische Erkrankungen stellen eine große Bedrohung für unsere moderne Gesellschaft und das Gesundheitssystem dar. Bei Patienten mit Adipositas sind Adipozyten chronischem metabolischem Stress ausgesetzt, was die Gesundheit und Plastizität dieser Zellen stark beeinträchtigt. Dies steht mit ektoper Lipidakkumulation, Entzündungen und Insulinresistenz in Verbindung. Das endoplasmatische Retikulum (ER) steuert metabolische Anpassungsmechanismen, die im Falle einer chronischen Überernährung versagen, was letztlich zu einer Dysfunktion der Adipozyten führt. Mechanismen, die die Gesundheit der Adipozyten und die Insulinsensitivität unter solchen Bedingungen fördern, werden jedoch nicht gut verstanden. Der im ER ansässige Transkriptionsfaktor Nfe2l1 (nuclear factor, erythroid derived 2,-like 1) ist ein Regulator der adaptiven Proteinhomöostase. Hier untersuchte ich die Rolle von Nfe2l1 bei der Anpassung von Adipozyten an die metabolischen Herausforderungen der Adipositas und deren Auswirkungen auf kardiometabolische Erkrankungen. Mit einem Cre-loxP-Mausmodell mit Adipozyten-spezifischer Nfe2l1-Deletion (Adipoq-Cre), sowohl auf einem regulären B6-Hintergrund als auch auf einem ApoE-defizienten ($ApoE^{-/-}$) Hintergrund für Atherosklerose-Studien, etablierte ich Nfe2l1 als einen Schlüsselregulator der Gesundheit und Insulinsensitivität von Adipozyten in diätinduzierter Adipositas (diet-induced obesity, DIO) und Atherosklerose. Mäuse ohne Adipozyten-Nfe2l1 zeigten während der DIO eine schwere Adipozytendysfunktion mit niedrigeren Adipokinspiegel, Steatose und Insulinresistenz. Auf einer westlichen Diät (WD) entwickelten $ApoE^{-/-}$ Adipoq-Cre Nfe2l1-Mäuse ein lipoatrophie-ähnliches Syndrom, was zu Dyslipidämie, systemischer Entzündung und Atherosklerose führte. Auf Gewebeebene verursachte der Verlust von Adipozyten-Nfe2l1 eine ausgeprägte Entzündungsreaktion mit Infiltration von Makrophagen und T-Zellen, vermittelt durch den stress-induzierten Transkriptionsfaktor Atf3 in den Adipozyten. Die Behandlung primärer oder 3T3-L1-Adipozyten mit Cholesterin und Proteasominhibitoren replizierte teilweise diese komplexe Entzündung. Überraschenderweise führte der Knockdown von Nfe2l1 nicht zu einer Verstärkung der cholesterininduzierten Entzündung. Knockdown von Atf3 linderte jedoch die entzündliche Komponente. Zuletzt zeigte ich eine inverse Korrelation zwischen dem gesamten Nfe2l1-Proteasomweg und dem Body-Mass-Index (BMI) bei der menschlichen Adipositas auf. Meine Ergebnisse verknüpfen zelluläre Protein- und Cholesterinhomöostase in weißen Adipozyten mit kardiometabolischer Gesundheit. Nfe2l1 schützt Adipozyten vor lipidinduzierter Entzündung, was die Insulinsensitivität bewahrt. Atf3 trat dabei als Schlüsselmediator der Entzündung des Fettgewebes in Reaktion auf Cholesterin hervor. Die Förderung der Proteinhomöostase in Adipozyten könnte daher die Adipozytendysfunktion bei Adipositas lindern und potenziell kardiometabolische Komplikationen abwenden.

Abstract

Obesity and its associated cardiometabolic diseases pose significant threats to our modern society and public health. During obesity, adipocytes are subjected to chronic metabolic stress, compromising their health and plasticity, which has been linked to ectopic lipid accumulation, inflammation, and insulin resistance. The endoplasmic reticulum (ER) governs metabolic adaptation mechanisms that fail in the event of chronic over-nutrition, which ultimately leads to adipocyte dysfunction. However, the mechanisms preserving adipocyte health and insulin sensitivity under such conditions are not well understood. The ER-resident transcription factor Nfe2l1 (nuclear factor, erythroid derived 2,-like 1) is a regulator of adaptive proteostasis under increased proteasomal activity demand. Here, I investigated the role of Nfe2l1 in the adaptation of adipocytes to the metabolic challenges of obesity and its impact on cardiometabolic diseases. Using a Cre-loxP mouse model with adipocyte-specific Nfe2l1 deletion (Adipoq-Cre), both on a regular B6 background and an ApoE-deficient ($ApoE^{-/-}$) background for atherosclerosis studies, this research established adipocyte Nfe2l1 as a key regulator of adipocyte health and insulin sensitivity in diet-induced obesity (DIO) and atherosclerosis. Mice lacking adipocyte Nfe2l1 displayed severe adipocyte dysfunction during DIO, characterized by lower adipokine levels, steatosis, and insulin resistance. On a Western Diet (WD), $ApoE^{-/-}$ Adipoq-Cre Nfe2l1 mice developed a lipoatrophy-like syndrome and exhibited a more unfavorable metabolic phenotype compared to Adipoq-Cre Nfe2l1 on DIO, resulting in enhanced dyslipidemia, systemic inflammation, and atherosclerosis. On the tissue level, loss of adipocyte Nfe2l1 caused a complex inflammatory response with a pronounced infiltration of macrophages and T cells mediated by the stress-induced transcription factor Atf3 in the adipocytes. Treating primary or 3T3-L1 adipocytes with cholesterol and proteasome inhibitors partially replicated this complex inflammation. Surprisingly, knockdown of Nfe2l1, which led to downregulation of the proteasome-pathway, did not enhance cholesterol-induced inflammation. However, silencing Atf3 alleviated the inflammatory component. Finally, this study revealed an inverse correlation between the entire Nfe2l1-proteasome-pathway and body mass index (BMI) in humans, emphasizing the relevance of Nfe2l1 in human obesity. My findings link cellular proteostasis and cholesterol homeostasis in white adipocytes to cardiometabolic health. Nfe2l1 protected adipocyte health from lipid-induced inflammation, which preserved insulin sensitivity *in vivo*. Importantly, Atf3 emerged as a key mediator of adipose tissue inflammation in response to lipids, most notably cholesterol. Promoting proteostasis in adipocytes may thus alleviate adipocyte dysfunction in obesity, potentially averting adverse cardiometabolic outcomes.

Figure index

Table index

Abbreviations

ANCOVA	analysis of covariance
ANOVA	analysis of variance
ATM	adipose tissue macrophages
BAT	brown adipose tissue
BMI	body mass index / Body-Mass-Index
CBA	conjugated bile acids
cDNA	complementary DNA
Chol	cholesterol
CL	CL 316,243
CL.	cleaved
CNC	Cap'n'collar
Cts	cycle thresholds
CVDs	cardiovascular diseases
DEGs	differentially expressed genes
DIO	diet-induced obesity
ECAT	epicardial adipose tissue
ER	endoplasmic reticulum / endoplasmatisches Retikulum
ERAD	ER-associated degradation
FFA	free fatty acids
FL.	full-length
gDNA	genomic DNA
GIP	glucose-dependent insulinotropic polypeptide
GLP-1	glucagon-like peptide-1
GO	gene ontology
GTT	glucose tolerance test
GWAT	gonadal white adipose tissue
HDL	high-density lipoprotein
i.p.	intraperitoneal
iBAT	interscapular brown-adipose tissue
ITT	insulin tolerance test
KO	knockout
LDL	low-density lipoprotein
LOBB	Leipzig Obesity Biobank
MAFLD	metabolic-dysfunction associated fatty liver disease

MbCD	methyl-beta-cyclodextrin
ORO	Oil Red-O
oxLDL	oxidized LDL
PCA	principal component analysis
PCR	polymerase chain reaction
PVAT	perivascular adipose tissue
qRT-PCR	quantitative reverse transcription polymerase chain reaction
RBC	red blood cells
RER	respiratory exchange ratio
s.c.	subcutaneous
s.e.m.	standard error of the mean
SCAT	subcutaneous adipose tissue
SMCs	smooth muscle cells
SVF	stromal-vascular fraction
T2DM	type 2 diabetes mellitus
Tregs	regulatory T cells
UBA	unconjugated bile acids
UPR	unfolded protein response
UPS	ubiquitin-proteasome-systems
VISAT	visceral adipose tissue
VO_2	oxygen consumption rate
WAT	white adipose tissue
WD	Western diet
WHO	World Health Organization
WT	wild-type

1. Introduction

1.1 The dual pandemic of obesity and cardiovascular diseases

1.1.1 Obesity epidemiology, pathophysiology, and treatments

Obesity is one of the major health concerns of our time. The World Health Organization (WHO) defines obesity as excessive accumulation of fat that might impair health, diagnosed at a body mass index (BMI) of ≥ 30 kg/m^2. Obesity is a well-established risk factor for non-communicable diseases, such as type 2 diabetes mellitus (T2DM), cardiovascular diseases (CVDs), certain cancer types and even death[1]. Depending on its severity, obesity is associated with a 5-to-20-year reduction in life expectancy. Importantly, during the COVID-19 pandemic it also became evident that obesity negatively affects the course of infectious diseases. Obesity is associated with severe COVID-19 progression and with evidence suggesting that adipose tissue is a significant target of the Severe Acute Respiratory Syndrome Coronavirus 2[2].

Obesity arises from a positive energy balance, where energy intake exceeds energy consumption, resulting in accumulation of nutrients as triglycerides in white adipose tissue (WAT)[3,4]. While humans have evolved to overeat as an adaptive response to periods of under-nutrition, our modern environment, characterized by constant food availability and sedentary behavior, has shifted the balance towards over-nutrition[3]. Consequently, the prevalence of obesity has surged to pandemic proportions since 1975[1]. Projections indicate that by 2030, over one billion people will be classified as obese, making it the most prevalent chronic disease globally[5]. Unfortunately, strategies to prevent or treat obesity, such as promoting healthy nutrition and physical activity, have proven largely ineffective and unsustainable[6].

Obesity is nowadays recognized as a multifactorial chronic disease based on the complex pathophysiology that leads to reprogramming of mechanisms that impede weight loss and promote further weight gain[3]. This understanding has led to a shift in treatment guidelines, moving beyond lifestyle modifications to include anti-obesity medications and bariatric surgeries. While surgical interventions achieve notable weight loss and improvements in blood pressure, lipid, and glucose metabolism, they cannot meet the global medical need. Until recently, anti-obesity medications offered limited benefits for long-term weight management due to modest weight loss and severe side effects such as adverse cardiovascular effects, increased suicidal risk, or a higher likelihood of drug

abuse[6]. However, recent breakthroughs, exemplified by the approval of injectable incretin-based glucagon-like peptide-1 (GLP-1) receptor agonist semaglutide for weight management[7], have achieved almost 15% weight loss with a reasonable side-effect profile. Clinical trials are also exploring dual and triple agonists targeting GLP-1, glucagon, and/or the glucose-dependent insulinotropic polypeptide (GIP) receptor. One notable example, the triple-hormone-receptor agonist retatrutide, demonstrated remarkable efficacy with 24% weight loss over 48 weeks in a phase II study, comparable to the weight loss achieved through bariatric surgery[8]. Nevertheless, despite these advances, obesity remains a major health burden. Obese patients are a very heterogenous group, thus it remains to be shown that incretin-based drugs will prove successful for the majority of the obese population. Moreover, the rapid development of these novel agonists necessitates cardiovascular outcome trials to assess potential cardiometabolic risk reduction and evaluate cardiovascular safety, which has been a primary challenge in the development of anti-obesity medication[6].

1.1.2 Obesity as a risk factor for cardiovascular diseases

Given that CVDs are the leading cause of obesity-related death, the primary objective of weight loss therapies is to improve cardiometabolic health[9]. Studies by the Global Burden of Disease Obesity Collaborators have reported in 2015 that CVDs caused two-thirds of all deaths accounted by high BMI. Moreover, CVDs caused large proportions of BMI-related deaths and BMI-related disability-adjusted life-years in obese individuals[9]. Obesity is often accompanied by a cluster of metabolic diseases, including hypertension, insulin resistance, abdominal obesity, and dyslipidemia, referred to as the metabolic syndrome, which are major contributors to the increase in CVDs prevalence. Especially diabetic dyslipidemia, the insulin resistance-linked elevation of atherogenic plasma lipids (elevated triglycerides, low high-density lipoprotein (HDL) cholesterol and high low-density lipoprotein (LDL) cholesterol), is a strong risk factor for CVDs[10].

Atherosclerosis is the leading cause of many CVDs, such as aortic valve stenosis and coronary artery disease. As a result, the obesity pandemic has coincided with a surge in atherosclerosis and cardiovascular diseases, doubling the number of individuals with heart and circulatory diseases worldwide since 1997[10–12]. While obesity was once considered purely an indirect factor in CVDs, emerging evidence now suggests that obesity directly influences cardiovascular risk factors such as T2D, dyslipidemia, and hypertension. It also independently fosters CVDs development, as supported by Mendelian randomization studies demonstrating a causal relationship between higher lifetime BMI, mortality and a variety of CVDs (Figure 1)[13,14]. In particular, visceral adipose tissue

(VISAT) has been demonstrated as an independent risk factor for CVDs, while subcutaneous adipose tissue (SCAT) is a weaker indicator of CVDs risk[15]. Emerging evidence now also suggests that ectopic lipid deposition in the liver, around the heart and around the vasculature linked to visceral obesity, contributes to cardiometabolic risk and atherosclerosis[10,15–17].

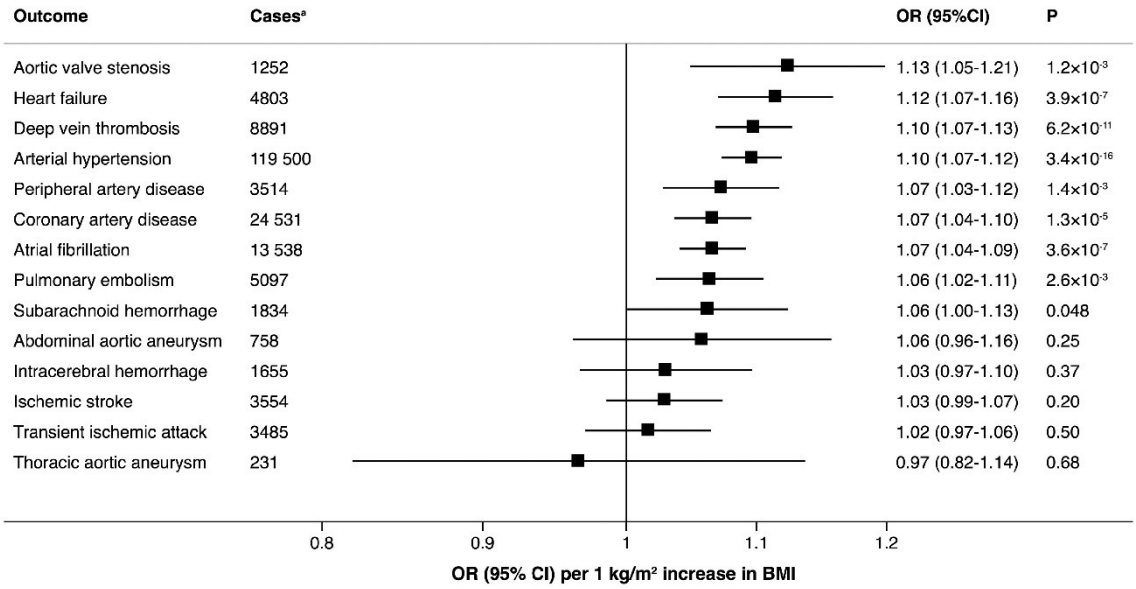

Figure 1 | BMI and CVDs risk

Genetically predicted increase of 1 kg/m^2 is associated with higher odds ratio for some CVDs (n = 367,703). Figure printed from Larsson et al. (2020)[14] under the Creative Commons CC BY license. CI: confidence interval, OR: odds ratio.

1.1.3 Obesity and Atherosclerosis

Atherosclerosis is the predominant cause of vascular disease[18,19]. It is a chronic inflammatory process of the arterial wall in middle- and large-sized arteries and characterized by the formation of lipid-rich atherosclerotic plaques. Atherosclerosis is initiated by damage of the endothelium of the *tunica intima*, the innermost layer of the arterial wall, which facilitates the accumulation of LDL in the subendothelial space[20]. Various factors, including high blood pressure, smoking, atherogenic dyslipidemia, and inflammation, can cause endothelial damage. Once LDL particles reside in the intima, they are oxidized by reactive oxygen species or inflammatory cells, resulting in oxidized LDL (oxLDL). This triggers an inflammatory response in the arterial wall, including the expression of adhesion molecules and the secretion of chemokines by endothelial cells and smooth muscle cells (SMCs), leading to recruitment of circulating monocytes and other leukocytes. Monocytes infiltrate the arterial wall and differentiate into macrophages, which then ingest oxLDL to become lipid-laden foam cells, which form the early "fatty streak" lesions[18–22] (Figure 2).

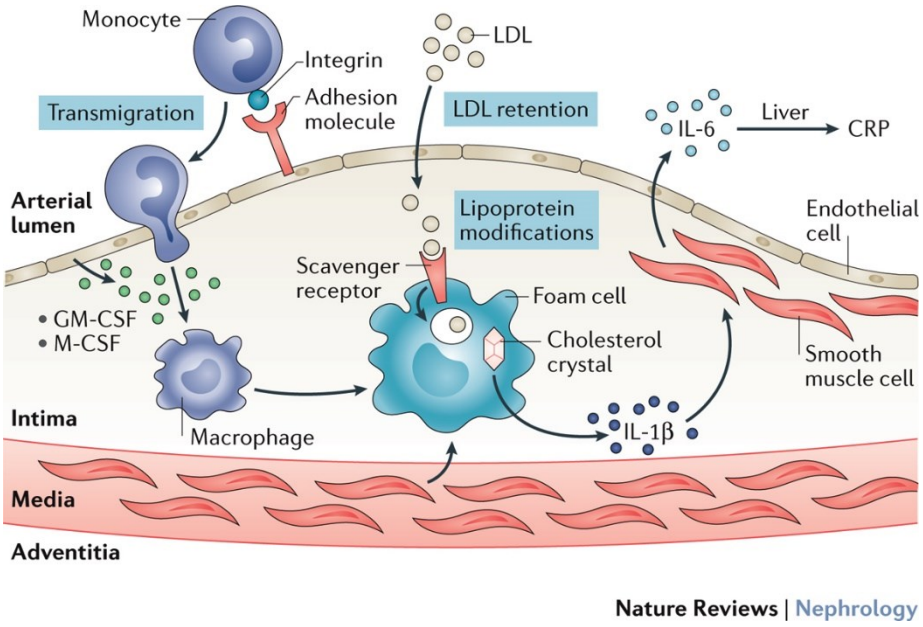

Figure 2 | Lipid-immune cell-interaction during the initiation of atherosclerosis.
Retention and modification of LDL leads to an inflammatory response in the arterial wall, which includes the upregulation of adhesion molecules on the endothelial surface and recruitment of monocytes to the lesion. Endothelial cells release macrophage colony-stimulating factor (M-CSF) and granulocyte-macrophage colony-stimulating factor (GM-CSF), triggering infiltrating monocytes to differentiate into macrophages. Macrophages take up modified lipoproteins such as ox-LDL, which leads to the formation of foam cells. Overtime, cholesterol crystals form in these cells, resulting in release of interleukin-1 β (IL-1β), which stimulates SMCs to produce interleukin-6 (IL-6), which both exert pro-inflammatory effects. In addition, IL-6 in the circulation might signal to the liver to produce pro-inflammatory C-reactive protein (CRP). Figure printed from Gisterå &Hansson (2017)[22] with permission of Springer Nature.

Over time, lesions evolve into advanced plaques with a necrotic core, composed of apoptotic foam cells, SMCs, cellular debris, and cholesterol crystals[18–22]. Calcification of these plaques further stiffens the arterial walls[20]. Advanced plaques are encapsulated by a fibrous cap made of collagen mainly produced by SMCs[19]. However, the cap may thin over time, rendering the plaques vulnerable to rupture or erosion, which can precipitate acute thrombus formation. This can lead to severe complications such as myocardial infarction or ischemic stroke [19,22].

Obesity and atherosclerosis share significant pathophysiological characteristics. These conditions have traditionally been categorized as lipid storage diseases, attributed to the excessive accumulation of triglycerides in obesity and LDL cholesterol in atherosclerosis[23]. Furthermore, both atherosclerosis and obesity are recognized within the spectrum of immunometabolic diseases characterized by chronic low-grade inflammation[24,25]. Inflammation mediates all stages of atherosclerosis[19] and it has been suggested that obesity accelerates atherosclerotic progression through several mechanisms, including adipose tissue inflammation[10]. Moreover, inflammation of the adipose tissue is a hallmark

of metabolic dysfunction in obesity. Visceral obesity is especially concerning, as it is associated with adipocyte dysfunction, the dysregulation of inflammatory cytokines and adipokines, insulin resistance, and dyslipidemia[10,15]. These factors collectively increase the risk of cardiometabolic diseases[10,15]. Notably, while many of these factors contribute indirectly to CVDs, secretion of bioactive mediators such as adipokines and cytokines from adipose tissue can exert effects on the heart and vasculature in an endocrine manner. Furthermore, adipose tissue depots located near the cardiovascular system, such as epicardial adipose tissue (ECAT) around the heart and perivascular adipose tissue (PVAT) surrounding blood vessels, may exert direct influences via paracrine mediators[26]. Inflammation in these depots has been observed in conditions like ischemic heart disease and myocardial infarction, and PVAT inflammation, especially around the aorta, has been linked to atherosclerosis[16,17].

Collectively, the expansion of adipocytes in obesity does not only serve as a risk factor for atherosclerosis and other CVDs but also exacerbates atherosclerosis through several mechanisms such as inflammation, insulin resistance, and dyslipidemia. In the same fashion, conditions such as lipodystrophy, defined by a deficiency of functional adipocytes, also display severe metabolic dysfunction and an elevated risk for cardiometabolic diseases[27], suggesting that a certain level of functional adipocytes is essential for maintaining cardiometabolic health. Thus, to elaborate on this observation, the next chapter will provide information on adipocyte types, their function and dysfunction in obesity.

1.2 Adipose tissue in health and disease

1.2.1 Adipose tissue depots, adipocyte types and functions

Adipose tissue is a multifaceted organ, which regulates central aspects of whole body energy homeostasis and insulin sensitivity rather than being just a simple lipid storage[28,29]. It is localized in distinct anatomical depots that can broadly be divided into VISAT, which surrounds the visceral organs in the thoracic and abdominal cavity, or SCAT, which is found under the skin[28,29]. Based on the exact anatomical location, VISAT can be further classified into many distinct depots for example PVAT and ECAT, that have attracted considerable interest in cardiovascular research[17,26,30]. While SCAT may confer protective effects on energy homeostasis, dysregulation of VISAT has been linked to an elevated cardiometabolic risk. Furthermore, based on phenotype and function, WAT and brown adipose tissue (BAT) can be distinguished[28,29]. An overview of adipose tissue distribution in humans and mice can be found in Figure 3.

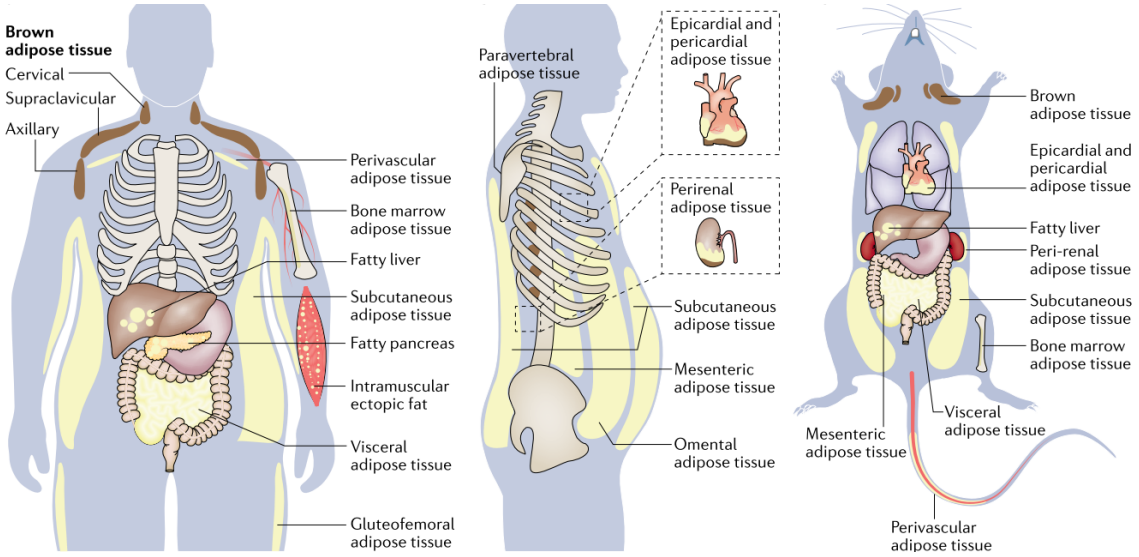

Figure 3 | Adipose tissue distribution in humans and mice

Adipose tissue is distributed throughout the body in both visceral and subcutaneous depots. Due to ectopic deposition in obesity, lipids and adipose tissue can also be found within other metabolic organs such as the liver and pancreas. There are also few BAT depots in several distinct locations in both humans and mice. Figure printed from Trim and Lynch (2022)[31] with permission from Springer Nature.

BAT predominantly consists of brown adipocytes, which are specialized cells proficient in generating heat through the metabolic conversion of lipids and glucose, a process known as non-shivering thermogenesis. Brown adipocytes are characterized by multilocular lipid droplets, abundant mitochondria and the expression of Uncoupling protein 1 (UCP1). UCP1 is responsible for uncoupling the proton gradient of the electron transport chain, diverting it from energy production to heat generation[29,32,33]. In addition to brown

adipocytes, there are also specialized thermogenic adipocytes in some WAT depots, called beige or “brown-in-white” (“brite”) adipocytes, equally adept at non-shivering thermogenesis. The emergence of thermogenic adipocytes in WAT is known as “browning”, a reversible process in response to cold exposure or exercise. Conversely, BAT can also undergo whitening when exposed to thermoneutral or obesogenic conditions[29,32].

WAT serves as the primary reservoir for energy storage within the body, predominantly comprising white adipocytes. White adipocytes feature a singular large lipid droplet, few mitochondria, and the absence of UCP1 expression[29,32]. In postprandial states, white adipocytes take up lipids from the blood stream and sequester them, predominantly as triglycerides, in lipid droplets. In catabolic states such as fasting, adipocytes release free fatty acids (FFA) from lipid droplets and provide them as energy substrates to other organs[29,32]. WAT also functions as cushioning to the inner organs and as insulation. Besides, WAT has emerged as an endocrine organ that is central to the regulation of energy metabolism, insulin sensitivity and inflammation. It secrets a variety of adipocyte-derived mediators, peptide hormones called adipokines, bioactive lipids (“lipokines”) and small RNAs. Although BAT also produces endocrine factors, the much larger WAT is most likely the more predominant source, especially in obesity[34,35]. The adipokines leptin and adiponectin are almost exclusively secreted by adipocytes and are well-established endocrine mediators. Whereas leptin suppresses appetite in the brain and regulates energy expenditure, adiponectin has anti-inflammatory and insulin-sensitizing properties. Interestingly, unlike other adipokines, adiponectin secretion decreases under obese or insulin-resistant conditions, which makes it a good marker for adipocyte health[36,37].

Although adipocytes make up the majority of the volume of adipose tissue, they only account for 20-40% of the cellular content[28]. Other cell types found in adipose tissue include endothelial cells, immune cells, fibroblasts, pre-adipocytes and stem cells, called the stromal-vascular fraction (SVF). Leukocytes, including adipose-tissue resident macrophages (ATM) and regulatory T cells (Tregs), comprise the majority of stromal-vascular cells and have important homeostatic functions in adipocytes.

1.2.2 Adipocyte dysfunction and cardiometabolic diseases

During periods of excessive energy intake, adipose tissue expansion occurs through two primary mechanisms: an increase in adipocyte number (hyperplasia) and an increase in adipocyte size (hypertrophy). While hyperplasia maintains vascularization and adiponectin levels, hypertrophy is associated with hypoxia, fibrosis, necrosis, and inflammation, marking it as a detrimental form of adipose tissue expansion[38,39]. Notably, adipocyte number is set early in life, therefore expansion of adipose tissue in adults is mostly driven

by adipocyte hypertrophy. However, certain conditions, such as overnutrition or cold exposure, can induce hyperplasia in specific adipogenic niches.

In obesity, adipocytes become severely dysfunctional, losing their capacity to expand properly in response to an energy surplus. In this state, adipose tissue contains insulin-resistant hypertrophic adipocytes with a decreased capacity to safely store lipids[40]. Consequently, dysfunctional adipocytes release free fatty acids in the circulation, which accumulate in other organs such as the liver and skeletal muscle, where they cause cellular stress, referred to as lipotoxicity. This is a hallmark of metabolic diseases and has been linked to systemic insulin resistance, T2DM, metabolic-dysfunction associated fatty liver disease (MAFLD) and CVDs[41–43]. Conversely, the absence of WAT, as seen in congenital or acquired forms of lipodystrophy, is also linked to an increased cardiometabolic risk and severe insulin resistance, mirroring the metabolic disturbances observed in obesity[4,27,44]. Moreover, generalized lipodystrophy is associated with more severe insulin resistance than partial lipodystrophy, suggesting that the impairment of adipocyte function and the inability to efficiently store excess nutrients are crucial drivers of metabolic derangements[44]. Current evidence implies that similar mechanisms of adipocyte overload and dysfunction in WAT contribute to insulin resistance and increased cardiometabolic risk in obesity[27,45].

Dysfunctional or unhealthy adipose tissue displays a plethora of pathophysiological features such as dysregulated adipokine secretion[35], immune cell infiltration[46], hypoxia and fibrosis[38,41], which fuels chronic inflammation (Figure 4).

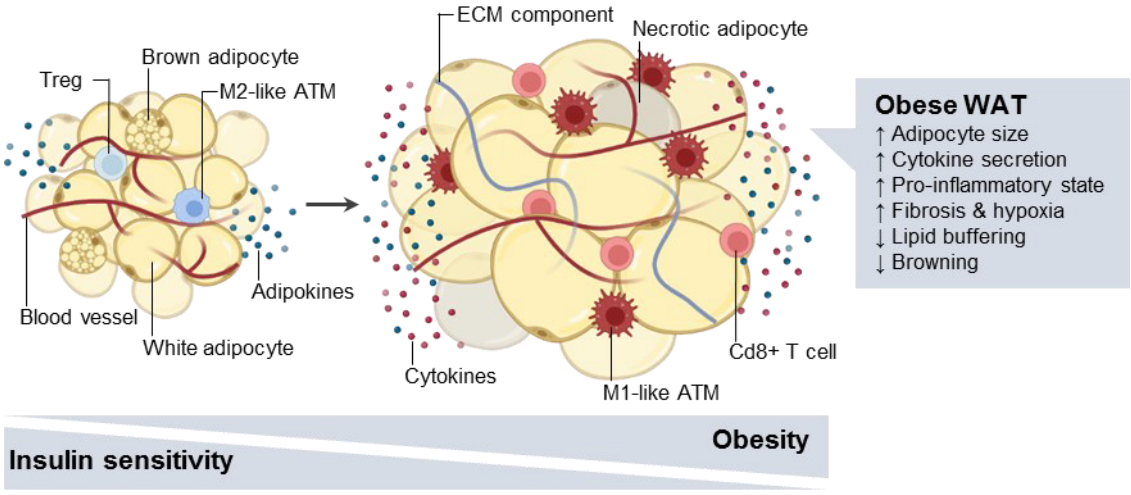

Figure 4 | Characteristics of dysfunctional WAT in obesity

During obesity, adipocytes are pushed towards their capacity to safely store lipids, which results in a continuous decline in WAT plasticity and function. Obese WAT is characterized by hypertrophic adipocytes, the production of pro-inflammatory cytokines, immune cell infiltration, diminished browning, fibrosis, and hypoxia. Figure based on Hagberg & Spalding (2023)[4].

As adipocytes expand, they undergo mechanical stress and hypoxia, pushing them to the limits of oxygen diffusion[38,41]. Unlike other tissues, hypoxic response mediated by hypoxia-inducible factor 1 is insufficient to promote vascularization in adipose tissue, which leads to tissue fibrosis and necrosis of hypoxic adipocytes[47]. Inflamed adipose tissue secretes pro-inflammatory cytokines, such as Tumor-necrosis-factor alpha (TNF-α), Monocyte Chemoattractant Protein-1 (MCP-1, encoded by *CCL2*) and IL-6, which derive from either ATM or adipocytes themselves[46]. At the same time, adipocytes secrete less anti-inflammatory and insulin-sensitizing adiponectin[35,48]. This can have local effects on the adipose tissue such as immune cell infiltration and polarization of tissue-resident cells, as well as effects on peripheral organs by secretion of pro-inflammatory mediators in the circulation[46]. Obesity increases the number of pro-inflammatory M1-like ATM[49–51] and Cd8+ cytotoxic T cells in WAT[52], whereas anti-inflammatory M2-like ATM[51] and Tregs[53,54] are depleted. Notably, inflammation in VISAT is more pronounced than in SCAT, presumably due to higher macrophage content and greater extent of adipocyte hypertrophy in VISAT.

Inflammation in obesity has been linked to activation of stress kinase pathways in adipose tissue including c-jun N-terminal kinase (JNK), p38 mitogen-activated protein kinase (p38) and nuclear factor kappa-B kinase subunit beta (IKKB), an activator of the nuclear factor of kappa light polypeptide gene enhancer in B cells (NF-κB) pathway[46,55,56]. Activation of Jnk and IKKB can phosphorylate insulin receptor substrate-1 (IRS-1) on serine residues, inhibiting its activity and thus insulin signal transduction[46,55]. Moreover, stress kinase signaling by Jnk and p38 have been linked to ER stress, which provides a mechanistic link between obesity, inflammation and insulin resistance in the adipose tissue[57–59]. The ER is a highly adaptive organelle, which orchestrates stress resistance pathways to maintain cellular homeostasis[60,61]. However, ER stress and inflammation become chronic in obesity and mediate the progression to metabolic diseases[25]. Therefore, an interesting hypothesis is whether maladaptation of these stress resistance pathways could be a cause of adipocyte dysfunction in obesity. The next subchapter will outline the role of the ER in metabolic homeostasis in health and obesity, as well as ER-associated mechanisms that enable cells to adapt to nutrient stress.

1.3 The endoplasmic reticulum as the central site of protein and cholesterol metabolism

1.3.1 ER structure and functions

The ER is a cytosolic organelle, and site of protein folding, calcium homeostasis, steroid and lipid biosynthesis. As such, it is critical for the maintenance of cellular homeostasis. The ER consists of a variety of contiguous structural domains developing from the nuclear envelope, which can be classified as membrane cisternae ("sheets") and tubules. ER sheets are covered with ribosomes for protein biosynthesis and are found close to the nucleus, while ER tubules are branched and spread through the cytosol[62]. It should be noted that the ER is a diverse organelle and that several distinct ER phenotypes exist, which can vary by tissue or physiological conditions. For example, adipose tissue only contains very little, mostly tubular ER[60]. Notably, lipid droplets, the hallmark of adipocytes, also derive from the ER, where they are synthesized to store energy in the form of neutral lipids[63].

In recent time, the ER has emerged as the central site for integrating nutrient sensing, stress signaling and inflammatory response. The ER responds to nutrient signals induced by glucose, free cholesterol, fatty acids and amino acids[64]. Conversely, glucose deprivation, excessive lipids, increased synthesis of secretory proteins, and accumulation of mutant or misfolded proteins can cause disturbances of ER homeostasis, commonly referred to as ER stress[65,66]. Based on the nature of the stressor, this is referred to as proteotoxicity, lipotoxicity or glucotoxicity[60]. In obese adipocytes, ER stress might be triggered by increased demand for protein synthesis during expansion and secretion of adipokines, as well as excessive nutrients such as free fatty acids and pro-inflammatory cytokines[67]. Disturbances in ER homeostasis cause accumulation of unfolded proteins, inflammation and cellular dysfunction, ultimately resulting in cell death if sustained[61,66,68]. Notably, ER stress can disrupt all ER functions, thus disturbances in protein homeostasis ("proteostasis") might impact lipid synthesis and vice versa[60]. To limit ER stress, the ER is equipped with adaptive stress resistance mechanisms, that operate in concert to restore proteostasis and limit proteotoxicity: the unfolded protein response (UPR), autophagy[60] and the ubiquitin-proteasome-systems (UPS). These can also be summarized as protein quality control mechanisms.

1.3.2 Protein quality control mechanisms

ER stress is sensed by at least three different ER membrane-anchored sensors, which mediate the UPR. These sensors initiate signaling pathways that alter gene transcription,

mRNA processing, and protein modification to enhance the cell's ability to fold proteins[68,69]. The first arm of the UPR is protein kinase R-like ER kinase (PERK), which phosphorylates eukaryotic translation initiation factor 2-alpha (EIF2α) to attenuate global mRNA translation[70]. Despite this inhibition, specific mRNAs such as activating transcription factor-4 (ATF4), are preferentially translated[71,72], thereby activating the transcription of UPR target genes involved in amino acid biosynthesis, antioxidative responses, autophagy, and apoptosis[68,73]. The second arm is mediated by inositol-requiring enzyme 1-alpha (IRE1α), which is an endoribonuclease. Upon activation, IRE1α splices X-box binding protein 1 (XBP1)[74,75], a transcription factor that induces the expression of genes involved in ER proteostasis. In addition, IRE1α can cleave ER-associated mRNAs and non-coding RNAs, a process known as regulated IRE1-dependent decay (RIDD), thereby modulating protein load, metabolism, and inflammation[76,77]. The third arm of the UPR involves activating transcription factor-6 (ATF6), which undergoes proteolytic cleavage upon translocation to the Golgi apparatus, yielding an active transcription factor[78]. This active ATF6 stimulates the expression of genes involved in maintaining ER protein folding homeostasis[79]. Overall, the UPR dynamically adjusts ER folding capacity to sustain proteostasis and cellular health under conditions of ER stress. However, if ER stress persists and cannot be resolved, the UPR can trigger apoptosis through the upregulation of pro-apoptotic factors such as C/EBP-homologous protein (CHOP, encoded by the gene *DNA Damage Inducible Transcript 3* (*DDIT3*))[80].

Autophagy, particularly induced under conditions of nutrient starvation, plays a crucial role in recycling large cellular components, including protein aggregates[81]. This process involves the formation of a double-membrane compartment known as the autophagosome, which engulfs protein aggregates and then fuses with lysosomes to form autolysosomes. Within these autolysosomes, protein aggregates are enzymatically broken down into amino acids[82]. The most common form of autophagy, macroautophagy, involves the bulk degradation of cellular components. However, other forms of autophagy, such as microautophagy and chaperone-mediated autophagy, also exist and serve distinct roles within the cell[83]. Notably, autophagy is not essential for cell survival when nutrients are abundant[81].

While macroautophagy mediates the bulk degradation of many proteins in a relatively non-selective manner, the UPS targets proteins for degradation in a highly selective process known as ubiquitination. This involves the covalent attachment of ubiquitin to proteins through a three-step enzymatic cascade. Initially, ubiquitin is activated by an ubiquitin-activating enzyme (E1) in an ATP-dependent manner. Subsequently, the activated ubiquitin is transferred to an ubiquitin-conjugating enzyme (E2), and finally, an ubiquitin ligase (E3) recruits the Ubiquitin-bound E2 complex to facilitate the transfer of ubiquitin

to the target protein. Mono-ubiquitination can direct proteins to the proteasome, but often, proteins undergo successive ubiquitination, forming lysine 48-linked poly-ubiquitin chains, signaling for proteasomal degradation[84,85].

Complementing the UPR, ER-associated degradation (ERAD) specifically targets misfolded or unassembled proteins within the ER for degradation. Proteins recognized by an ubiquitin-ligase complex in the ER membrane[86,87] are retrotranslocated to the cytosol, ubiquitinated, and directed to the proteasome with the assistance of valosin-containing protein (VCP, also known as p97)[88].

The 26S proteasome, a complex comprising two regulatory 19S particles and a 20S core particle, performs the actual degradation. The core particle, composed of α- and β-subunits arranged in four stacked rings, features a proteolytic chamber where proteolysis is executed[89] (Figure 5A). Interestingly, of the seven β-subunits only β1, β2 and β5 have proteolytic activities - caspase-like activity, trypsin-like activity and chymotrypsin-like activity, respectively[90,91]. The regulatory 19S particle is responsible for substrate recognition, unfolding, and translocation into the core for degradation[84,85]. This process not only recycles proteins into amino acids for de novo protein synthesis but also recycles ubiquitin molecules through deubiquitinating enzymes[92].

Importantly, both UPS and autophagy are essential for maintaining amino acid homeostasis[85]. While autophagy is only required in conditions of nutrient starvation[93], proper functioning of the UPS is essential for cell survival, since UPS turnover of proteins is also high when nutrients are abundant[92]. Thus, regulation of the UPS must be tightly controlled to match cellular metabolism[85].

1.3.3 Transcriptional control of the proteasome by Nfe2l1

Proteasomal degradation is regulated by selective substrate targeting and proteasome abundance[85]. Recent studies identified the ER-resident transcription factor NFE2L1 (also known as NRF1 or TCF11) as a novel regulator of proteasome abundance in mammals[94,95]. It mediates the induction of proteasome subunits genes in a bounce-back response when the level of ubiquitinated proteins exceed proteasomal activity (Figure 5B).

NFE2L1 belongs to the family of Cap'n'collar (CNC) transcription factors, which also includes the homologous NFE2L2 and NFE2L3[96]. They are expressed in many tissues and are found in all animals[97]. Interestingly, invertebrates such as *Caenorhabditis elegans* and *Drosophila melanogaster* contain only one NFE2L gene, *skn-1* and CNC respectively. In mammals, the three homologs have distinct biological functions and their target genes only partially overlap[98,99]. While NFE2L1 is unique in regulating proteasome

subunit genes[94,95], NFE2L2 activates the antioxidant defense[100]. The functions of NFE2L3 are not well understood[101].

NFE2L1 undergoes extensive post-translational modification to become transcriptionally active. First, NFE2L1 is glycosylated and subsequently retrotranslocated to the outer ER membrane facilitated by VCP[94,102,103]. There, it is ubiquitinated by ERAD-E3 ligase HRD1[94,102], deglycosylated by N-glycanase1 (NGLY1)[104] and proteolytically cleaved by protein DNA damage- inducible 1 homolog 2 (DDI2)[105]. This process releases a transcriptionally active basic leucine zipper (bZIP)-DNA binding domain-containing fragment[105] that is rapidly degraded by the proteasome under normal conditions[94,102]. However, when ubiquitination levels surpass proteasome activity, the bZIP fragment evades degradation, translocates to the nucleus, where it forms heterodimers with small Maf proteins[106,107]. These heterodimers bind to antioxidant response elements in the DNA, where they function as transcriptional activators of proteasome subunit genes, thus promoting the formation of new proteasomes[94,95].

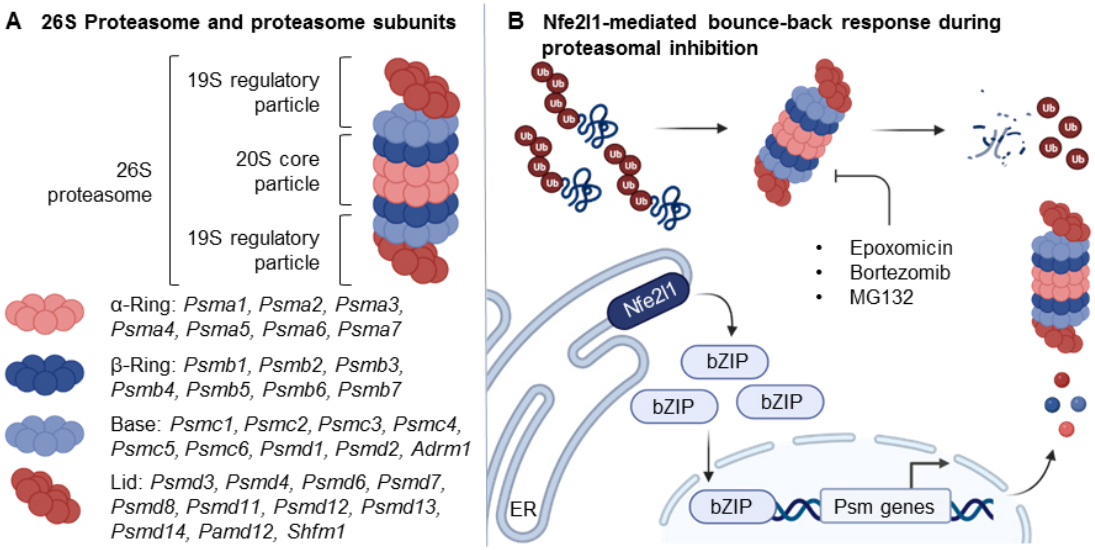

Figure 5 | Transcriptional control of the proteasome by Nfe2l1

A The constitutive 26S proteasome consists of two 19S regulatory particles and a 20S core particle, in which the proteolytical cleavage occurs. The particles consist of ring-shaped structures made of the distinct proteasome subunits[84,85]. **B** In conditions of proteasome overload or inhibition e.g. by epoxomicin, the active bZIP fragment can escape proteasomal degradation and translocate to the nucleus. There, it activates the transcription of proteasome subunit genes, which can assemble to form new proteasome to restore proteostasis[94,95,108]. Psm genes: proteasome subunit genes, Ub: Ubiquitin.

Notably, there is accumulating evidence that Nfe2l1-mediated proteasomal activity is critical for regulating metabolism and inflammation under conditions of metabolic stress. In the liver, Nfe2l1 has been shown to protect against ER stress and steatosis by maintaining proteostasis[108,109], as well as to prevent excessive cholesterol accumulation by

suppressing inflammation and promoting cholesterol removal[110]. Moreover, Widenmaier et al. discovered Nfe2l1 as a cholesterol sensor that regulates its turnover, post-translational processing, and activity through binding to cholesterol via its CRAC domain[110]. In cardiomyocytes, Nfe2l1 has been found to promote heart regeneration following myocardial infarction[111]. In brown adipocytes, Nfe2l1 is essential for cellular adaptation to cold and non-shivering thermogenesis[112]. The absence of Nfe2l1 in brown and white adipocytes, however, was linked to whitening of the BAT, adipocyte hypertrophy, insulin resistance and inflammation[112–114]. Collectively, these studies suggest that NFE2L1-mediated proteasomal activity affects adipocyte metabolism, inflammation, insulin resistance, and cholesterol homeostasis, highlighting a central role of NFE2L1 in maintaining metabolic health. Dysregulation of NFE2L1 in adipocytes could thus provide a mechanistic link between obesity and the onset of cardiometabolic diseases.

1.3.4 Regulation of cellular cholesterol homeostasis in the ER

Cholesterol serves as an essential component for plasma membranes, steroid hormones, and bile acids[115]. However, exposure to excessive dietary cholesterol or elevated levels of circulating cholesterol is associated with metabolic diseases such as insulin resistance, metabolic dysfunction-associated fatty liver disease MAFLD, and atherosclerosis[116]. On the cellular level, excess cholesterol is toxic, since it decreases membrane fluidity, alters membrane protein function, and ultimately leads to cellular dysfunction. The ER is particularly sensitive as it has a limited capacity for free cholesterol[117]. Surplus cholesterol leads to lipotoxicity, which can deplete ER calcium stores, triggering the UPR and potentially leading to apoptosis[117].

Cells predominantly acquire cholesterol from LDL-cholesterol via the LDL receptor (LDLR). LDLR facilitates the internalization of LDL particles into cells through the lysosomal-endosomal system. Lysosomal hydrolases then liberate cholesterol esters from LDL. In addition to LDL-cholesterol uptake, cells can synthesize cholesterol endogenously via the mevalonate pathway[118]. Both uptake and synthesis are meticulously regulated by a complex involving the ER membrane-bound sensor, sterol response element-binding protein (SREBP) cleavage-activating protein (SCAP), and the transcription factor SREBP-2. SCAP interacts with inactive SREBP-2 in the ER membrane, guiding it to the Golgi apparatus through coat protein II coated vesicles. In the Golgi, SREBP-2 is activated through proteolytic cleavage by site-1 and site-2 proteases, initiating the transcription of genes involved in cholesterol synthesis and uptake, such as HMG CoA reductase (HMGCR) and LDLR[119,120]. SCAP serves as the principal sensor for low cholesterol levels, detecting rising ER cholesterol levels through direct interaction. This interaction induces a conformational change in SCAP, promoting its binding to the insulin-induced

gene (INSIG) protein. INSIG binding retains SCAP and associated SREBP-2 in the ER membrane, thus inhibiting further cholesterol synthesis and uptake when cellular levels are sufficient[119,120].

Adipocytes are unique in the way they handle cholesterol. They have limited ability for endogenous synthesis, which is why they depend on cholesterol uptake[121] and store cholesterol almost exclusively in its free form. Besides uptake via the LDLR, adipocytes have multiple ways to extract cholesterol from circulating lipoproteins, such as scavenger receptor BI (SR-BI) and CD36[122]. With weight gain, adipocytes accumulate triglycerides and cholesterol, which leads to hypertrophy and a subsequent expansion of the plasma membrane. As a result, membrane cholesterol is diluted in relative terms, which is perceived as cholesterol depletion as indicated by activation of SREBP-2[123]. In addition to the plasma membrane, adipocytes store around one third of free cholesterol in the phospholipid monolayer of lipid droplets.

While mechanisms to guard against low cholesterol levels are well understood, those protecting from excessive cholesterol and its precursors are less defined. Excess cholesterol can undergo esterification by acyl-coenzyme A: cholesterol acyltransferase (ACAT), resulting in cholesteryl esters. These esters can be temporarily stored in lipid droplets. Additionally, they can be removed from the cell by efflux transporters such as ATP binding cassette subfamily A member 1 (ABCA1). Alternatively, cholesteryl esters can enter biosynthetic pathways, contributing to oxysterol formation or bile synthesis[115,116]. An overview of cellular cholesterol metabolism can be found in Figure 6.

Recently, a novel mechanism has been proposed to protect cells from cholesterol overload, which includes the retention of NFE2L1 in the ER by binding to cholesterol[110]. Under low or normal cholesterol levels, NFE2L1 is activated and translocates to the nucleus, where it represses transcription mediated by liver-x-receptor (LXR) and inflammatory signaling driven by scavenger receptor CD36. During transient cholesterol elevations, partial retention of NFE2L1 de-represses LXR, enhancing cholesterol efflux and primes for inflammation. However, when cholesterol level exceed ER membrane capacity, NFE2L1 is almost completely retained in the ER. NFE2L1 deficiency de-represses CD36, which promotes inflammation-induced inhibition of cholesterol efflux. However, this response comes at the expense of NFE2L1's canonical action in the nucleus, the promotion of transcription of proteasome subunits[110]. It is important to note that this intricate mechanism has been exclusively identified in hepatocytes, thus its applicability across different cell types, especially adipocytes, is unclear.

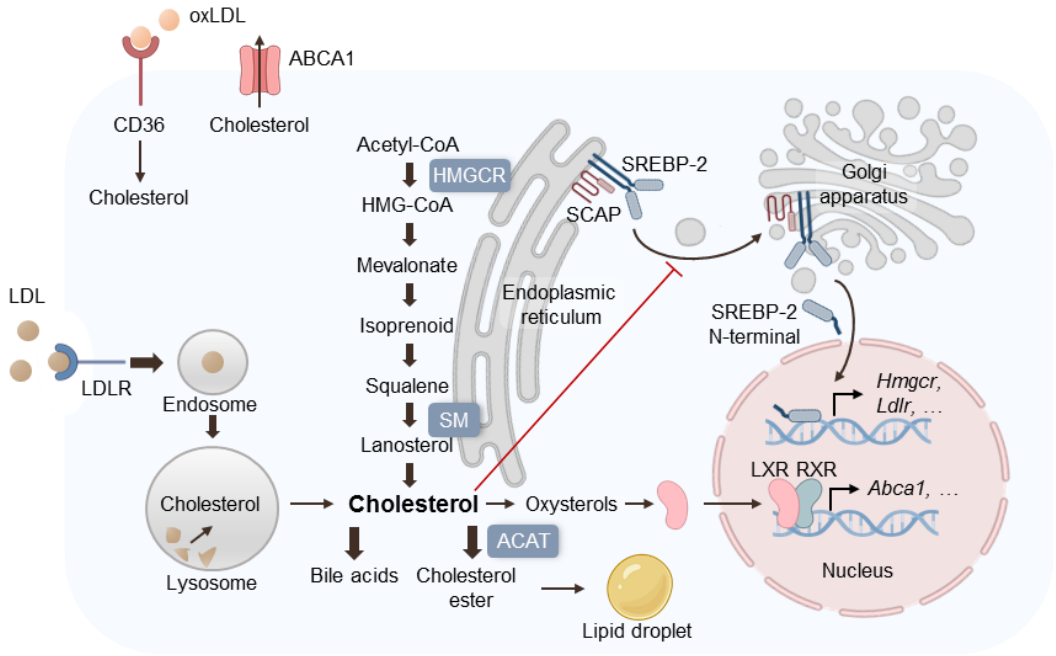

Figure 6 | Cellular cholesterol metabolism

Cellular cholesterol metabolism involves uptake via LDLR-mediated endocytosis, synthesis through the mevalonate pathway with HMGCR and squalene monooxygenase (SM) as rate-limiting enzymes, and efflux through ABC transporters like ABCA1. Excess cholesterol is esterified by ACAT and stored in lipid droplets, or used for bile acid synthesis. Moreover, cholesterol surplus retains the SCAP-SREBP2 complex in the ER, which reduces cholesterol biosynthesis and uptake, and activates liver-x-receptor (LXR) to enhance cholesterol efflux. Figure based on Song et al. (2023)[116]. RXR: retinoid-x-receptor.

In summary, cholesterol is a critical nutrient that must be tightly regulated to prevent cholesterol-induced inflammation and lipotoxicity. Adipocytes accumulate enormous amounts of cholesterol and triglycerides in obesity. However, how they adapt to excess cholesterol and maintain ER homeostasis and cellular integrity is unknown.

2. Objective

The objective of this thesis is to decipher the role of the ER-resident transcription factor NFE2L1 in adipocyte adaptation to the metabolic challenges posed by obesity and its consequent impact on cardiometabolic health. In obesity, chronic over-nutrition disrupts metabolic adaptation mechanisms, rendering adipocytes dysfunctional, which is associated with ectopic lipid accumulation, inflammation, and insulin resistance. I hypothesize that this dysfunction is partly attributed to the failure of proteostasis - encompassing protein synthesis, folding, and degradation - which is critical for cellular health and regulated by NFE2L1. As a transcription factor, NFE2L1 mediates the bounce-back response of the proteasome to help cells adapt to increased demand for proteasomal activity. In addition, NFE2L1 has also been shown to play an important role in the regulation of cholesterol metabolism and inflammation under metabolic stress. Therefore, dysregulation of NFE2L1 in obese adipocytes may represent a mechanistic link between obesity and adipocyte dysfunction. However, the specific contribution of NFE2L1 to the maintenance of adipocyte function and the prevention of cardiometabolic diseases associated with obesity is still poorly understood.

This thesis aims to elucidate these mechanisms, offering potential insights into novel therapeutic strategies for obesity and its associated cardiometabolic disorders by addressing the following aims:

1) Determine the role of adipocyte NFE2L1 in obesity and cardiometabolic diseases.

2) Assess the interaction of adipocyte NFE2L1 with diets varying in lipid composition.

3) Explore the molecular mechanisms linking NFE2L1 to cholesterol homeostasis in white adipocytes.

4) Evaluate the relevance of the NFE2L1-proteasome pathway to human obesity.

3. Material and Methods

3.1 Human data

The human data utilized in this study were obtained from the Leipzig Obesity Biobank (LOBB), which includes paired samples of abdominal SCAT and omental VISAT, as well as body fluids and associated anthropometric data. The study received approval from the Ethics Committee of the University of Leipzig (approval no: 159-12-21052012) and was conducted in compliance with the Declaration of Helsinki principles. All participants provided written informed consent prior to their inclusion in the study.

The first cohort consisted of 478 individuals, categorized into non-obese (N = 68; age: 62.7 ± 17.4 years old; BMI: 24.4 ± 2.9 kg/m^2) and obese (N = 410; age: 46.6 ± 11.4 years old; BMI: 49.7 ± 9.0 kg/m^2) groups. *NFE2L1* expression in SCAT and VISAT was quantified using quantitative real-time polymerase chain reaction (qRT-PCR), and the expression levels were normalized to *HPRT1* (hypoxanthine phosphoribosyltransferase 1).

The second cohort comprised 31 non-obese individuals (age: 55.8 ± 13.4 years old; BMI: 25.7 ± 2.7 kg/m^2) and 1,448 obese individuals (age: 46.9 ± 11.7 years old; BMI: 49.2 ± 8.3 kg/m^2). In this cohort, gene expression analysis of *NFE2L1* and proteasome subunit genes was performed by RNA sequencing.

3.2 Animal care and use

All animal experiments were performed according to procedures approved by the animal welfare committees of the government of Upper Bavaria, Germany (ROB-55.2-2532.Vet_02-20-32) and performed in compliance with German Animal Welfare Laws. I housed animals in individually ventilated cages at room temperature (22 °C) with a 12 h-light-dark cycle and *ad libitum* access to standard chow diet (Ssniff) and water. The previously described Nfe2l1 floxed ($^{fl/fl}$) mice[112] were crossed with B6.FVB-Tg(Adipoq-cre)1Evdr/J mice (The Jackson Laboratory, stock no. 028020) to generate Nfe2l1 adipocyte-specific knockout (Adipoq-KO) mice. I used Cre negative littermates carrying floxed Nfe2l1 alleles as wild-type (WT) controls. For atherosclerosis studies I have crossed Adipoq-Cre Nfe2l1 mice with whole-body ApoE knock-out mice (ApoE$^{-/-}$, The Jackson Laboratory, stock no. 002052), to create ApoE$^{-/-}$ Adipoq-KO and ApoE$^{-/-}$ Nfe2l1 floxed wild-type controls. I also studied brown adipocyte-specific Nfe2l1 KO mice by using Ucp1-Cre, as previously described [112]. For diet-induced obesity (DIO) studies, I fed mice high-fat diet (HFD) 60 kJ% fat (E15742-34, Ssniff) for 16 weeks starting at age 4-8 weeks, and for atherosclerosis studies, I fed Western diet (E15721-34, Ssniff) containing 42 kJ%

fat enriched with 0.21 % cholesterol for 12 weeks. I measured respiration, energy expenditure, food and water intake, as well as activity using a Promethion Core system (Sable Systems). BAT-specific energy expenditure was measured by subcutaneous injection of CL316,243 (CL, Tocris, 0.5 mg/kg in 0.9% w/v in NaCl) at ~12:00 p.m. I assessed glucose and insulin tolerance with intraperitoneal (i.p.) glucose tolerance test (GTT) and i.p. insulin tolerance test (ITT). For both GTT and ITT, mice were starved for 6 h, baseline blood glucose was measured and then mice were injected i.p. with glucose (1 g/kg body weight, Gibco) and insulin (0.25-0.75 U/kg body weight, Abbott, in DPBS + 0.2 % BSA), respectively. Blood glucose was subsequently measured at 15 min, 30 min, 60 min, 90 min and 120 min after injection. At the end of the study, mice were anesthetized with a lethal dose of ketamine-xylazin (120 mg/kg and 8 mg/kg body weight, respectively). After ensuring deep anesthesia, the chest of the mouse was disinfected, opened, and blood was collected via cardiac puncture. I perfused with cold Dulbecco's Balanced Salt Solution (DPBS, with 50 U/mL heparin), dissected the organs and weighed them. Organs were snap frozen in liquid nitrogen and stored at -80 °C. I estimated sample size by pilot experiments that showed trends of effects and their sizes. In most cases, n = 6 was the minimum number of mice used. During feeding studies, I excluded mice for poor body condition or barbering. All experiments were reproduced at least in two independent cohorts.

3.3 *Ex vivo*

3.3.1 Aorta dissections and *en face* Oil Red O staining

After cardiac blood collection and perfusion with cold DPBS, gastrointestinal tract, liver, lung, and thymus were removed to expose the aorta. PVAT was carefully removed *in situ* under a stereomicroscope using Vannas spring scissors and Dumont forceps. I harvest the aorta, including parts of the brachiocephalic and subclavian arteries, and transferred it on a black pinning bed. The remaining adipose tissue was removed, the aorta was split longitudinally and pinned down with minutiae needles. Pinned aortas were fixed in zinc formalin (Sigma) overnight and transferred to DBPS (Gibco) the next day. For the staining, I diluted Oil Red-O (ORO) stock solution (Sigma) to 60 % with ddH_2O (v/v) and filtered it through a 0.22 µm syringe filter. I first dipped the pinned aorta in 60 % 2-propanol (v/v, 10x) and then stained it with 60 % ORO (v/v) for 15 min. Excessive stain was removed by dipping in 60 % 2-propanol (v/v, 10x) and aortas were transferred to ddH_2O until imaging. I took macroscopic pictures using a Canon EOS 4000D. Total aorta area and plaque area were quantified using ImageJ. For long-term conservation, I mounted aortas on microscopy slides with Kaiser’s glycerol (Roth).

3.3.2 Histology

Tissues were collected in histology cassettes, fixed in zinc formalin overnight (12-24 h) and dehydrated by successively immersing the tissues in 70 % ethanol (v/v), 96 % ethanol (v/v), 100 % ethanol (v/v), and Xylene (Sigma) in an ASP200S (Leica) apparatus The tissues were embedded in paraffin (Roth) sliced in 4-5 µm sections using a microtome (Leica). The sections underwent deparaffination and rehydration procedures, by dipping the slides in 2x Xylene (5 min), 2x 100 % ethanol (v/v, 5x), 96 % ethanol (v/v, 5x), 70 % ethanol (v/v, 3x), and ddH_2O (10x). I stained sections with hematoxylin (5 min), washed with ddH_2O and then stained with eosin (5 min), followed by dehydration with 3x 70 % ethanol (v/v), 5x 96 % ethanol (v/v), 5x 100 % ethanol (v/v), 5x 100 % ethanol (v/v) and 2x Xylene (5 min). Finally, I mounted the slides with Histokitt II (Roth), and took images with a DMi8 (Leica).

3.3.3 Plasma analysis

Whole blood was collected by heart puncture and transferred to EDTA blood collection tubes. I separated the plasma by centrifuging at 2,000 x g for 10 min at 4 °C. I used Mouse/Rat Leptin Quantikine ELISA Kit (R&D systems), Mouse Adiponectin/Acrp30 Quantikine ELISA Kit (R&D systems) and Ultra Sensitive Mouse Insulin ELISA Kit (Crystal Chem) according to manufacturer's instructions to quantify plasma leptin, adiponectin and insulin level, respectively. Plasma cholesterol and triglyceride level were measured using Cholesterol FS and Triglyceride FS kits (Diasys) according to manufacturer's instructions. I assessed pro- and anti-inflammatory cytokine and chemokine concentrations using the LEGENDplex™ Mouse Anti-Virus Response Panel (Biolegend), which I analyzed on a MACSQuant® Analyzer 10 (Miltenyi).

3.3.4 Liver lipids

Liver tissue (max. 200 mg) was lysed in cold DPBS by shaking in a TissueLyser II (30.0 1/s for 2x 3:00 min). For protein and triglyceride quantification, liver lysates were diluted 1:10 with DPBS and measured using Triglyceride FS kits (Diasys) and Pierce BCA Protein Assay (Thermo Fisher Scientific) according to the manufacturer's instructions. For cholesterol quantification, I mixed 100 µL of the undiluted liver lysate with 1 ml of Folch reagent (8:5 w/w Chloroform-Methanol), vortexed well and centrifuged at 1000 x g for 5 min at room temperature. I let 200 µl of the supernatant evaporate at 80 °C in a thermoshaker (600 rpm) for 10-15 min to remove any organic solvents. Lipid extract was dissolved in 200 µl of 1x reaction buffer of the Amplex® Red Cholesterol Assay Kit (Invitrogen), by thorough vortexing and subsequent incubation for 20 min at 60 °C with

shaking at 1000 rpm. Resulting cholesterol extracts were quantified using the Amplex® Red Cholesterol Assay Kit according to manufacturer's instructions.

3.3.5 Flow cytometry analysis of white adipose tissue SVF

For flow cytometry analysis of immune cell population in WAT, I dissected GWAT and minced it with surgical scissors. To each fat pad I added DMEM/F-12 (Sigma-Aldrich), 1 % PenStrep (Sigma-Aldrich), 15 mg/mL fatty acid free BSA (Sigma-Aldrich), 1 mg/ml collagenase type 2 (Worthington) and 0.1 mg/mL DNase 1 (Roche) and incubated at 37 °C in a thermoshaker for approx. 30 min, shaking at 800 rpm with manually shaking every 10 min. The digestion was stopped by adding staining buffer (DPBS, 1 % FBS v/v, 2 mM EDTA, 0.1 % sodium azide w/v) in a 1:1 ratio. SVF were filtered through a 70 µm filter and centrifuged at 500 x g for 5 min (4 °C). Red blood cells (RBC) were lysed by incubation with RBC lysis buffer (Qiagen) for 3 min at room temperature. I stopped the lysis by adding staining buffer in a 5:1 ratio and centrifuged at 500 x g for 5 min (4 °C). The cell pellet was re-suspended in staining buffer supplemented with 1:100 anti-mouse CD16/32 (Fc block, BioLegend) and incubated on ice for 10 min. After centrifugation at 500 x g for 5 min (4 °C), supernatant was decanted. Cells were stained for 30 min in the dark (4 °C) with either anti-Cd45.2, anti-Cd11b, anti-F4/80 and anti-Cd11c fluorescence-labeled antibodies for macrophages or anti-Cd45.2, anti-Cd11b, anti-Cd19, anti-Cd8a, anti-Cd4 fluorescence-labeled antibodies for T cells (antibody details in Table 1).

Table 1 │ Flow cytometry antibodies

Antibody	Supplier	Order number	Working dilution
Purified anti-mouse CD16/32 Antibody (Fc Block)	BioLegend	101302	1:100
F4/80 Monoclonal Antibody PE	eBioscience	12-4801-82	1:100
Cd11b Monoclonal Antibody APC-eFluor 780	eBioscience	47-0112-82	1:125
Cd45.2 Monoclonal Antibody PerCP-Cyanine5.5	eBioscience	45-0454-82	1:100
Cd11c Monoclonal Antibody PE-Cyanine7	BioLegend	117318	1:100
Cd4 Monoclonal Antibody PE	eBioscience	12-0041-82	1:200
Cd8a Monoclonal Antibody APC	BioLegend	100712	1:200
PE/Cy7 anti-mouse CD19 Antibody	BioLegend	115519	1:800
CD3e Monoclonal Antibody (145-2C11), FITC	eBioscience	11-0031-85	1:100

Cells were washed by adding staining buffer in a 4:1 with subsequent centrifugation 500 x g for 5 min (4 °C). After removing the supernatant, I re-suspended the pellet in

staining buffer, added countbright beads (Invitrogen) and mixed by vortexing for 30 s. After centrifugation at 500 x g for 5 min (4 °C), pellets were re-suspended in staining buffer and analyzed on a MACSQuant® Analyzer 10 (Miltenyi). Data was analyzed using FlowJo (V10). I corrected for spectral overlap by applying compensation values derived from single stained samples and assured correcting gating with Fluorescence Minus One controls. The gating strategies can be found in Supplementary Figures 1 and 2. I calculated absolute cell numbers according to countbright beads (Invitrogen) instructions and normalized cell number to tissue weight.

3.3.6 Detection of gene recombination in tissue

I detected Cre-mediated recombination of floxed *Nfe2l1* alleles in genomic DNA (gDNA) by polymerase chain reaction (PCR). Briefly, selected tissues from wild-type and Adipoq-KO animals were dissected and lysed with DirectPCR Lysis Reagent (VWR) supplemented with 0.2 mg/ml proteinase K (Merck) for 2 h at 50 °C, following inactivation for 45 min at 85 °C. The gDNA was precipitated by adding NaCl to a final concentration of 250 mM and 0.7 volume of 100 % isopropanol. After centrifugation at 4 °C for 2 min, the supernatant was discarded, the DNA pellet washed with 70 % EtOH, dried and eluted in 50 µl 10 mM Tris-HCl (pH 8.0). For the PCR reaction, 1 µL purified gDNA, 12.5 µL Dream Taq Green PCR Master Mix (Thermo Fisher Scientific), 1 µL of 5 µM primer stock (Table 2) and 10.5 µl ddH_2O were used. The PCR was run on a TRIO thermal cycler (Biometra). The program was 2:00 min 94 °C, followed by 34 cycles of 0:20 min 94 °C, 0:30 min 64 °C (-0.5 °C per cycle), 0:45 min 72 °C and a final step of 5:00 min 72 °C. The PCR products were analyzed on a 1.5 % agarose gel.

Table 2 │ Primer sequences for detection of gene recombination

Gene	Forward primer	Reverse primer
Cre	CCGTCTCTGGTGTAGCTGAT	CCGGTATTGAAACTCCAGCG
Nfe2l1	AGAGGGTACCAATTTGCTCTGGCT	AGACTGGCCATTGTGTGCTTAGGT CTAATTTGTGCAAGCAGCAGCCCA

3.4 *In vitro*

3.4.1 Cell culture and treatments

I used 3T3-L1 cells (Sigma), which I differentiated into mature white adipocytes. The cells were induced at confluence for 2 days and differentiated for 2 more days followed

by 1 day of cultivation in standard medium (DMEM GlutaMax (Gibco), 10 % iron-fortified calf serum (Sigma-Aldrich), 1 % penicillin-streptomycin (Sigma-Aldrich)). For both induction and differentiation, the standard medium was supplemented with 850 nM human insulin (Sigma-Aldrich), 1 µM dexamethasone (Sigma-Aldrich, in 100 % ethanol), 1 µM rosiglitazone (Cayman Chemicals, in 100 % DMSO) and 500 µM IBMX (Sigma-Aldrich, in 100 % DMSO). All treatments were performed on the 5th day of differentiation. Proteasome inhibitor epoxomicin (Millipore) was used at 100 nM in 100 % DMSO. For cholesterol treatments, cholesterol powder (Sigma) was dissolved in 100 % (v/v) ethanol at 65 °C and conjugated to methyl-beta-cyclodextrin (MbCD) at a concentration of 5 mM cholesterol to 42 mg/ml MbCD. The conjugation to MbCD keeps cholesterol solubilized and causes the cells to accumulate cholesterol, as indicated by down-regulation of Srebp2 target genes[110].

3.4.2 Primary cell preparation and culture

For primary cell experiments, mature adipocytes were differentiated from pre-adipocytes, isolated from the SVF of adipose tissue of 4 weeks old C57BL/6J (Janvier) wild-type mice. The mice were sacrificed by cervical dislocation, the respective adipose tissues were harvested and pooled. The tissues were minced, weighted and digested in DMEM/F-12 (Sigma-Aldrich), 1 % PenStrep (Sigma-Aldrich), 15 mg/mL fatty acid free BSA (Sigma-Aldrich), 1 mg/mL collagenase type 2 (Worthington) and 0.1 mg/ml DNase 1 (Roche) for 30 – 45 min at 37 °C. For BAT, the digestion mix was supplemented with 1.2 U/ml Dispase (Roche). The digestion was stopped by adding DMEM/F-12 (+10% FBS, +1% PenStrep) in a 1:5 ratio. The digest was filtered through a 100 µm strainer and centrifuged at room temperature for 10 min at 500 x g. The mature adipocytes and the supernatant were aspirated, the pellet suspended in DMEM/F-12 (+10 % FBS, +1 % PenStrep) and filtered through a 70 µm and a 30 µm strainer before plating in a T75 flasks. The medium was changed the next day, and then every other day until the cells reached confluency. To differentiate pre-adipocytes into mature adipocytes, cells were induced for 2 days and differentiated for 2 days followed by 1 day cultivation in standard medium. The induction medium consisted of DMEM/F-12 (+10 % FBS, +1 % PenStrep) supplemented with 340 nM human insulin (Sigma-Aldrich), 1 µM dexamethasone (Sigma-Aldrich, in 100 % ethanol), 1 µM T3 (Sigma-Aldrich, in 1 M NaOH), 1 µM rosiglitazone (Cayman Chemicals, in 100 % DMSO), 500 µM IBMX (Sigma-Aldrich, in 100 % DMSO). The differentiation medium for white adipocytes from the SCAT consisted of DMEM/F-12 (+10 % FBS, +1 % PenStrep) with 10 nM human insulin and 2 µM T3.

3.4.3 Cell viability

Viability of cells was assessed with AquaBluer™ (MultiTarget Pharmaceuticals LLC). Briefly, 6000-8000 cells were seeded in 96 well plates and cultured at 37 °C overnight. The respective treatment was applied the next day, and incubated until 4 h before the desired treatment endpoint. The treatment solution was replaced with AquaBluer™ diluted 1:100 (v/v) in phenolred-free DMEM (Gibco) and the cells were incubated for 4 h. AquaBluer™ is a redox-indicator that changes color, when metabolized by viable cells. This color change was quantified at 540 nm excitation/590 nm emission using a Tecan plate reader. Absolute fluorescence intensity was normalized to untreated control cells.

3.4.4 Reverse transfection and RNAi

To knock-down genes of interest, I reverse transfected 3T3-L1 and primary white adipocytes with SMARTpool siRNA (Dharmacon) and Lipofectamine™ RNAiMAX transfection reagent (Thermo Fisher Scientific) on the 3rd day of differentiation. In brief, I diluted RNAiMAX and SMARTpool siRNAs, respectively, with Opti-MEM® (Gibco) according to RNAiMAX manufacturer's instructions and incubated for 5 min at room temperature. SMARTpool siRNAs for *Nfe2l1* and *Atf3* were used in a final concentration of 30 nM for single knockdowns. For double knockdown of *Nfe2l1* and *Atf3*, SMARTpool siRNAs were mixed in an equimolar ratio with final concentrations of 60 nM. Afterwards, diluted Lipofectamine® RNAiMAX was mixed 1:1 with diluted SMARTpool siRNAs and incubated for another 20 min. In the meantime, cells were trypsinized, centrifuged and the pellet re-suspended in the appropriate amount of differentiation medium. Finally, the siRNA-RNAiMAX mix was distributed in a cell culture plate and the adipocytes were pipetted on top. Careful shaking of the plate ensured an even distribution of the reaction mixture and the cells were allowed to reattach at room temperature for approximately 30 min before being transferred to the incubator. After 24 h, the transfection mix was replaced with the differentiation medium and the cells were incubated for another 24 h, after which I treated or directly harvested them.

3.4.5 RNA extraction, cDNA synthesis and qRT-PCR

To extract total RNA from frozen adipose tissue and cells, I used the NucleoSpin® RNA kit (Macherey-Nagel). Cells were lysed by adding RA1 supplemented with 1 % β-mercaptoethanol (Sigma), whereas tissue samples were lysed with TRIzol reagent (Thermo Fisher Scientific) in a TissueLyser II at 30.0/s for 3:00 min. Cell lysates were filtered using a filter column (Macherey-Nagel) and the flow-through was mixed with 70 % ethanol (v/v) in a 1:1 ratio. The tissue lysates were supplemented with 100 % chloroform (Sigma) in a

1:5 ratio (v/v), mixed and centrifuged for 15 min at 4 °C and maximum speed. The resulting clear phase was collected and also mixed with 70 % ethanol (v/v) in a 1:1 ratio. From here on, the lysate-ethanol mixture was applied to RNA columns (Macherey-Nagel) and the RNA was further processed according to the manufacturer's instructions. RNA concentrations were measured on a NanoDrop spectrophotometer (Thermo Fisher Scientific). To synthesize complementary DNA (cDNA), I reverse-transcribed 500 ng RNA with the Maxima™ H Master Mix 5x (Thermo Fisher Scientific) in a total volume of 10 µl according to manufacturer's instructions (10 min 25 °C, 15 min 50 °C, 5 min 85 °C). cDNA was diluted 1:40 with RNase-free H_2O. Relative gene expression was quantified using quantitative real time-polymerase chain reaction (qRT-PCR). Each reaction contained 4 µL cDNA, 5 µL PowerUp™ SYBR Green Master Mix (Applied Biosystems) and 1 µL of 5 µM primer stock (Table 3).

Table 3 │ qPCR primer sequences

Gene	Forward primer	Reverse primer
Atf3	GAGGATTTTGCTAACCTGACACC	TTGACGGTAACTGACTCCAGC
Atf4	CCTTCGACCAGTCGGGTTTG	CTGTCCCGGAAAAGGCATCC
Atf6	GGACGAGGTGGTGTCAGAG	GACAGCTCTTCGCTTTGGA
Ccl2	TTAAAAACCTGGATCGGAACCAA	GCATTAGCTTCAGATTTACGGGT
Cd68	CTCCGTGGAGTCTTCCATTTAC	GCACTATCTAGCTCCTCCATTTC
Cxcl10	GTGTTGAGATCATTGCCACG	AAGGAGCCCTTTTAGACCTT
Ddit3	CTGGAAGCCTGGTATGAGGAT	CAGGGTCAAGAGTAGTGAAGGT
Hmgcr	CGTAAGCGCAGTTCCTTCC	TTGTAGCCTCACAGTCCTTGG
Hspa5	TCATCGGACGCACTTGGAA	CAACCACCTTGAATGGCAAGA
Ldlr	CAAGAGGCAGGGTCCAGA	CCAATCTGTCCAGTACATGAAGC
Psma1	TGCGTGCGTTTTTGATTTTAGAC	CCCTCAGGGCAGGATTCATC
Psmb1	CGTTGAAGGCATAAGGCGAAAA	TTCCACTGCTGCTTACCGAG
sXbp1	GGTCTGCTGAGTCCGCAGCAGG	AGGCTTGGTGTATACATGG
Tbp	AGAACAATCCAGACTAGCAGCA	GGGAACTTCACATCACAGCTC

I used standard run conditions for Applied Biosystems SYBR Green Gene Expression Assays (2:00 min 50 °C, 10:00 min 95 °C, 40 cycles of 0:15 min 95 °C, 1:00 min 60 °C). Cycle thresholds (Cts) of genes of interest were normalized to *TATA-box binding protein* (*Tbp*) levels by the ΔΔCt-method and displayed as relative copies per Tbp or relative expression normalized to experimental control groups.

3.4.6 Protein extraction and Western blotting

I lysed cells in RIPA buffer (150 mM NaCl (Merck), 5 mM EDTA (Merck), 50 mM Tris pH 8 (Merck), 0.1 % w/v SDS (Carl Roth), 1 % w/v IGEPAL® CA-630 (Sigma-Aldrich), 0.5 % w/v sodium deoxycholate (Sigma-Aldrich)) freshly supplemented with complete EDTA protease inhibitors (Roche) and PhosStop (Roche). The lysates were centrifuged at 4 °C for 30 min at 21,000 x g to clear from debris and lipids. Protein concentrations were determined using the Pierce BCA Protein Assay (Thermo Fisher Scientific) according to the manufacturer's instructions. For western blotting, lysates were adjusted to a final concentration of 20-30 µg/lane in 1x Bolt™ LDS Sample buffer (Thermo Fisher Scientific) supplemented with 5 % (v/v) 2-mercaptoethanol (Sigma-Aldrich). For SDS-PAGE, we used Bolt™ 4-12 % Bis-Tris gels (Thermo Fisher Scientific) with Bolt™ MOPS SDS running buffer. After separation, proteins were transferred onto a 0.2 µm PVDF membrane (Bio-Rad) using the Trans-Blot® Turbo™ system (Bio-Rad) at 12 V, 1.4 A for 16 min. The membranes were briefly stained with Ponceau S (Sigma-Aldrich) to verify successful transfer. Afterwards, membranes were blocked in 5 % milk (w/v) in TBS-T (200 mM Tris (Merck), 1.36 mM NaCl (Merck), 0.1 % v/v Tween 20 (Sigma)) for 1 h at room temperature. Primary antibodies were used in a 1:1,000 ratio in 5 % milk (w/v) in TBS-T for regular antibodies and 5 % BSA (w/v) in TBS-T for phospho-antibodies and incubated overnight at 4 °C. After washing 4× for 10 min with TBS-T, secondary antibodies were applied in a 1:10,000 ratio in 5 % milk (w/v) in TBS-T for 1 h at room temperature. All antibodies used are listed in Table 4.

Table 4 │ Western blot antibodies

Antibody	Supplier	Order number	Host	Clonality
β-Tubulin	Cell Signaling	2146S	rabbit	polyclonal
Ubiquitin (P4D1)	Cell Signaling	3936S	mouse	monoclonal
Anti-rabbit IgG HRP-linked	Cell Signaling	7074S		
Anti-mouse IgG HRP-linked	Cell Signaling	7076S		
Nfe2l1: TCF11/NRF1 (D5B10)	Cell Signaling	8052S	rabbit	monoclonal
GAPDH (D16H11)	Cell Signaling	5174S	rabbit	monoclonal
Phospho-p38 MAPK (Thr180/Tyr182)	Cell Signaling	9211S	rabbit	polyclonal
p38 MAPK	Cell Signaling	9212S	rabbit	polyclonal
Phospho-NF-κB p65 (Ser536) (93H1)	Cell Signaling	3033S	rabbit	monoclonal
NF-κB p65 (D14E12)	Cell Signaling	8242S	rabbit	monoclonal
Phospho-SAPK/JNK (Thr183/Tyr185)	Cell Signaling	9255S	rabbit	monoclonal
SAPK/JNK	Cell Signaling	9252S	rabbit	polyclonal
Phospho-eIF2α (Ser51) (119A11)	Cell Signaling	3597S	rabbit	monoclonal
eIF2alpha	Cell Signaling	9722S	rabbit	polyclonal

Membranes were then washed again 3× for 10 min in TBS-T and developed using SuperSignal West Pico PLUS Chemiluminescent Substrate (Thermo Fisher Scientific) and a Chemidoc imager (Bio-Rad). I analyzed the digital images with the Image Lab software (Bio-Rad).

3.4.7 RNA Sequencing

I isolated RNA from primary white adipocytes using the NucleoSpin® RNA kit as described in subchapter 3.4.5. I measured RNA concentration and quality by Nanodrop and shipped the samples to Novogene (UK), where they performed bulk mRNA-Seq with the Illumina Novaseq platform. Briefly, after quality control of the RNA samples, mRNA was enriched, fragmented and reverse-transcribed into cDNA. After library preparation, the samples were sequenced and the resulting reads were filtered and aligned to the mouse genome (GRCm39/mm39) using HISAT2. I performed differential gene expression analysis using R (4.3.0) with the DESeq2[124] and ashr[125] packages, together with the dplyr package for data handling. Further analysis and visualization of results were performed using ggplot2, annotables, clusterProfiler, ComplexHeatmap, EnhancedVolcano and VennDiagram packages. Differentially expressed genes were filtered by $p_{adj}<0.05$ and absolute $\log_2$ fold change >0.3 for comparing the effect of genetic manipulation in untreated cells and absolute $\log_2$ fold change >1 for cells treated with cholesterol for downstream analysis.

3.5 Statistics

Data are expressed as the mean ± standard error of the mean (s.e.m.). For comparing two groups, I used Student's t test, when samples followed normal distribution or Mann-Whitney U-test where appropriate. I used one-way analysis of variance (ANOVA) for comparing three and more groups and two-way ANOVA for comparing two factors with post-hoc multiple comparisons. P values were adjusted for multiple testing where appropriate as indicated in the figure legends. Analyses were performed using R (4.3.0), Microsoft Excel and/or GraphPad Prism (10.0.1) and ImageJ. $p<0.05$ and $p_{adj}/q<0.05$ were considered significant, as indicated by asterisks and letters in the figures legends.

4. Results

4.1 Functional analysis of adipocyte Nfe2l1 in murine models of obesity and atherosclerosis

Obesity and its associated cardiometabolic diseases pose significant threats to our modern society and public health. During obesity, adipocytes fail to respond appropriately to sustain energy excess, rendering them unhealthy and dysfunctional. This has been linked to chronic low-grade inflammation, ectopic lipid accumulation and insulin resistance[4,40,41]. Nfe2l1 is a regulator of proteostasis, which involves synthesis, folding, and degradation of proteins – a crucial mechanism governing cellular health[94,95]. Recent discoveries have also identified a critical role for Nfe2l1 in regulating liver cholesterol metabolism by suppressing inflammation and promoting cholesterol removal[110]. Adipocytes are the main storage site for free cholesterol, especially under obese conditions. However, how adipocytes protect themselves from excessive cholesterol and how this affects adipocyte health is unknown. I hypothesized that the ER-resident transcription factor Nfe2l1 could play a protective role in conferring adipocyte health to the challenges of obesity.

This study aimed to explore the potential role of Nfe2l1 in the adaptation of adipocytes to the metabolic challenges of obesity and its impact on the development of cardiometabolic diseases. To study adipocyte Nfe2l1 in obesity, I used loss of function Cre-loxp mouse models, in which Nfe2l1 was specifically ablated in adipocytes, under the control of Adipoq-Cre or specifically in thermogenic adipocytes with Ucp1-Cre. For investigating Nfe2l1 role in cardiometabolic diseases, I used Adipoq-Cre$^{wt/tg}$ Nfe2l1$^{fl/fl}$ mice that were crossed on a whole body ApoE$^{-/-}$ background, to study adipocyte Nfe2l1 in the context of atherosclerosis. An overview of all the different mouse models, their gender and the interventions used in this study can be found in Table 5.

Table 5 │ Overview of mouse models and dietary interventions.

Mouse model		Gender	Diet
Adipoq-Cre$^{wt/tg}$ Nfe2l1$^{fl/fl}$	Adipocyte-specific KO of Nfe2l1	Male	DIO
		Male	WD
		Male	DIO + 0.21% cholesterol
ApoE$^{-/-}$ Adipoq-Cre$^{wt/tg}$ Nfe2l1$^{fl/fl}$	ApoE-deficient adipocyte-specific KO of Nfe2l1 for atherosclerosis studies	Female	Chow
		Female	WD
		Male	WD
Ucp1-Cre$^{wt/tg}$ Nfe2l1$^{fl/fl}$	Thermogenic adipocyte-specific KO of Nfe2l1	Male	WD

4.1.1 Role of adipocyte Nfe2l1 in diet-induced obesity

To study adipocyte Nfe2l1 in the context of DIO, I fed 8-week-old male Adipoq-Cre$^{tg/wt}$ Nfe2l1$^{fl/fl}$ mice a 60% kcal HFD for 16 weeks (Figure 7A). Following 16 weeks of DIO, there was no significant difference in body weight between wild-type and Adipoq-Cre knock-out (Adipoq-KO) mice (Figure 7B). However, the Adipoq-KO mice exhibited smaller and lighter SCAT and GWAT depots while having larger and heavier livers, but interscapular BAT (iBAT) weights were similar between the groups (Figure 7C,D).

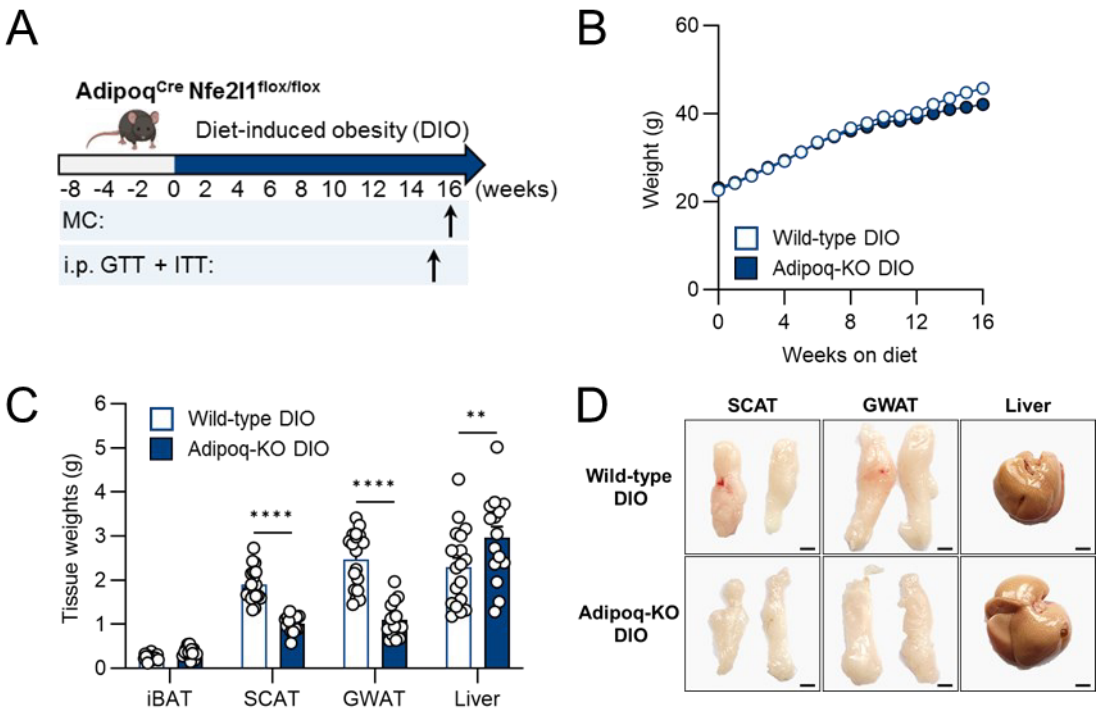

Figure 7 | Body and tissue weights of male Adipoq-Cre Nfe2l1$^{fl/fl}$ mice on DIO.

A Study design DIO (60%kcal fat, 16 weeks), indirect calorimetry in metabolic cages (MC) at diet end, intraperitoneal (i.p.) glucose tolerance test (GTT) and insulin tolerance test (ITT) at week 15, **B** body weight, **C** tissue weights and **D** representative tissue pictures (scale bar 0.5 cm) of male wild-type and Adipoq-KO mice after 16 weeks of DIO. **B,C** Data are mean + s.e.m, n=15-18 (from two independent cohorts), ** p<0.01, **** p<0.001 by Repeated Measures ANOVA with Šidák post-hoc test (**B**) and Student's t test (**C**).

Considering the larger livers and lower adipose tissue mass, loss of adipocyte Nfe2l1 might cause lipid deposition in the liver, which is associated with insulin resistance. To assess this, I performed i.p. GTT and i.p. ITT in these mice. There was no difference in baseline blood glucose nor any differences in glucose tolerance (Figure 8A). However, Adipoq-KO returned to basal glucose level more slowly, indicating that they are more insulin-resistant compared to their wild-type littermates (Figure 8B).

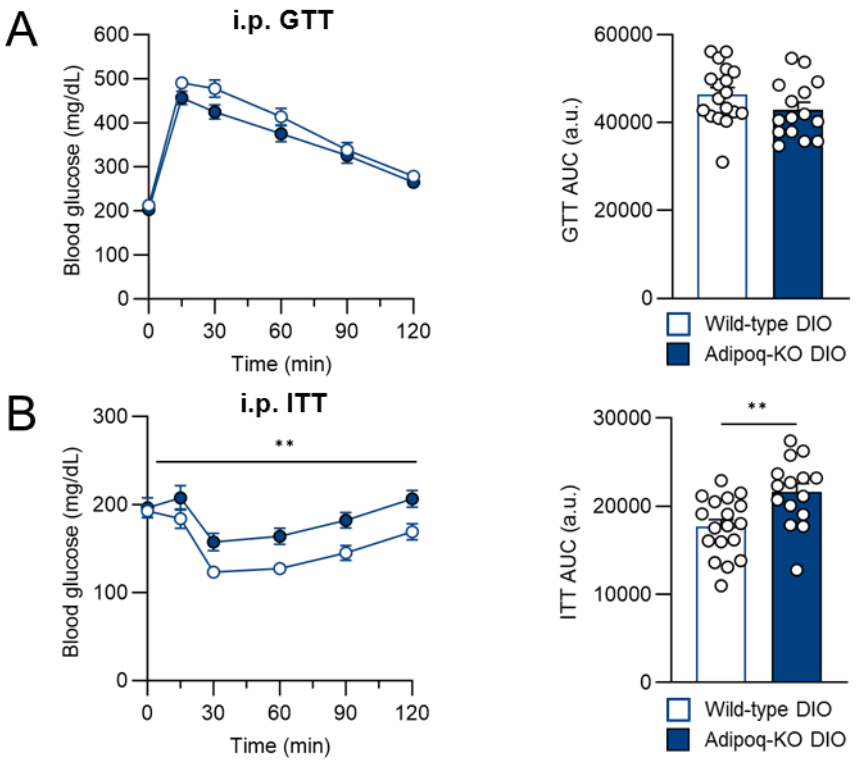

Figure 8 | Glucose and insulin tolerance of male Adipoq-Cre Nfe2l1$^{fl/fl}$ mice on DIO.

A i.p. GTT and **B** i.p. ITT of male wild-type and Adipoq-KO mice after 15 weeks of DIO. Throughout data are mean + s.e.m, n=15-18 (from two independent cohorts), ** p<0.01, by Student's t test of area under the curve (AUC).

A hallmark of adipocyte dysfunction is the decreased capacity to safely store lipids, which causes lipids to accumulate in the circulation or other organs[4], as well as alterations in the adipokine profile[35]. Thus, to characterize adipocyte health in further detail, I measured circulating lipids, adipokines and insulin in the plasma. Cholesterol and triglyceride plasma levels showed no significant differences between Adipoq-KO and wild-type mice (Figure 9A,B). Notably, Adipoq-KO mice displayed lower plasma levels of the adipokines adiponectin (Figure 9C) and leptin (Figure 9D). The secretion of adiponectin is a well-established marker of adipocyte health and function. Conversely, low levels of adiponectin, which is an anti-inflammatory and insulin-sensitizing mediator, have been linked to adipocyte hypertrophy and insulin resistance[35,126]. Finally, I measured plasma insulin levels to check if insulin resistance was compensated by hyperinsulinemia, but they were similar in both wild-type and Adipoq-KO mice (Figure 9E). To summarize, cholesterol, triglyceride and insulin levels did not differ between groups, but Adipoq-KO DIO mice had lower plasma adiponectin and leptin levels compared to their littermates.

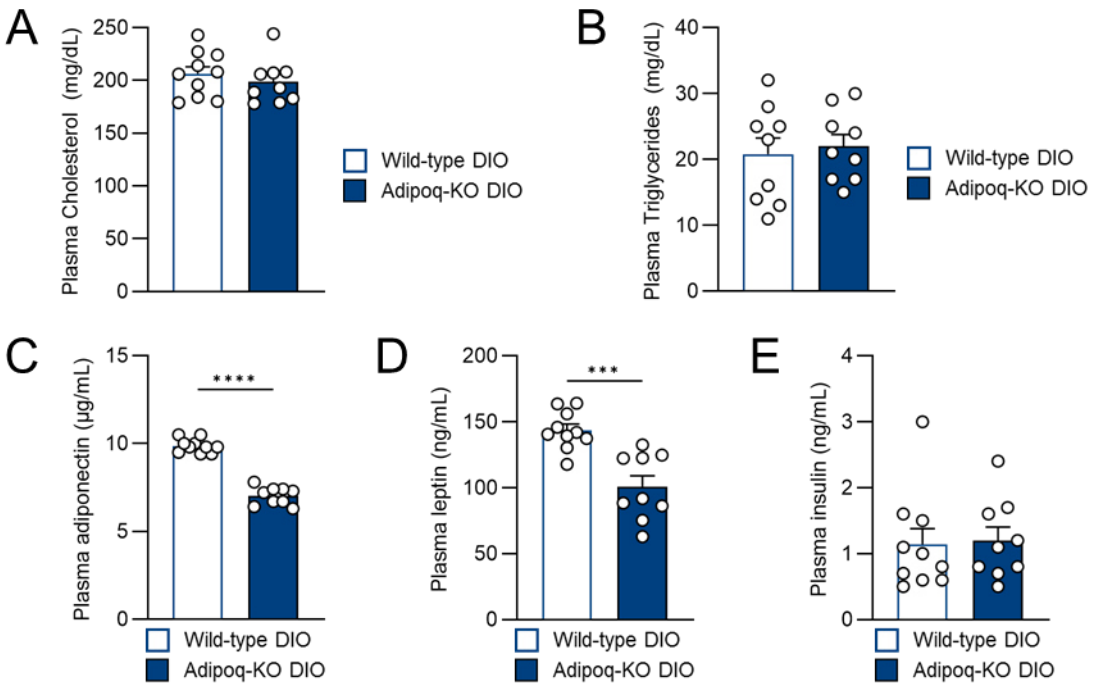

Figure 9 | Plasma parameter of male Adipoq-Cre Nfe2l1$^{fl/fl}$ mice on DIO.

A Cholesterol, **B** triglyceride, **C** adiponectin, **D** leptin and **E** insulin plasma concentration of male wild-type and Adipoq-KO mice after 16 weeks of DIO. Throughout data are mean + s.e.m, n=9-10, *** p<0.001, **** p<0.001 by Student's t test.

To determine whether the differences in WAT mass were due to variations in energy expenditure or caloric intake, the mice were subjected to indirect calorimetry to assess whole-body energy metabolism.

No differences in baseline oxygen consumption rate (VO_2) were observed in either the light or dark phase (Figure 10A). However, upon injecting the mice with the β3-adrenergic receptor agonist CL316.243 (CL) to assess BAT function *in vivo*, a marked up-regulation of VO_2 was observed in the wild-type but not in the Adipoq-KO animals. This suggests that upon loss of adipocyte Nfe2l1, mice are not able to activate their BAT for non-shivering thermogenesis. To investigate alterations in energy expenditure in either light, dark or CL-stimulated phase, I used analysis of covariance (ANCOVA) to model the relationship between energy expenditure and body weight. I found that Adipoq-KO mice displayed significantly higher energy consumption based on their genotype and body weight in both light and dark phase (Figure 10B,C). In contrast, I detected a trend, albeit not significant, that wild-type animals exhibited higher energy consumption in response to CL injections (Figure 10D).

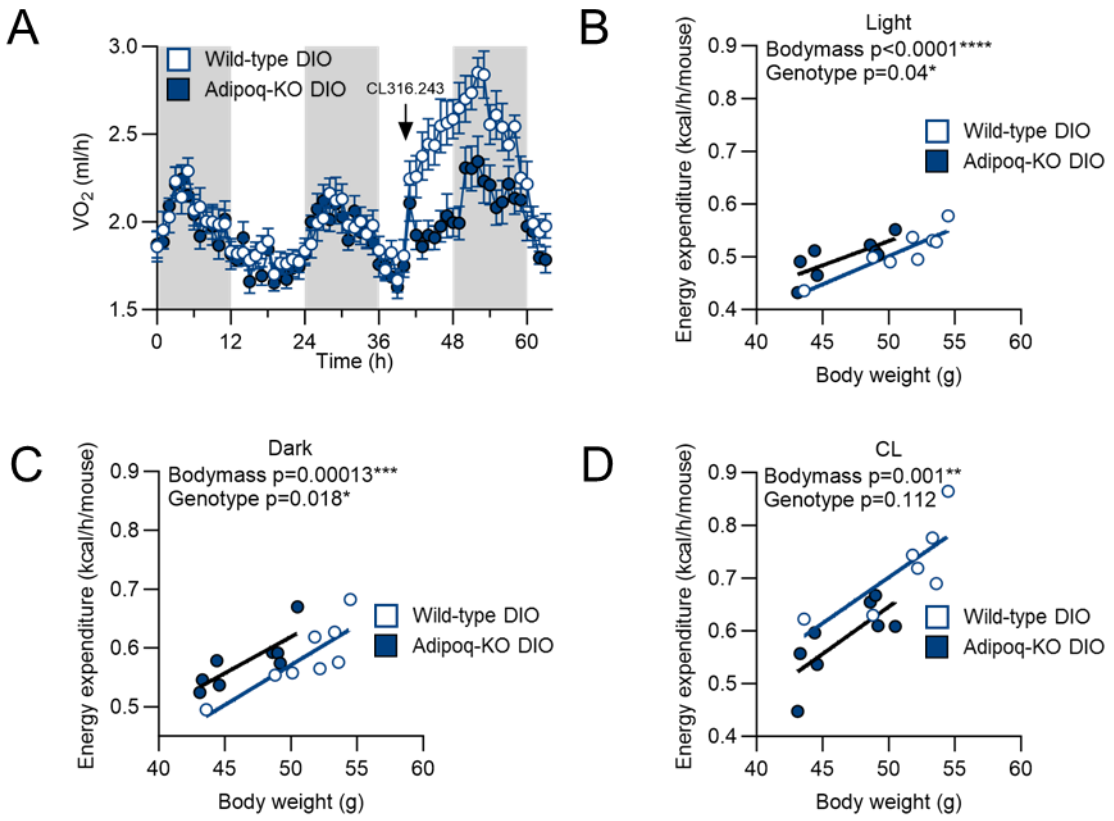

Figure 10 | Energy expenditure of male Adipoq-Cre Nfe2l1$^{fl/fl}$ mice on DIO.
A VO_2, **B** light phase, **C** dark phase and **D** CL-stimulated whole-body energy expenditure of male wild-type and Adipoq-KO mice after 16 weeks of DIO. **A** data are mean + s.e.m, **B-D** data are mean, **A-C** n=8, **D** n=7-8, ** p<0.01, *** p<0.001, **** p<0.001 by ANCOVA (**B-C**).

To check if the higher energy expenditure of the Adipoq-KO was a result of higher physical activity, I also analyzed the movement of the animals. However, there were no significant differences in activity as measured by pedestrian locomotion and locomotor activity (Figure 11A,B). I also assessed metabolic flexibility and food intake, but there were no differences in respiratory exchange ratio (RER) or food intake (Figure 11C,D) between Adipoq-KO mice and wild-type littermates. Thus, the lower WAT mass is likely a result of higher energy expenditure independently of higher activity, which the mice do not compensate for by overeating.

To sum up, Nfe2l1 is required to confer adipocytes to the challenges of DIO by protecting adipocyte health and insulin sensitivity independently of the body weight.

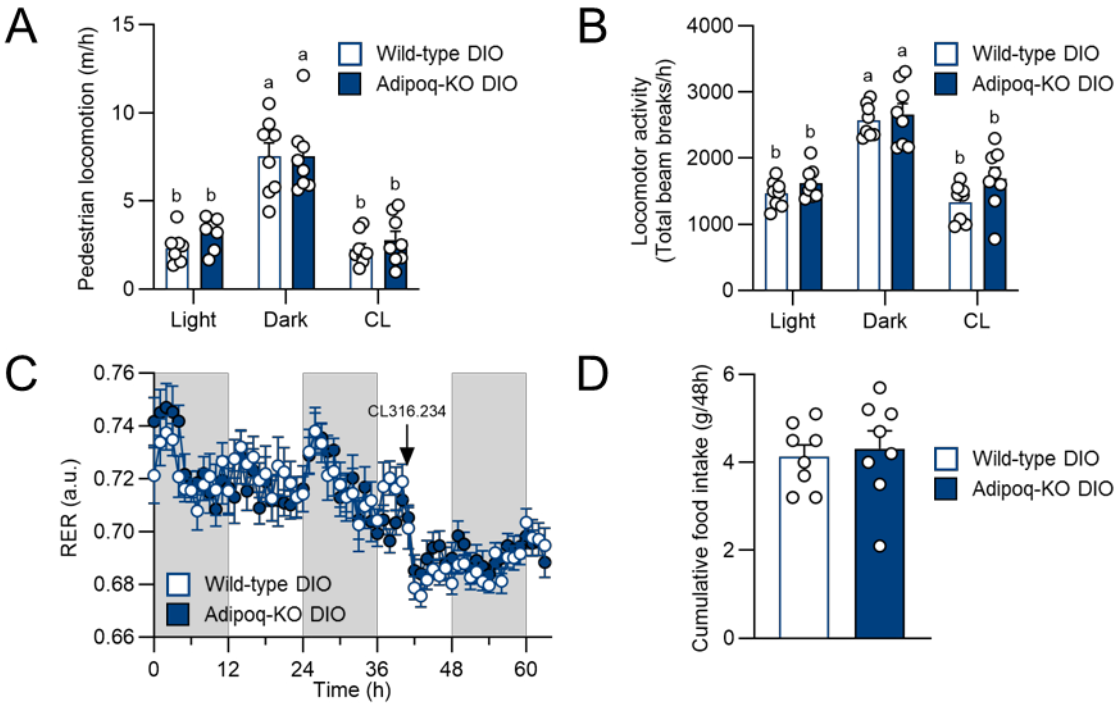

Figure 11 | Activity and food utilization of male Adipoq-Cre Nfe2l1$^{fl/fl}$ mice on DIO.

A Pedestrian locomotion, **B** locomotor activity, **C** RER and **D** cumulative food intake (average over 48h) of male wild-type and Adipoq-KO Nfe2l1 mice after 16 weeks of DIO. Throughout data are mean + s.e.m, n=8, distinct letters indicate significant differences (p_{adj}<0.05) between groups tested by two-way ANOVA with Tukey post-hoc test (**A,B**).

4.1.2 Characterization of ApoE-deficient Adipoq Nfe2l1 knockout mice

Obesity and insulin resistance are major contributors to the increase in CVDs and atherosclerosis prevalence[10–12]. Thus, given the more insulin-resistant phenotype of Adipoq-KO mice on DIO, I hypothesized that adipocyte Nfe2l1 could be protective of atherosclerosis development. However, while the Adipoq-Cre Nfe2l1$^{fl/fl}$ model is adequate to study DIO, it does not develop atherosclerosis even when fed a cholesterol-rich diet[127]. Thus, in the pursuit of understanding adipocyte Nfe2l1's involvement in cardiometabolic diseases, Adipoq-Cre Nfe2l1$^{fl/fl}$ mice were crossed with whole-body ApoE$^{-/-}$ mice, a widely used atherosclerosis model[127].

Before subjecting the ApoE$^{-/-}$ Adipoq-Cre Nfe2l1$^{fl/fl}$ mice to a cholesterol-rich diet to induce atherosclerotic plaque development, I characterized adult female ApoE$^{-/-}$ wild-type and ApoE$^{-/-}$ Adipoq-KO mice that were fed a standard chow diet. While there were no differences in body weight (Figure 12A), iBAT and SCAT were markedly smaller and lighter and iBAT appeared white in ApoE$^{-/-}$ Adipoq-KO mice (Figure 12B,C). GWAT weight, however, was similar between ApoE$^{-/-}$ Adipoq-KO and ApoE$^{-/-}$ wild-type mice, but the livers of the ApoE$^{-/-}$ Adipoq-KO were significantly heavier (Figure 12B).

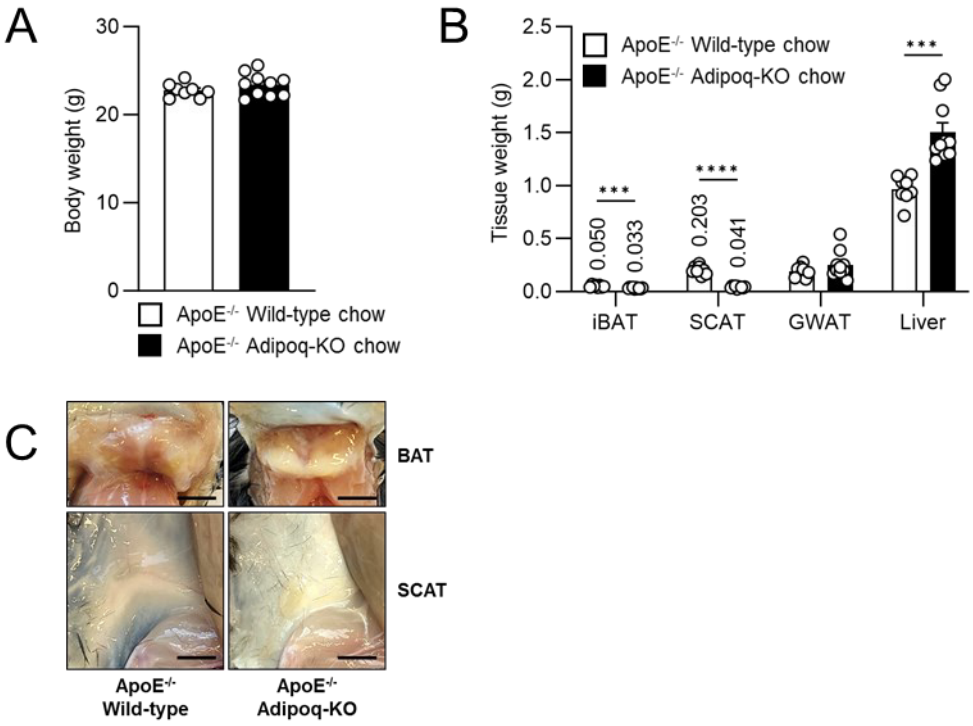

Figure 12 | Body and tissue weights of female ApoE$^{-/-}$ Adipoq-Cre Nfe2l1$^{fl/fl}$ mice.

A Body weight, **B** tissue weights, **C** tissue pictures (scale bar 0.5 cm) of 20 weeks old female ApoE$^{-/-}$ wild-type and Adipoq-KO mice on chow diet. **A,B** Data are mean ± s.e.m, n=8-10, *** p<0.001, **** p<0.001 by Student's t test (**B**).

To test whether loss of adipocyte Nfe2l1 might already disturb insulin sensitivity on chow diet on the ApoE$^{-/-}$ background, I assessed whole body glucose tolerance and insulin sensitivity by i.p. GTT and i.p. ITT in ApoE$^{-/-}$ Adipoq-Cre Nfe2l1$^{fl/fl}$. There was no difference in glucose tolerance (Figure 13A). Notably, the i.p. ITT had to be discontinued for ApoE$^{-/-}$ wild-type mice after 60 minutes, since they developed critically low blood glucose levels. Albeit this made analysis of the experiment difficult, it clearly showed that ApoE$^{-/-}$ Adipoq-KO mice were severely more insulin-resistant compared to ApoE$^{-/-}$ wild-type littermates (Figure 13B).

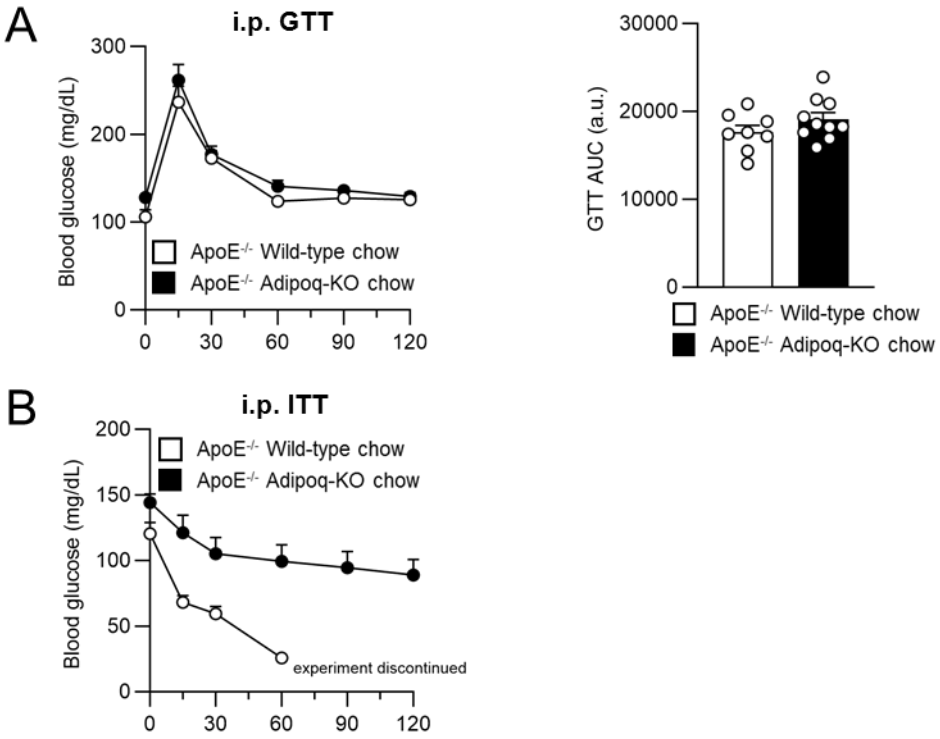

Figure 13 | Glucose and insulin tolerance of female ApoE$^{-/-}$ Adipoq-Cre Nfe2l1$^{fl/fl}$ mice.
A i.p. GTT and **B** i.p. ITT of 20 weeks old female ApoE$^{-/-}$ wild-type and Adipoq-KO mice on chow diet. Throughout data are mean ± s.e.m, n=8-10.

Since ApoE$^{-/-}$ Adipoq-KO mice had very little SCAT, whitened iBAT and were more insulin-resistant, I measured plasma adipokine and insulin level to determine adipocyte health. ApoE$^{-/-}$ Adipoq-KO mice exhibited lower plasma adiponectin levels (Figure 14A), but no difference in plasma leptin levels (Figure 14B). Plasma insulin levels showed no difference between ApoE$^{-/-}$ wild-type and Adipoq-KO mice (Figure 14C).

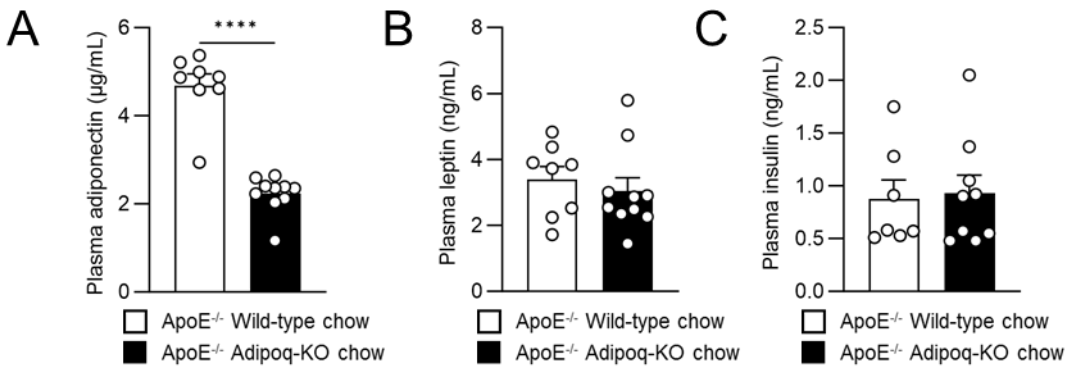

Figure 14 | Plasma parameter of female ApoE$^{-/-}$ Adipoq-Cre Nfe2l1$^{fl/fl}$ mice.

A Adiponectin, **B** leptin and, **C** insulin plasma concentration of 20 weeks old female ApoE$^{-/-}$ wild-type and Adipoq-KO mice on chow diet. Throughout data are mean ± s.e.m, n=8-10, **** p<0.001 by Student's t test.

Even in the absence of dietary cholesterol, ApoE$^{-/-}$ mice develop atherosclerotic plaques due to their higher level of atherosclerotic cholesterol-rich lipoproteins[127]. To investigate if adipocyte Nfe2l1 affected plaque formation on chow diet, aortas were dissected and stained with ORO *en face*. There was only little plaque formation found in both ApoE$^{-/-}$ wild-type and ApoE$^{-/-}$ Adipoq-KO mice, which was primarily located in the aortic arch area (Figure 15A). There was no difference in plaque content between the two groups (Figure 15B). Interestingly, while plasma cholesterol level were similarly high, plasma triglyceride levels were significantly higher in ApoE$^{-/-}$ Adipoq-KO mice compared to wild-type littermates (Figure 15C). In summary, adipocyte Nfe2l1 did not affect atherosclerosis progression on chow diet.

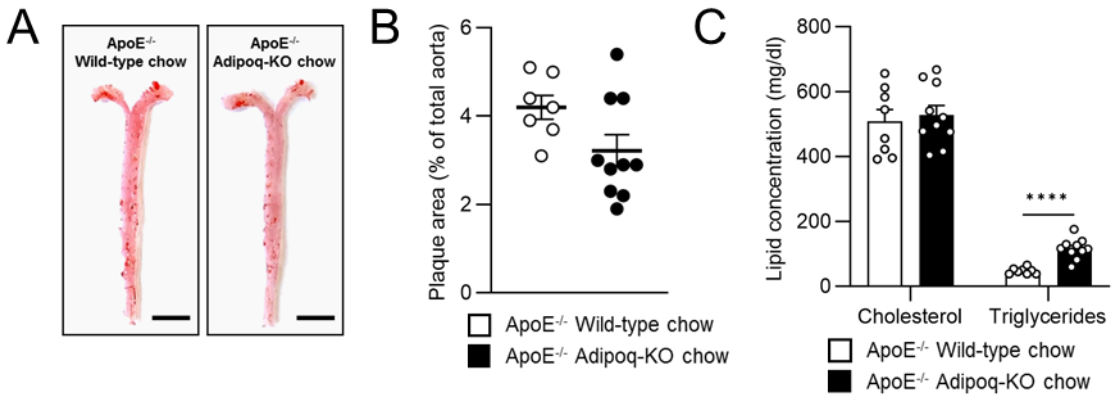

Figure 15 | Atherosclerosis assessment and plasma lipids of female ApoE$^{-/-}$ Adipoq-Cre Nfe2l1$^{fl/fl}$ mice.

A Representative pictures of *en face* ORO stained aortas (scale bar 0.5 cm), **B** quantification of plaque area, **C** plasma cholesterol and triglyceride concentration of 20 weeks old female ApoE$^{-/-}$ wild-type and Adipoq-KO mice on chow diet. **B,C** Data are mean ± s.e.m, n=7-10. **** p<0.001 by Student's t test.

4.1.3 Impact of adipocyte Nfe2l1 on diet-induced atherogenesis

As I did not observe differences in aortic plaque content on chow diet, I fed ApoE$^{-/-}$ Adipoq-Cre Nfe2l1$^{fl/fl}$ mice a cholesterol containing WD (42% kcal fat + 0.21% cholesterol) for 12 weeks starting from age 8 weeks to significantly induce atherosclerosis (Figure 16A). WD feeding did not cause differences in body weight gain (Figure 16B), but ApoE$^{-/-}$ Adipoq-KO on WD exhibited more pronounced lipoatrophy than those on a chow diet. This was evident not only in lower iBAT and SCAT mass, but also GWAT mass. Liver weights were again higher in ApoE$^{-/-}$ Adipoq-KOs compared to ApoE$^{-/-}$ wild-type littermates (Figure 16C,D).

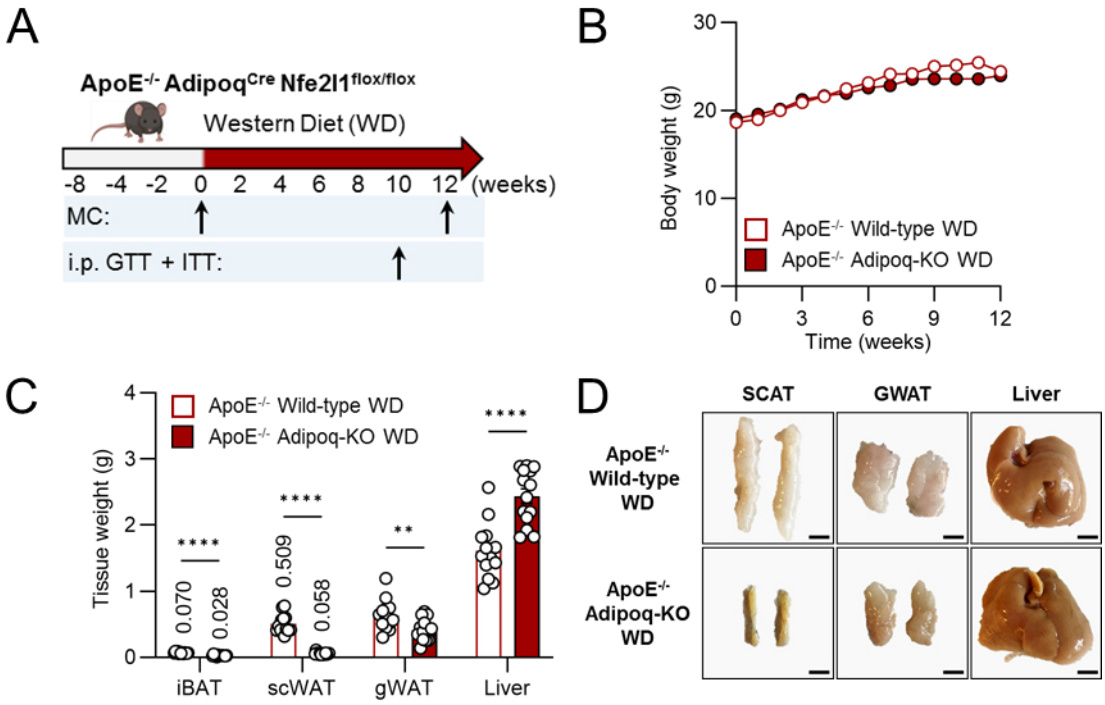

Figure 16 | Body and tissue weights of female ApoE$^{-/-}$ Adipoq-Cre Nfe2l1$^{fl/fl}$ mice on WD.
A Study design WD (WD, 42%kcal fat + 0.2% cholesterol, 12 weeks), indirect calorimetry in MC at diet start and end, i.p. GTT and ITT at week 10, **B** body weights, **C** tissue weights and **D** representative tissue pictures (scale bar 0.5 cm) of female ApoE$^{-/-}$ wild-type and Adipoq-KO mice after 12 weeks on WD. **B**,**C** Data are mean + s.e.m., n=14-17, ** p<0.01, **** p<0.001 by Student's t test (**C**).

To test whether WD ameliorated insulin resistance and altered glucose tolerance, i.p. GTT and i.p. ITT was also performed in this study. Glucose tolerance was similar in both wild-type and Adipoq-KO mice (Figure 17A), but Adipoq-KO mice were considerably more insulin-resistant compared to their wild-type littermate controls (Figure 17B).

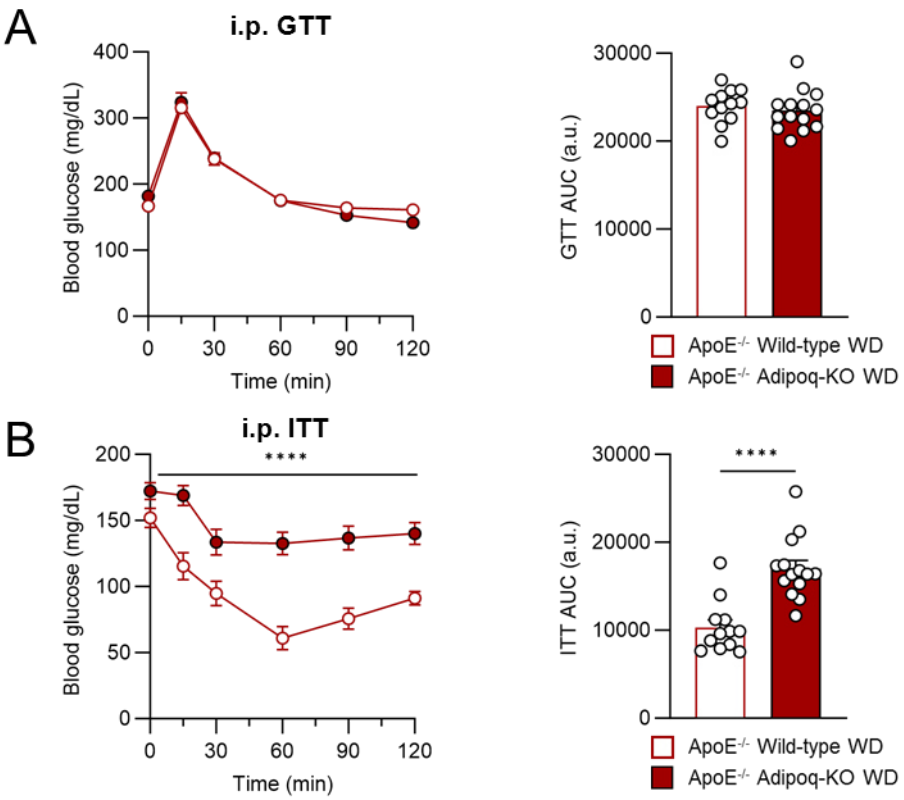

Figure 17 | Glucose and insulin tolerance of female ApoE$^{-/-}$ Adipoq-Cre Nfe2l1$^{fl/fl}$ mice on WD.
A i.p. GTT and **B** i.p. ITT of female ApoE$^{-/-}$ wild-type and Adipoq-KO mice after 10 weeks on WD. Throughout data are mean + s.e.m., n=12-14, **** p<0.001 by Student's t test.

The partial absence of adipose tissue, in combination with larger liver and insulin resistance, suggested severe adipocyte dysfunction in ApoE$^{-/-}$ Adipoq-KO mice. Thus, I measured plasma adipokine and insulin level to assess this. Indeed, plasma adiponectin and leptin level were significantly lower and plasma insulin level higher (Figure 18A-C).

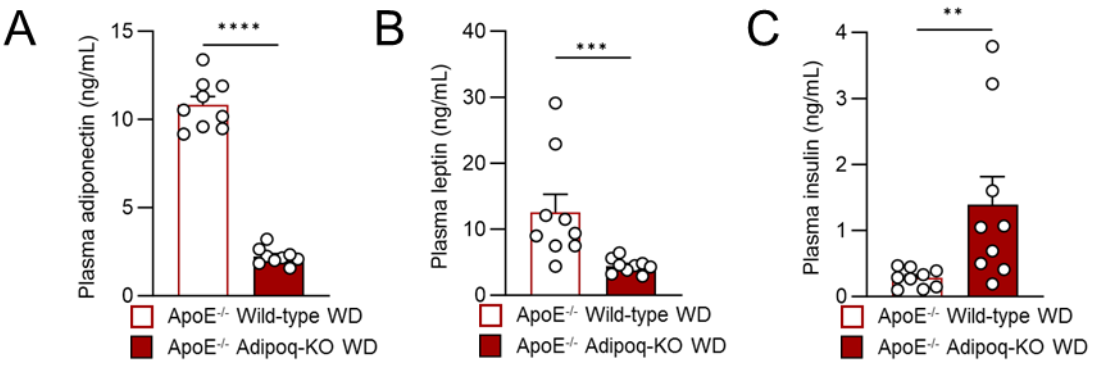

Figure 18 | Plasma parameter of female ApoE$^{-/-}$ Adipoq-Cre Nfe2l1$^{fl/fl}$ mice on WD.
A Adiponectin, **B** leptin and **C** insulin plasma concentration of female ApoE$^{-/-}$ wild-type and Adipoq-KO mice after 12 weeks on WD. Throughout data are mean + s.e.m, n=9, ** p<0.01, *** p<0.001, **** p<0.001 by Student's t test.

I hypothesized that the absence of adipose tissue mass in the ApoE$^{-/-}$ Adipoq-KO mice might be a result of higher energy expenditure or lower food intake. Thus, I used indirect calorimetry to study energy metabolism in these mice at 8 weeks before giving them WD ("pre-diet") and at the end of the diet. At 8 weeks of age, there was no difference in VO_2 during either the light or dark phase (Figure 19A). However, comparable to male Adipoq-KO mice on DIO subcutaneous (s.c.) injection of CL to assess BAT function *in vivo*, led to an increase in VO_2 in wild-type mice but not in Adipoq-KO mice. Analysis of energy expenditure in relation to body weight using ANCOVA, demonstrated no differences between genotypes in the light phase (Figure 19B) and the dark phase (Figure 19C). Variations in overall energy expenditure were solely attributed to differences in body weight. Notably, only CL-stimulated whole-body energy expenditure was higher in wild-type mice than in Adipoq-KO mice (Figure 19D).

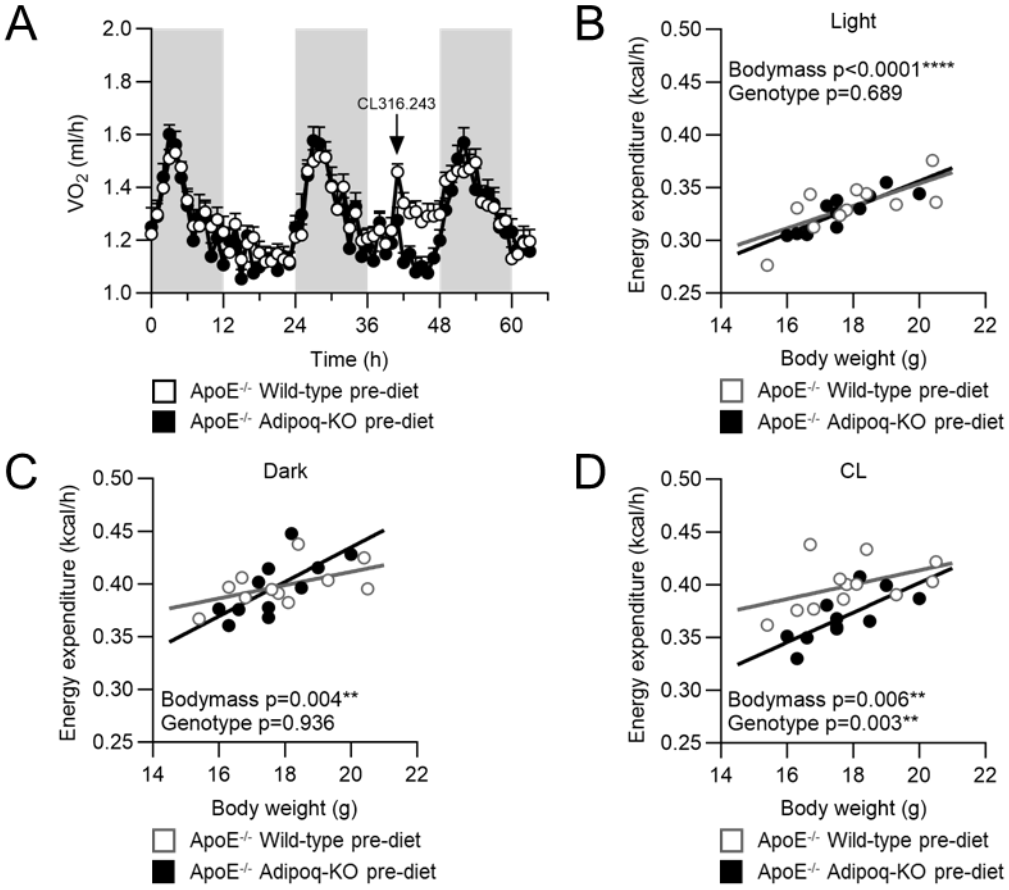

Figure 19 | Energy expenditure of female ApoE$^{-/-}$ Adipoq-Cre Nfe2l1$^{fl/fl}$ before WD.
A VO_2, **B** light phase, **C** dark phase and **D** CL316,243 (CL)-stimulated whole-body energy expenditure of female ApoE$^{-/-}$ wild-type and Adipoq-KO mice before being put on WD. **A** Data are mean + s.e.m., **B-D** data are mean, n=11-12, ** p<0.01, **** p<0.0001 by ANCOVA.

After 12 weeks of a WD, overall VO_2 increased in both wild-type and Adipoq-KO mice compared to baseline measurement. Of note, also here s.c. injection of CL did increase VO_2 in wild-type but not in Adipoq-KO mice (Figure 20A). Energy expenditure in both

light (Figure 20B) and dark phase was similar between ApoE$^{-/-}$ wild-type and Adipoq-KO mice (Figure 20C). However, there was a tendency for the Adipoq-KO to have higher energy expenditure in the dark phase, yet insignificant (p=0.123). Nevertheless, CL-stimulated whole body energy expenditure remained higher in wild-type mice than in Adipoq-KO mice (Figure 20D).

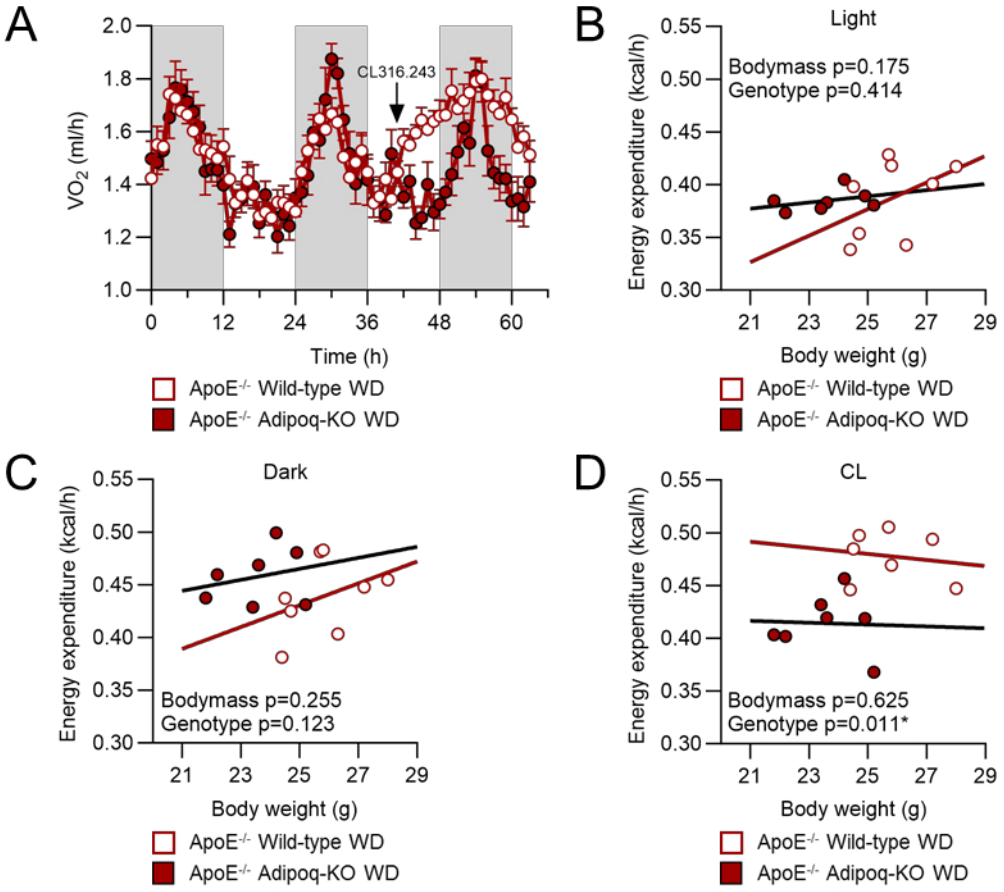

Figure 20 | Energy expenditure of female ApoE$^{-/-}$ Adipoq-Cre Nfe2l1$^{fl/fl}$ after 12 weeks of WD. **A** VO_2, **B** light phase, **C** dark phase and **D** CL-stimulated whole-body energy expenditure of female ApoE$^{-/-}$ wild-type and Adipoq-KO mice after 12 weeks of WD. **A** Data are mean + s.e.m., **B-D** data are mean, n=7-8, * p<0.05 by ANCOVA.

Since, there was no visible difference in energy expenditure between ApoE$^{-/-}$ wild-type and Adipoq-KO mice, food utilization and activity were analyzed in these animals. RER and food intake were comparable in ApoE$^{-/-}$ wild-type and Adipoq-KO mice at the baseline measurement (Figure 21 A,B). There was also no difference in activity, as measured by pedestrian locomotion and locomotor activity in the light and dark phase (Figure 21 C,D). However, Adipoq-KO mice displayed significantly higher locomotor activity during the CL-stimulated phase (Figure 21D).

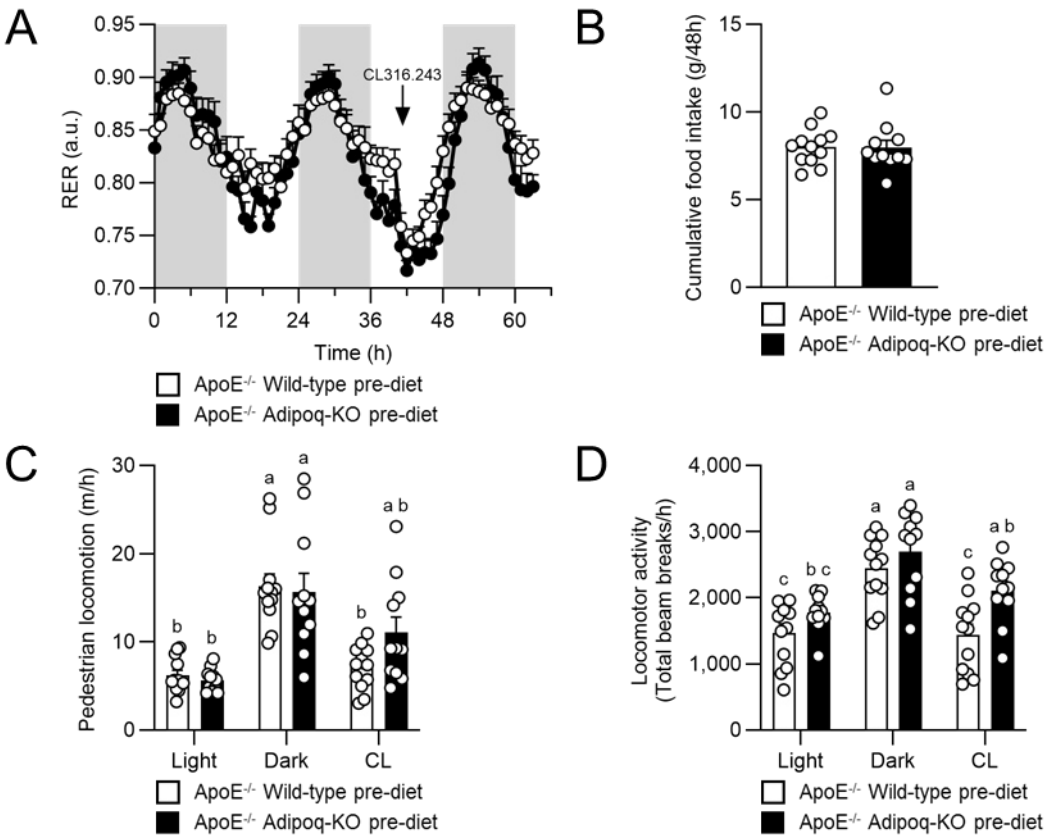

Figure 21 | Food utilization and activity of female ApoE$^{-/-}$ Adipoq-Cre Nfe2l1$^{fl/fl}$ before WD.
A RER, **B** cumulative food intake (average over 48h), **C** pedestrian locomotion **D** and locomotor activity of female ApoE$^{-/-}$ wild-type and Adipoq-KO mice before being put on WD. Throughout data are mean + s.e.m., n=11-12, distinct letters indicate significant differences (p_{adj}<0.05) between groups tested by two-way ANOVA with Tukey post-hoc test (**C,D**).

Interestingly, after being on WD for 12 weeks, ApoE$^{-/-}$ wild-type mice and Adipoq-KO mice exhibited lower overall RER and disrupted circadian oscillation of RER, compared to before the diet. The latter was more pronounced in wild-type mice than in Adipoq-KO mice. Notably, after stimulation with CL, the wild-type's RER stayed low at approx. 0.72 for more than 12h, whereas the knockout's RER went up again after 4h (Figure 22A). Food intake was significantly higher in ApoE$^{-/-}$ Adipoq-KO mice compared to their wild-type littermates (Figure 22B), however there was no difference in activity (Figure 22C,D). Thus, lower adipose tissue mass in the ApoE$^{-/-}$ Adipoq-KO mice cannot be explained by alterations in energy expenditure or consumption.

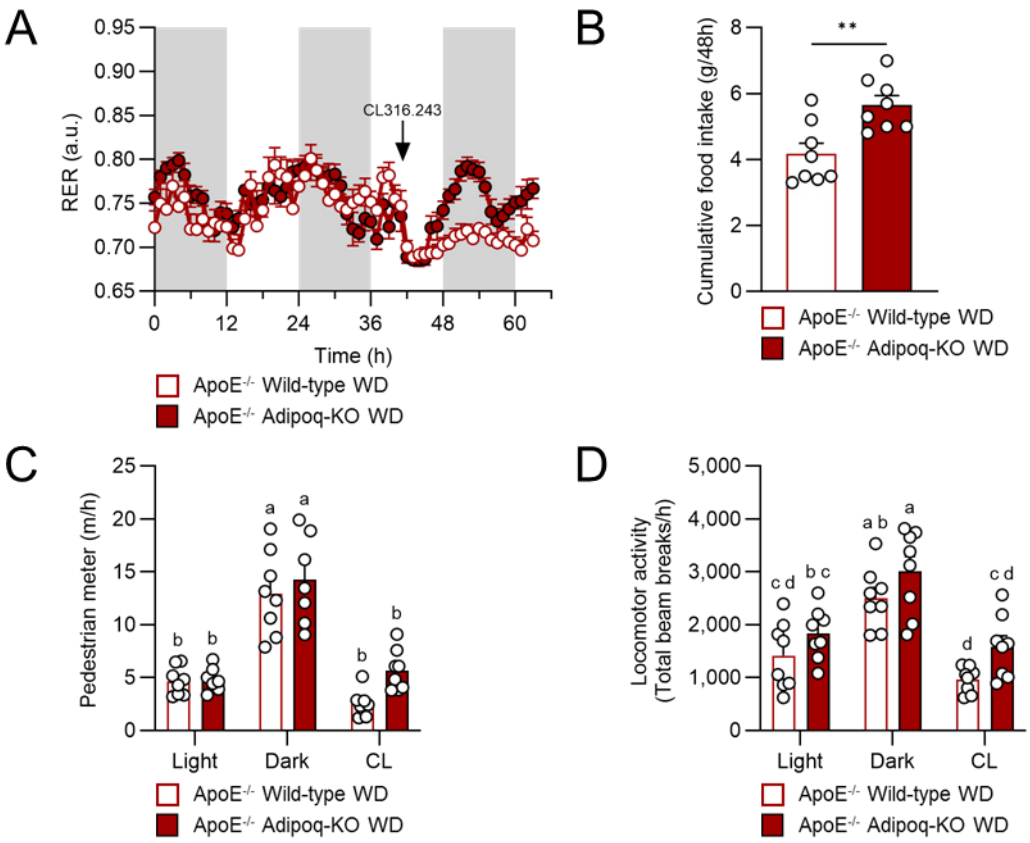

Figure 22 | Food utilization and activity of female ApoE$^{-/-}$ Adipoq-Cre Nfe2l1$^{fl/fl}$ after 12 weeks of WD.

A RER, **B** cumulative food intake (average over 48h), **C** pedestrian locomotion **D** and locomotor activity of female ApoE$^{-/-}$ wild-type and Adipoq-KO mice after 12 weeks of WD. Throughout data are mean + s.e.m., n=7-8, ** p<0.01 by Student's t test (**B**), distinct letters indicate significant differences (p_{adj}<0.05) between groups tested by two-way ANOVA with Tukey post-hoc test (**C,D**).

Since ApoE$^{-/-}$ Adipoq-KO displayed more severe lipoatrophy and insulin resistance on WD compared to chow diet, I hypothesized that the cholesterol-rich WD would promote atherosclerotic plaque formation in ApoE$^{-/-}$ Adipoq-KO compared to ApoE$^{-/-}$ wild-type littermates. To determine atherosclerosis progression in these mice, aortas were dissected and stained to visualize and quantify plaque content. Interestingly, ApoE$^{-/-}$ Adipoq-KO mice had almost twice as many atherosclerotic plaques after 12 weeks of WD compared to their wild-type littermates (Figure 23A,B). This was accompanied by significantly higher plasma total cholesterol level (Figure 23C). However, plasma triglycerides were unaffected (Figure 23D). Moreover, ApoE$^{-/-}$ Adipoq-KO mice exhibited more severe dyslipidemia, with higher levels of pro-atherogenic lipoproteins compared to ApoE$^{-/-}$ wild-types (Figure 23E,F).

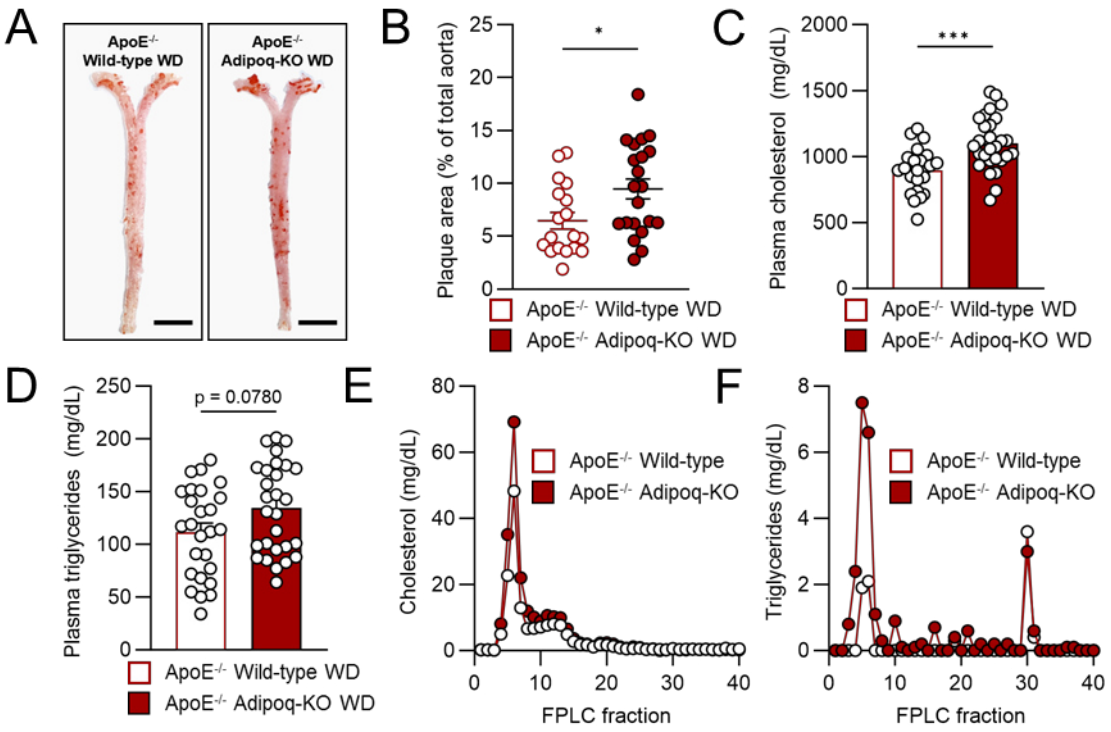

Figure 23 | Atherosclerosis assessment and plasma lipids of female ApoE$^{-/-}$ Adipoq-Cre Nfe2l1$^{fl/fl}$ mice on WD.

A Representative pictures of *en face* oil-red o stained aortas (scale bar 0.5 cm), **B** quantification of plaque area, **C** cholesterol and **D** triglyceride plasma concentration, **E** fast protein liquid chromatography (FPLC) analysis of plasma cholesterol and **F** triglyceride fractions provided by Anna Worthmann (UKE Hamburg) of female ApoE$^{-/-}$ wild-type and Adipoq-KO mice after 12 weeks on WD. **B-D** Data are mean + s.e.m., **B** n=18-21 (from three independent cohorts), **C-D** n=24-29 (from four independent cohorts), * p<0.05, *** p<0.001 by Student's t test (**B,C**) and Mann-Whitney U test (**D**). **E, F** Data is from a single sample pool, each generated by pooling of n=8 individual samples.

Atherosclerosis is an immunometabolic disease, initiated by the retention modified of cholesterol-rich lipoproteins leading to inflammation involving endothelial cells, SMCs and immune cells. The secretion of pro-inflammatory cytokines, chemokines and metabolites mediates the progression of atherosclerosis[19]. Dysfunctional adipose tissue is a relevant source of pro-inflammatory cytokines and inflammation of PVAT have been linked to atherosclerosis[16,26]. Thus, secretion of pro-inflammatory cytokines and chemokines were assessed to test whether loss of adipocyte Nfe2l1 affected systemic inflammation. Interestingly, pro-inflammatory chemokines C-X-C motif chemokine ligand 1 (Cxcl1), C-X-C motif chemokine ligand 10 (Cxcl10) and C-C Motif Chemokine Ligand 5 (Ccl5) as well as interleukin-10 (IL-10) plasma levels were significantly higher in ApoE$^{-/-}$ Adipoq-KO mice compared to wild-type littermates (Figure 24).

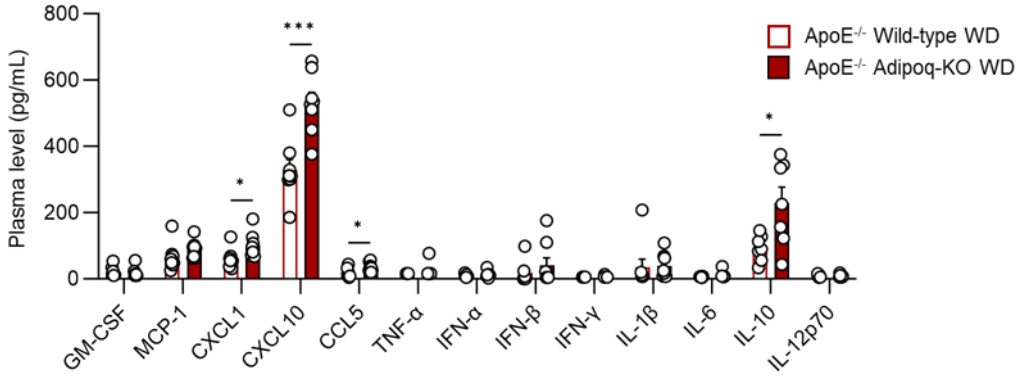

Figure 24 | Cytokine and chemokine profile of female ApoE$^{-/-}$ Adipoq-Cre Nfe2l1$^{fl/fl}$ mice on WD. Cytokine and chemokine plasma concentrations of female ApoE$^{-/-}$ wild-type and Adipoq-KO mice after 12 weeks on WD. Data are mean + s.e.m, n=7-8, * p<0.05, ** p<0.01, *** p<0.001 by Student's t test.

What was particularly striking in this study, apart from intensified plaque formation, were the significantly larger livers in the ApoE$^{-/-}$ Adipoq-KO mice. Due to the partial absence of adipose tissue, I assumed that there must be substantial ectopic lipid deposition in the liver. Indeed, livers of ApoE$^{-/-}$ Adipoq-KO mice had higher cholesterol content (Figure 25A) and a higher, albeit insignificant, triglyceride content (Figure 25B). Histological assessment of the liver also pointed towards aggravated steatosis in the ApoE$^{-/-}$ Adipoq-KO mice, as demonstrated by higher lipid droplet content and droplet size (Figure 25C).

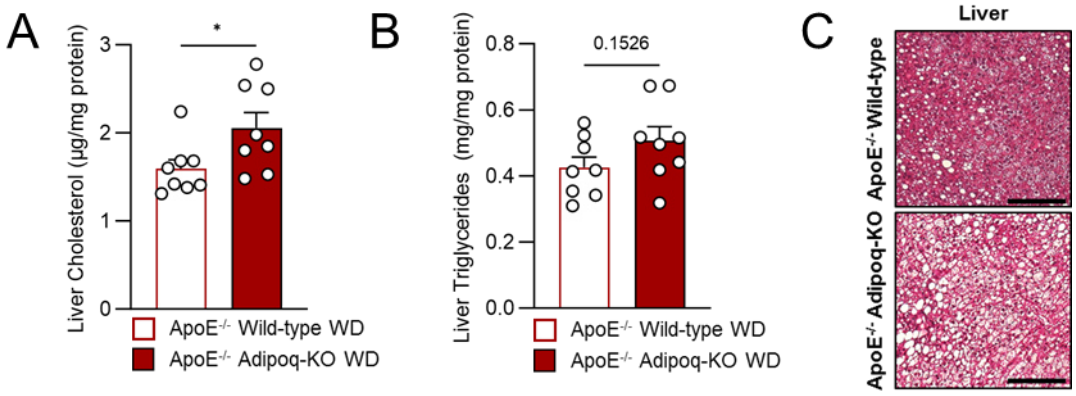

Figure 25 | Liver lipids of female ApoE$^{-/-}$ Adipoq-Cre Nfe2l1$^{fl/fl}$ mice on WD.

A Liver cholesterol and **B** triglyceride concentration, **C** representative liver hematoxilin-eosin staining (scale bar 200 µm) of female ApoE$^{-/-}$ wild-type and Adipoq-KO mice after 12 weeks on WD. Throughout data are mean + s.e.m, n=6-8, * p<0.05 by Student's t test.

Cholesterol is an important building block for various biosynthetic pathways in the liver, e.g. bile acid metabolism. Thus, I hypothesized that the liver might compensate for hypocholesteremia by up-regulation of bile acid metabolism and excretion of both cholesterol and bile acids to eliminate cholesterol. In fact, there were higher levels of conjugated bile acids (CBA) but not unconjugated bile acids (UBA) in both liver (Figure 26A) and

plasma of ApoE$^{-/-}$ Adipoq-KO mice (Figure 26B). However, bile acid as well as cholesterol and triglyceride excretion inthe feces was unaffected by loss of adipocyte Nfe2l1, suggesting cholestasis in ApoE$^{-/-}$ Adipoq-KO mice (Figure 26C,D). Despite higher cholesterol and bile acid content in the liver, mRNA expression of enzymes involved in bile acid synthesis, conjugation and transport as well as cholesterol metabolism were not different in ApoE$^{-/-}$ wild-type and Adipoq-KO liver (Figure 26H).

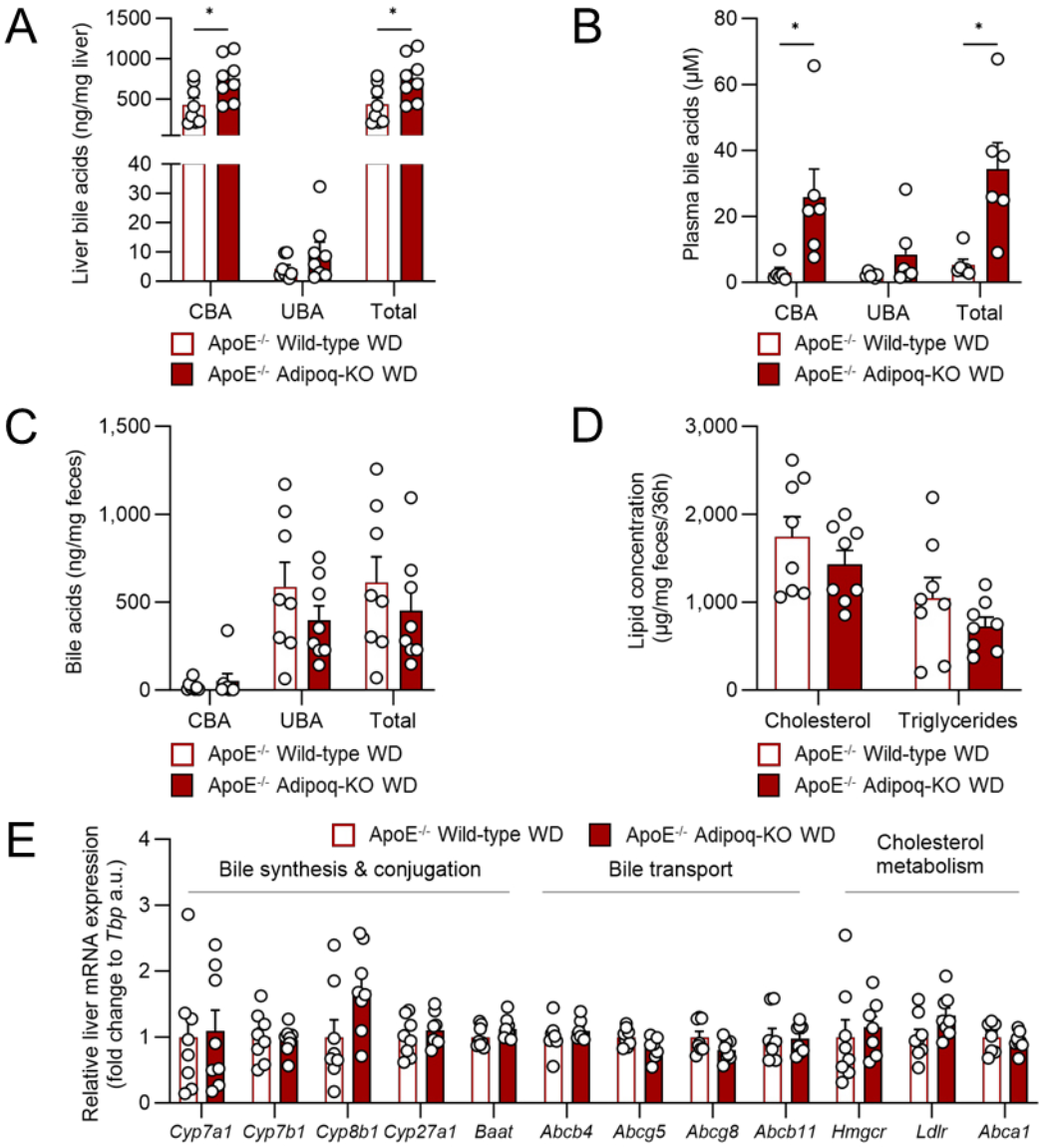

Figure 26 | Bile acid metabolism of female ApoE$^{-/-}$ Adipoq-Cre Nfe2l1$^{fl/fl}$ mice on WD.

A Liver, **B** plasma and **C** feces concentration of conjugated (CBA), unconjugated (UBA) and total bile acids, **D** feces cholesterol an triglyceride concentration and **E** relative liver mRNA expression of bile and cholesterol metabolism genes in female ApoE$^{-/-}$ wild-type and Adipoq-KO mice after 12 weeks on WD. Throughout data are mean + s.e.m., n=6-8, * q<0.05 by multiple t tests adjusted for multiple testing by false discovery rate. **A-D**, measurements provided by Anna Worthmann (UKE Hamburg).

Circulating bile acids are able to promote BAT energy expenditure by inducing thyroid hormone activating enzyme deiodinase, iodothyronine, type II (encoded by *Dio2*)[128]. Thus, the higher circulating bile acid concentration prompted me to the hypothesis that ApoE$^{-/-}$ Adipoq-KO mice might display higher BAT energy expenditure. This could have potentially been overlooked by indirect calorimetry and might account for the lower adipose tissue mass. However, in line with the indirect calorimetry data, showing no response of ApoE$^{-/-}$ Adipoq-KO mice to CL-stimulation of BAT (Figure 20A,D), there was no evidence of BAT activation despite higher circulating bile acid level. ApoE$^{-/-}$ Adipoq-KO have whitened iBAT with hypertrophic adipocytes (Figure 27A). Moreover, gene expression of thermogenic marker ELOVL fatty acid elongase 3 (encoded by *Elovl3*) and *Dio2* was similar in iBAT and SCAT of ApoE$^{-/-}$ wild-type and Adipoq-KO mice (Figure 27B).

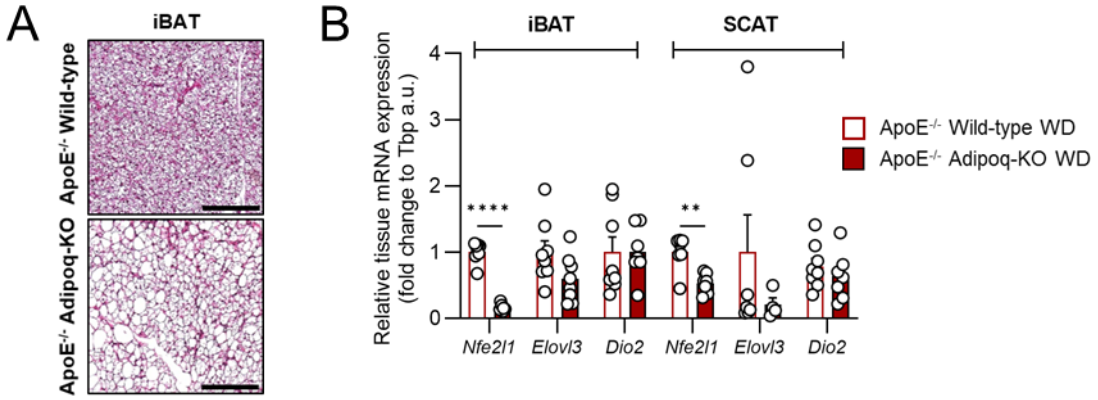

Figure 27 | Thermogenic adipose tissue of female ApoE$^{-/-}$ Adipoq-Cre Nfe2l1$^{fl/fl}$ mice on WD.
A Representative iBAT hematoxilin-eosin staining (scale bar 200 µm), **B** relative iBAT and SCAT mRNA expression of thermogenic marker genes in female ApoE$^{-/-}$ wild-type and Adipoq-KO mice after 12 weeks on WD. **B** Data are mean + s.e.m., n=4-8, ** p<0.01, **** p<0.001 by Student's t test.

So far, this study has only focused on female ApoE$^{-/-}$ Adipoq-Cre Nfe2l1$^{fl/fl}$ mice, since female ApoE$^{-/-}$ mice generally develop more atherosclerotic plaques compared to males. However, to address potential gender-specific effects of adipocyte Nfe2l1 in atherosclerosis, male ApoE$^{-/-}$ Adipoq-Cre Nfe2l1 mice were also included in this study. Interestingly, while the ApoE$^{-/-}$ wild-type mice gained weight during the 12 weeks of WD and reached a final body weight of 35.0 g on average, ApoE$^{-/-}$ Adipoq-KO mice stagnated at approximately 27.6 g (Figure 28A). This difference in body weight was at least partly explained by the extensive absence of SCAT and the lower mass of iBAT and GWAT (Figure 28B,C). The liver weights were comparable between both groups in male mice.

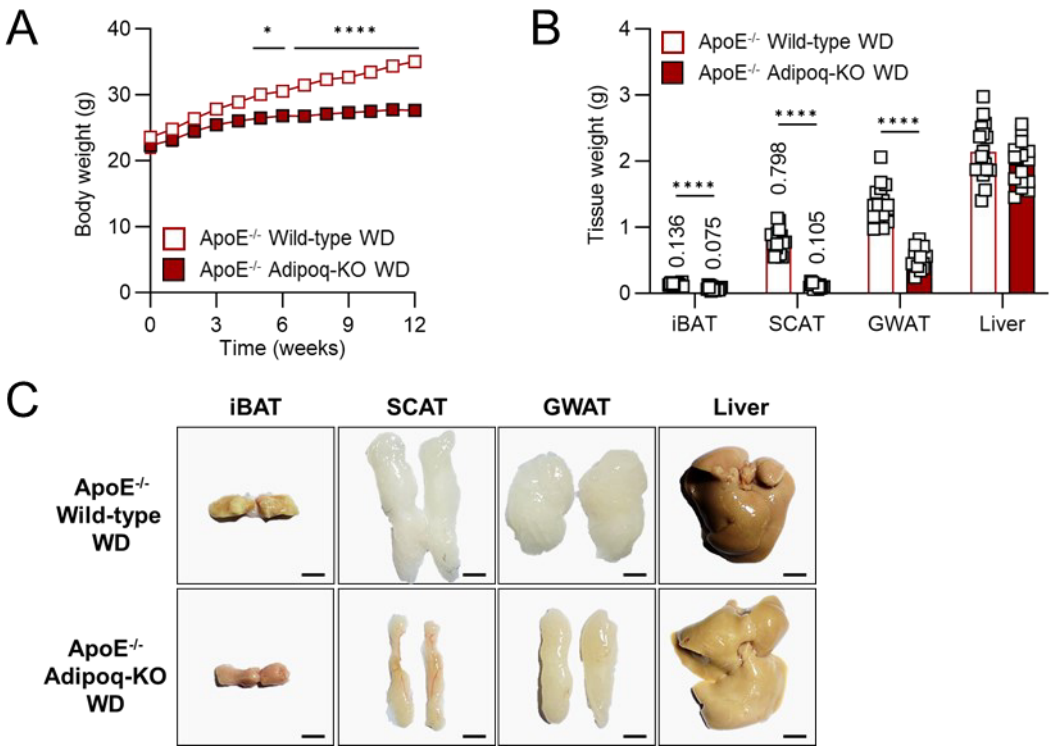

Figure 28 | Body and tissue weights of male ApoE$^{-/-}$ Adipoq-Cre Nfe2l1$^{fl/fl}$ mice on WD.

A Body weight curve, **B** tissue weights and **C** representative tissue pictures (scale bar 0.5 cm) of male ApoE$^{-/-}$ wild-type and Adipoq-KO mice after 12 weeks on WD. **A,B** Data are mean + s.e.m., n=15-17, * p_{adj}<0.05, **** p_{adj}<0.0001 by Repeated Measures ANOVA with Šidák post-hoc test (**A**) and **** p<0.0001 Student's t test (**B**).

Nevertheless, as seen in both in ApoE$^{-/-}$ females and DIO males, also male ApoE$^{-/-}$ Adipoq-KO displayed lower adiponectin and leptin plasma levels (Figure 29A,B).

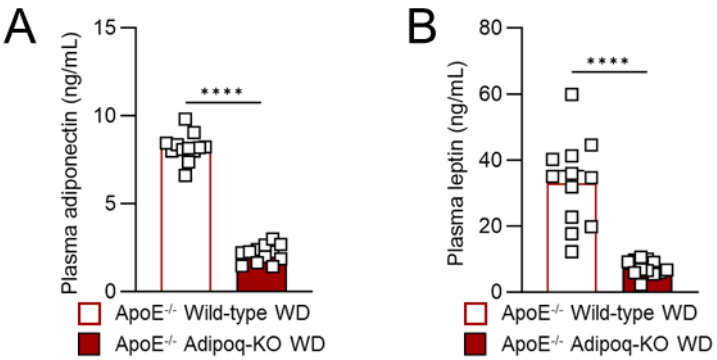

Figure 29 | Plasma parameter of male ApoE$^{-/-}$ Adipoq-Cre Nfe2l1$^{fl/fl}$ mice on WD

A Adiponectin and **F** leptin plasma concentration of male ApoE$^{-/-}$ wild-type and Adipoq-KO mice after 12 weeks on WD. Throughout data are mean + s.e.m., n=12, **** p<0.0001 by Student's t test.

In contrast to the female mice, male ApoE$^{-/-}$ Adipoq-KO did not exhibit higher susceptibility to atherosclerosis, since plaque area was comparable to the wild-type mice (Figure 30A,B). Male ApoE$^{-/-}$ Adipoq-KO also did not display higher plasma cholesterol level but

they had lower plasma triglyceride level compared to their wild-type littermates (Figure 30C,D).

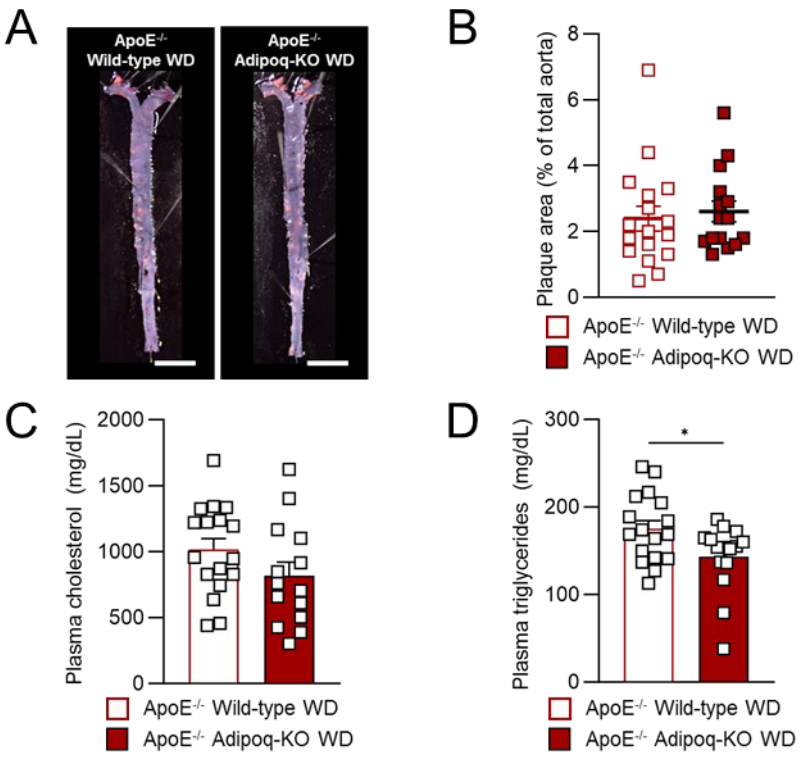

Figure 30 | Atherosclerosis assessment and plasma lipids of male ApoE$^{-/-}$ Adipoq-Cre Nfe2l1$^{fl/fl}$ mice on WD.

A Representative image of oil-red o stained aortas, **B** quantification of plaque area, **C** cholesterol and **D** triglyceride plasma concentration of male ApoE$^{-/-}$ wild-type and Adipoq-KO Nfe2l1 mice after 12 weeks on WD. **B-D** Data are mean + s.e.m., n=15-17, * $p<0.05$ by Student's t test.

In summary, the role of adipocyte Nfe2l1 in atherosclerosis is complex and gender-specific. In female mice, the absence of adipocyte Nfe2l1 promotes atherosclerotic plaque formation, dyslipidemia, and steatosis. However, the scenario is different in male ApoE$^{-/-}$ Adipoq-KO mice, where no higher plaque formation is observed. Instead, male mice exhibit more pronounced lipoatrophy and a plateau in body weight gain.

4.2 Interactions of Nfe2l1 with different lipid compositions in the diet

To elucidate the intricate interplay between dietary composition and genetic factors underlying the lower body weight phenotype in male mice, I undertook a comprehensive examination of dietary-gene interactions. Initially, I revisited the Adipoq-Cre Nfe2l1$^{fl/fl}$ model on a B6 background to ensure the phenotype was not solely due to an interaction between ApoE and Nfe2l1 (Figure 31A). The study revealed significantly lower body weights in the Adipoq-KO group (Figure 31B), with some Adipoq-KO animals appearing smaller compared to their wild-type littermates (Figure 31C). Similar to their ApoE$^{-/-}$ counterparts, Adipoq-KO mice exhibited smaller and lighter adipose tissue depots, especially in SCAT, but liver sizes and weights remained comparable to wild-types (Figure 31D).

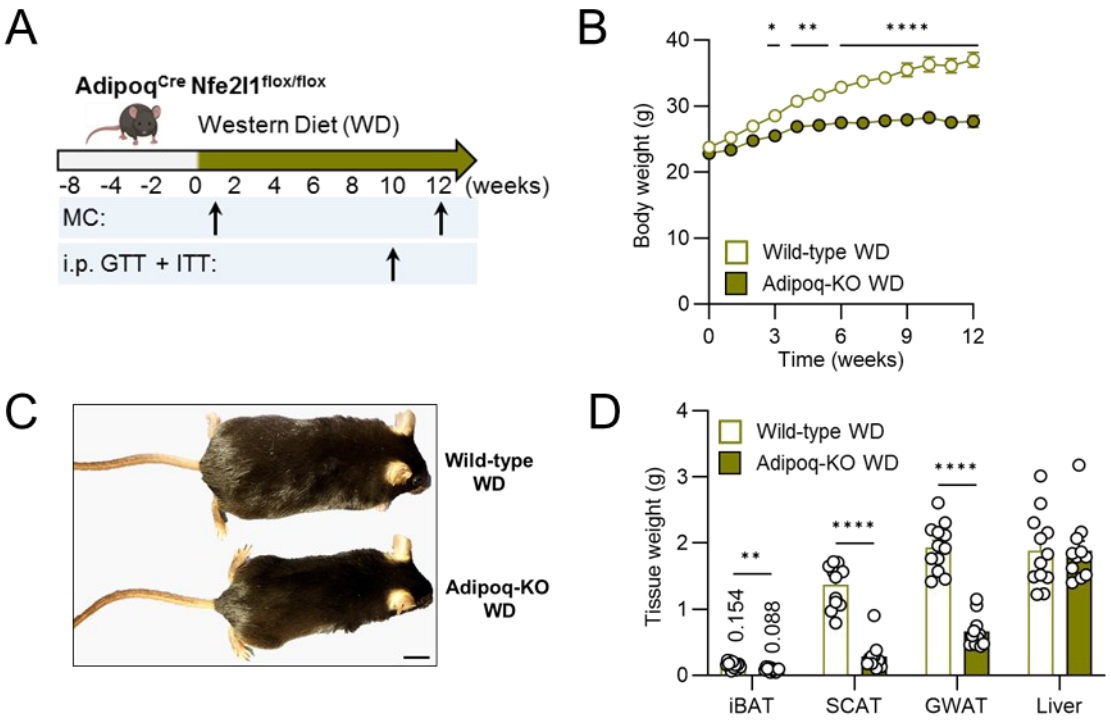

Figure 31 | Body and tissue weights of male Adipoq-Cre Nfe2l1$^{fl/fl}$ mice on WD.

A Study design Western diet (WD, 42%kcal fat + 0.2% cholesterol, 12 weeks), indirect calorimetry in MC at diet start and end, i.p. GTT and ITT at week 10, **B** body weight curve, **C** representative image (scale bar 1 cm) and **D** tissue weights of male wild-type and Adipoq-KO mice after 12 weeks of WD. **B,D** Data are mean + s.e.m., n=11-12, * p_{adj}<0.05, **p_{adj}<0.01, **** p_{adj}<0.0001 by Repeated Measures ANOVA with Šidák post-hoc test (**B**) and **p<0.01, **** p<0.0001 by Student's test (**D**).

Given the more severe insulin resistance observed in Adipoq-KO mice on DIO compared to wild-type littermates, I hypothesized that Adipoq-KO mice on WD would exhibit even greater insulin resistance, due to the previously observed lipoatrophy. To test this, I measured glucose and insulin tolerance at 10 weeks of WD in these mice. Interestingly,

glucose tolerance was better in Adipoq-KO mice and insulin resistance showed no significant differences between Adipoq-KO mice and wild-type littermates (Figure 32A,B).

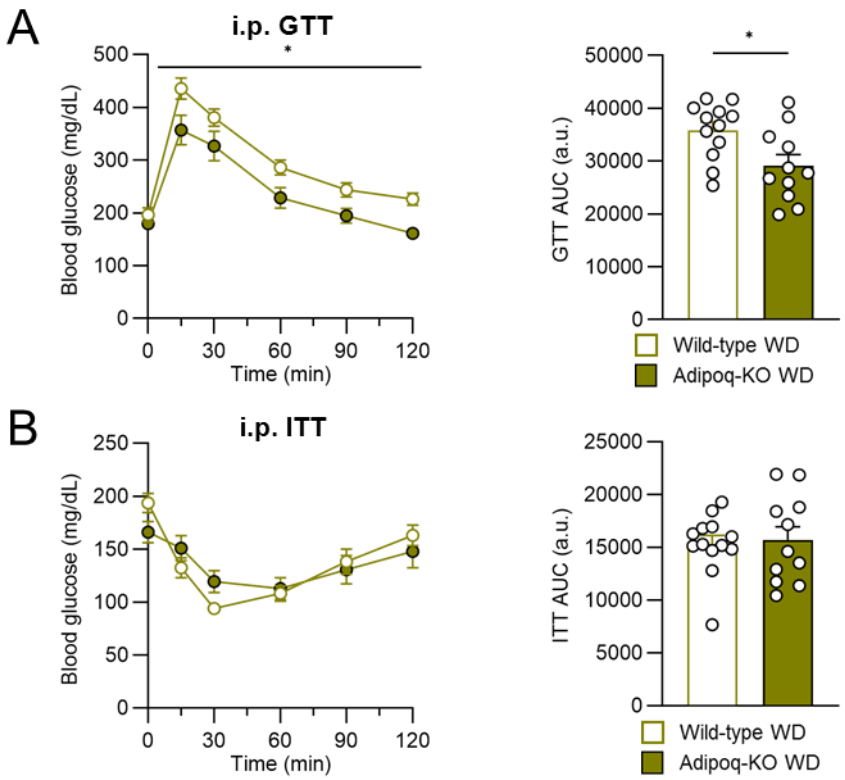

Figure 32 | Glucose and insulin tolerance of male Adipoq-Cre Nfe2l1$^{fl/fl}$ mice on WD.
A i.p. GTT and **B** i.p. ITT of male wild-type and Adipoq-KO mice after 10 weeks of WD. Throughout data are mean + s.e.m., n=11-12, * p<0.05 by Student's t test of AUC (**A**).

Further analysis assessed plasma parameters, including plasma lipids, adipokine and insulin secretion to evaluate adipocyte functions and systemic metabolism. Plasma cholesterol level were lower in Adipoq-KO mice whereas triglyceride levels were similar between wild-type and Adipoq-KO mice (Figure 33A,B). However, similarly to male Adipoq-KO mice on DIO as well as ApoE$^{-/-}$ Adipoq-KO mice on WD, Adipoq-KO mice on WD had markedly lower adiponectin and leptin plasma levels (Figure 33C,D). Insulin plasma levels, however, were similar between the Adipoq-KO and wild-type littermates (Figure 33E).

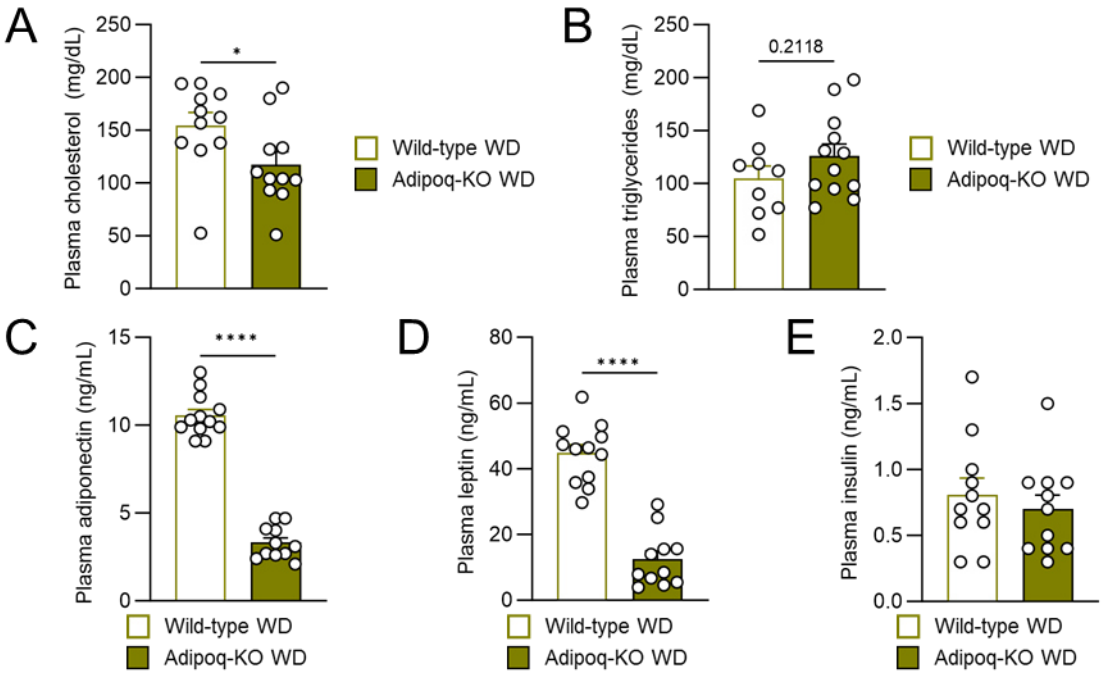

Figure 33 | Plasma parameter of male Adipoq-Cre Nfe2l1$^{fl/fl}$ mice on WD.

A Cholesterol, **B** triglyceride, **C** adiponectin, **D** leptin and **E** insulin plasma concentration of male wild-type and Adipoq-KO mice after 12 weeks of WD. Throughout data are mean + s.e.m. n=11-12. * p<0.05, **** p<0.0001 by Student's t test.

To investigate the underlying reasons for the differences in body weight, I analyzed energy metabolism by indirect calorimetry at the beginning of the WD intervention in week 1 ("pre-diet") as well as at the end in week 12. In week 1, Adipoq-KO animals exhibited lower total VO_2 in both light and dark phase. Moreover, in line with the DIO study and the ApoE$^{-/-}$ Adipoq-KO females, Adipoq-KO males on WD failed to respond to β_3-adrenergic stimulation with CL (Figure 34A). Indeed, when corrected for body weight Adipoq-KO mice had significantly lower energy expenditure in light and dark phase (Figure 34B,C). CL-stimulated BAT energy expenditure was higher in wild-type mice compared to Adipoq-KO mice (Figure 34D).

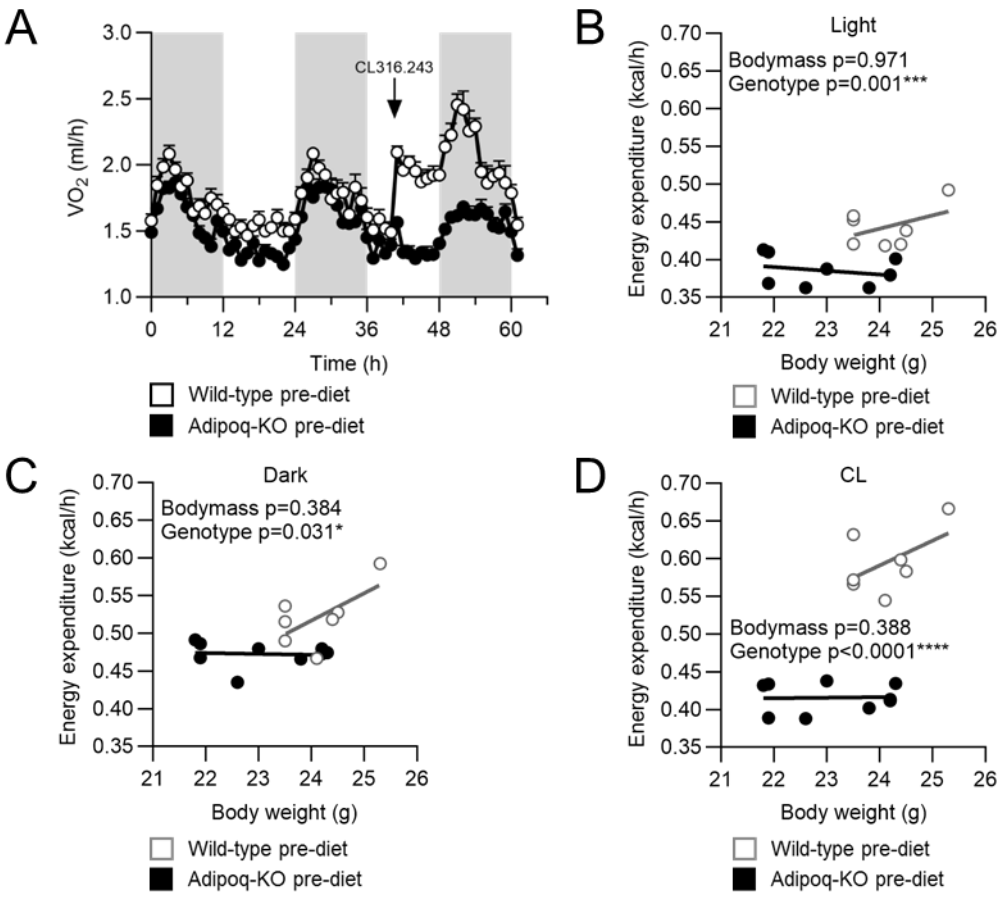

Figure 34 | Energy expenditure of male Adipoq-Cre Nfe2l1$^{fl/fl}$ mice before WD.
A VO_2, **B** light phase, **C** dark phase and **D** CL316,243 (CL)-stimulated whole-body energy expenditure of male wild-type and Adipoq-KO mice before being put on WD. **A** Data are mean + s.e.m., **B-D** data are mean, n=7-8, * p<0.05, *** p<0.001, **** p<0.0001 by ANCOVA.

After 12 weeks of WD, the differences in total VO_2 became less pronounced (Figure 35A), despite considerable body weight differences (Figure 31B). However, similar to prior to the diet, Adipoq-KO mice did not exhibit an increase in VO_2 following CL injection, whereas wild-type mice showed a significant increase in VO_2 in response to CL injections (Figure 35A). There was no difference in energy expenditure in the light phase (Figure 35B). In the dark phase, Adipoq-KO mice had higher energy expenditure than wild-type littermates; however, this was only attributed to differences in body weight according to ANCOVA analysis, there was only a trend for the genotype term (p=0.123) (Figure 35C). The CL-stimulated BAT energy expenditure was higher in wild-type mice attributed to both differences in body weight and the genotype (Figure 35D).

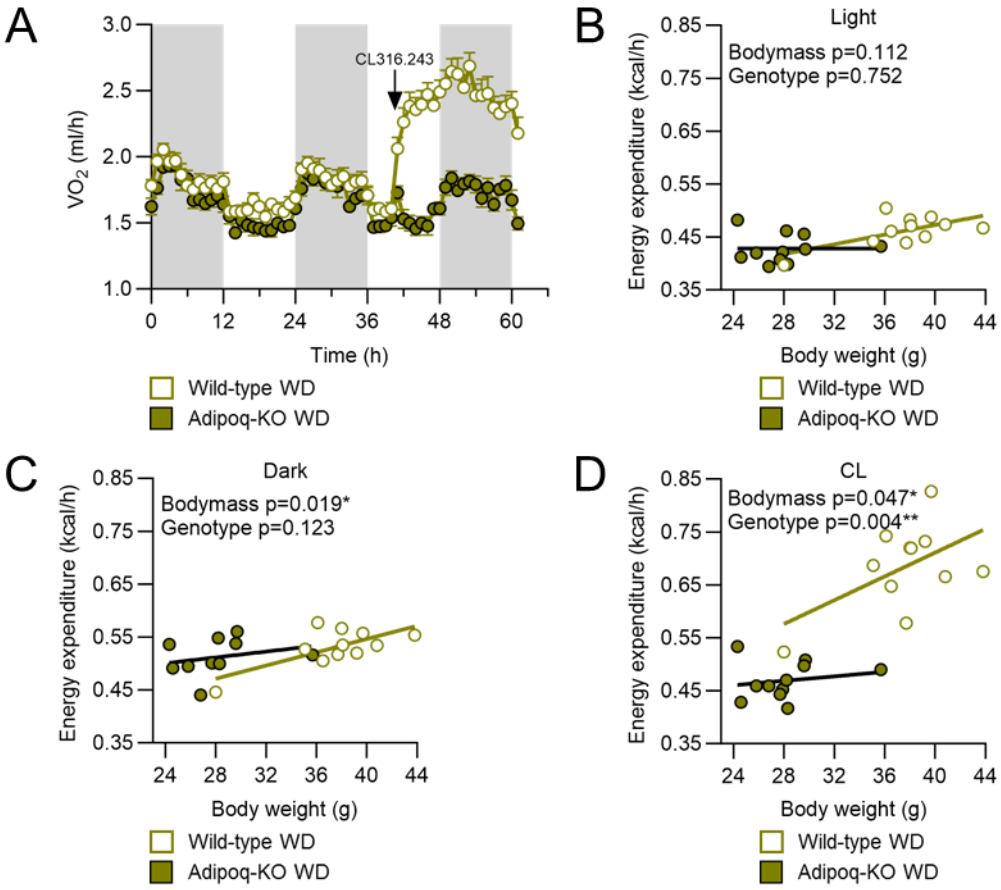

Figure 35 | Energy expenditure of male Adipoq-Cre Nfe2l1$^{fl/fl}$ mice after WD.

A VO_2, **B** light phase, **C** dark phase and **D** CL316,243 (CL)-stimulated whole-body energy expenditure of male wild-type and Adipoq-KO mice after 12 weeks of WD. **A** Data are mean + s.e.m., **B-D** data are mean, n=10-11, * p<0.05, ** p<0.01 by ANCOVA.

Since the Adipoq-KO mice displayed lower energy expenditure in week 1 of the WD intervention, I analyzed food consumption and physical activity, to see whether higher activity or lower food intake could be responsible for the lower body weight. The RER was higher in the wild-type mice both light and dark phase compared to Adipoq-KO mice. RER ranged between 0.85 and 0.7, with irregular circadian oscillation in both groups. Notably, after CL injection, RER dropped to approximately 0.67 and rose to almost 0.8 after 12 hours in both groups (Figure 36A). However, there were no differences in food intake, pedestrian locomotion or locomotor activity (Figure 36B-D).

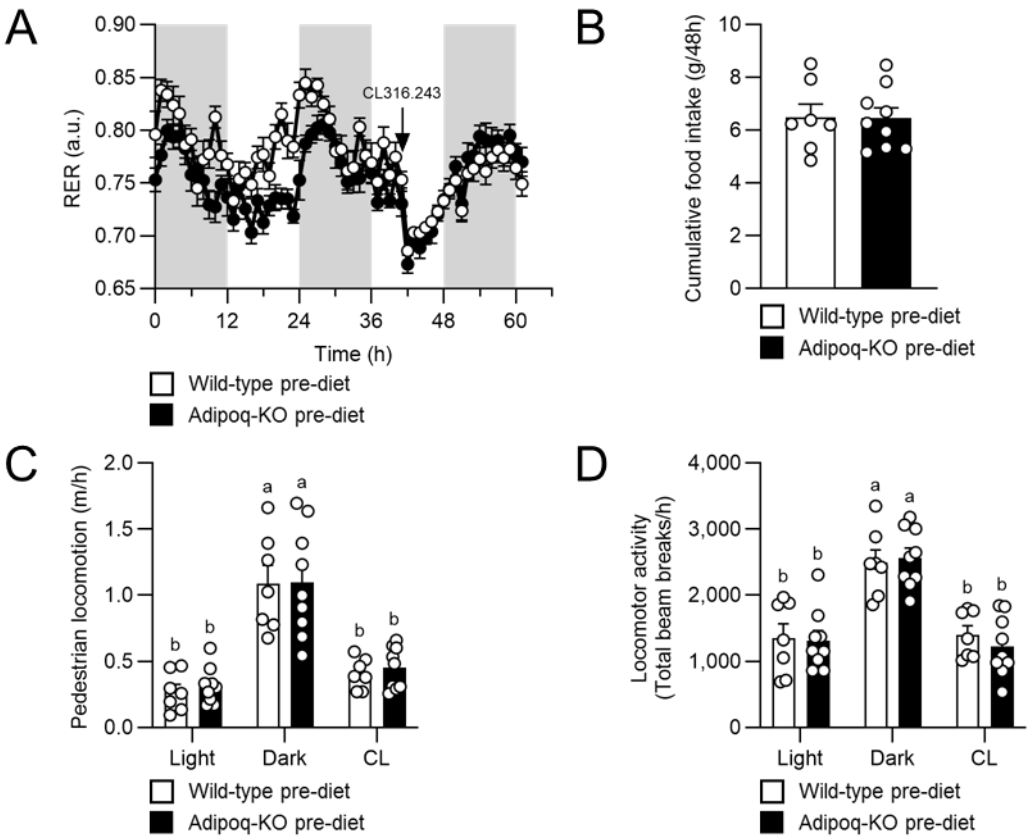

Figure 36 │ Food utilization and activity of male Adipoq-Cre Nfe2l1$^{fl/fl}$ mice before WD.

A RER, **B** cumulative food intake (average over 48h), **C** pedestrian locomotion **D** and locomotor activity of male wild-type and Adipoq-KO mice before being put on WD. Throughout data are mean + s.e.m., n=7-8**,** distinct letters indicate significant differences (p_{adj}<0.05) between groups tested by two-way ANOVA with Tukey post-hoc test (**C,D**).

After 12 weeks of WD, RER ranged between approx. 0.83 in the light phase and 0.75 in the dark phase, similar in both wild-type and Adipoq-KO mice. While both groups dropped below 0.7 in RER after CL injection, RER only rebounded to 0.77 in wild-types, but not in Adipoq-KO mice (Figure 37A). Additionally, there was a tendency for higher food intake (p=0.0543) in Adipoq-KO mice (Figure 37B) but only mild differences in activity. Adipoq-KO mice exhibited higher pedestrian locomotion in the CL phase and higher locomotor activity in the dark phase. In all other phases, measures of activity were comparable between wild-type and Adipoq-KO mice (Figure 37C,D).

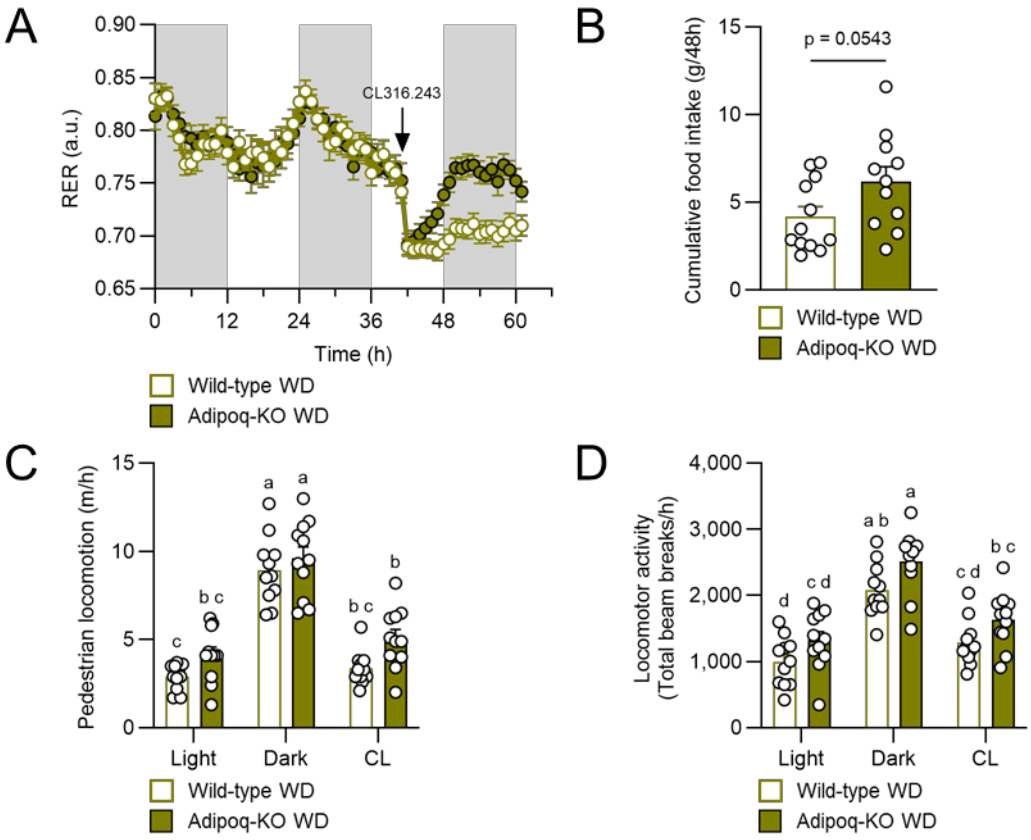

Figure 37 | Food utilization and activity of male Adipoq-Cre Nfe2l1$^{fl/fl}$ mice after WD

A RER, **B** cumulative food intake (average over 48h), **C** pedestrian locomotion **D** and locomotor activity of male wild-type and Adipoq-KO mice after 12 weeks of WD. Throughout data are mean + s.e.m., n=7-8**.** * p<0.05 by Student's t test (**B**), distinct letters indicate significant differences (p_{adj}<0.05) between groups tested by two-way ANOVA with Tukey post-hoc test (**C,D**).

In addressing the fundamental question of the lipoatrophy, my investigation also aimed to identify the adipocyte type primarily responsible for the observed outcome. Considering that Adipoq-Cre targets all three types of adipocytes (i.e. white, brown, and beige), I extended my study to include Ucp1-Cre Nfe2l1$^{fl/fl}$ mice, in which Nfe2l1 is selectively ablated in thermogenic brown and beige adipocytes. As for the Adipoq-Cre Nfe2l1$^{fl/fl}$ mice, I subjected 8-week-old male Ucp1-Cre Nfe2l1$^{fl/fl}$ mice to WD for 12 weeks. No significant differences in body weight were observed (Figure 38A). Tissue weights of iBAT, SCAT and liver showed no distinctions between the two groups, only GWAT was slightly smaller and lighter in Ucp1-KO mice (Figure 38B). Thus, the lipoatrophy is likely a consequence of Nfe2l1 ablation specifically in white adipocytes.

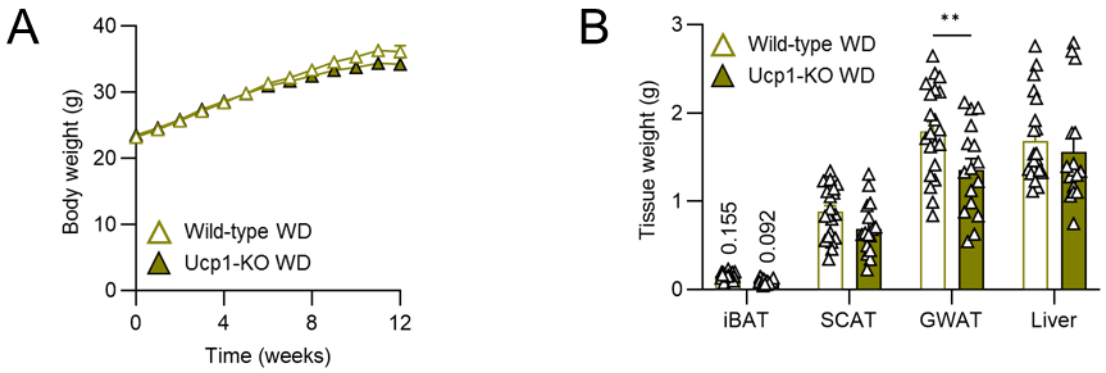

Figure 38 | Body and tissue weights of male Ucp1-Cre Nfe2l1$^{fl/fl}$ mice on WD.

A Body weight curve and **B** tissue weights of male wild-type and Ucp1-KO mice after 12 weeks of WD. Throughout data are mean + s.e.m. n=16-21. ** p<0.01 by Student's t test.

Finally, the remaining question pertained to the dietary component in the WD responsible for lipoatrophy and lower body weight in male Adipoq-KO mice. I hypothesized that Nfe2l1 might interact with the dietary cholesterol, given previous findings that Nfe2l1 regulates cholesterol homeostasis in the liver. In the absence of hepatocyte Nfe2l1, livers accumulated cholesterol, which led to inflammation and liver disease [110]. Moreover, in DIO I did not observe difference in body weight between male wild-type and Adipoq-KO mice, despite lower WAT mass. Thus, it is rather unlikely that other dietary lipid species were responsible for the observed phenotype on WD.

To eliminate the possibility that these effects were solely attributed to lower metabolizable energy in the WD (19.1 versus 21.6 MJ/kg in DIO), I supplemented DIO with an equivalent amount of cholesterol (DIO+Chol) and fed male mice for 16 weeks, comparing them with littermates on regular DIO (Figure 39A). No significant differences in body weight were observed between genotypes or diet groups (Figure 39B). Tissue weights of iBAT and liver remained similar across all groups, while SCAT and GWAT weights were consistently lighter in the Adipoq-KO groups, irrespective of dietary cholesterol supplementation (Figure 39C).

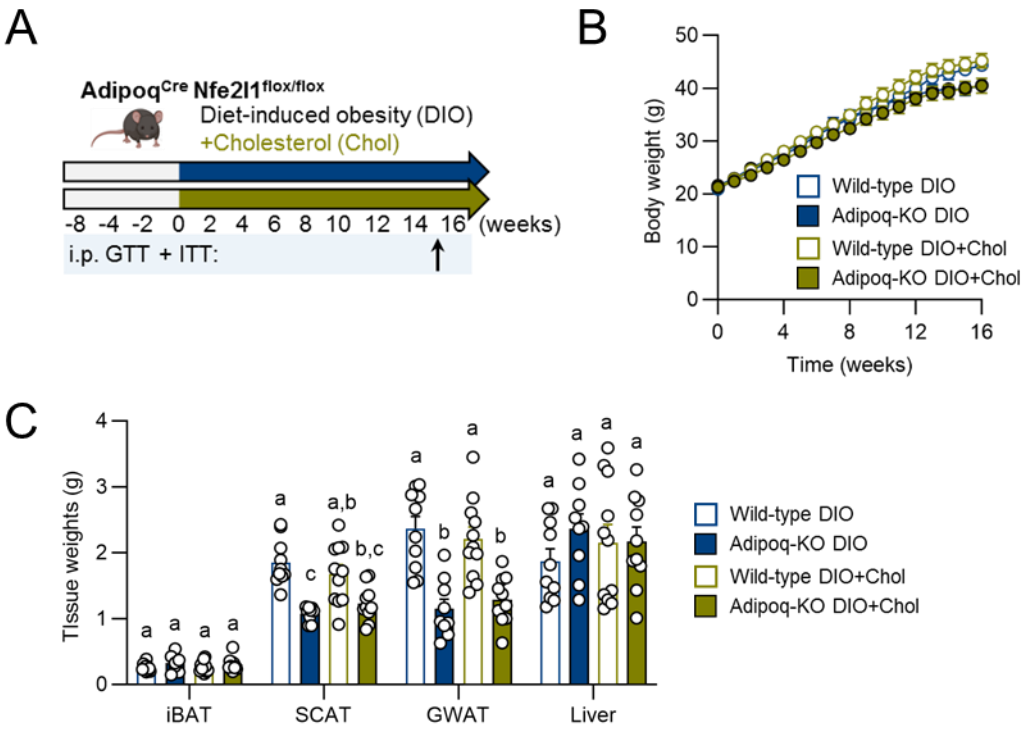

Figure 39 | Body and tissue weights of male Adipoq-Cre Nfe2l1$^{fl/fl}$ mice on DIO supplemented with cholesterol.

A Study design (60%kcal fat ± 0.21% cholesterol (Chol), 16 weeks), i.p. GTT and ITT at 15 weeks, **B** body weight curve, **C** tissue weights of male wild-type and Adipoq-KO mice after 16 weeks on DIO with or without Chol. **B,C** Data are mean + s.e.m., n=9-12, distinct letters indicate significant differences (p_{adj}<0.05) between groups tested by one-way ANOVA with Tukey post-hoc test.

Since Adipoq-KO mice on DIO were more insulin-resistant than wild-type littermates in previous studies, I tested if Adipoq-KO mice on DIO+Chol would be equally insulin resistance. However, there was no difference in glucose tolerance in the i.p. GTT for any of the groups (Figure 40A). Moreover, in the i.p. ITT, Adipoq-KO mice on DIO were most-insulin resistant, but this was not significantly different from wild-type mice on DIO. Only wild-type mice on DIO+Chol were significantly less insulin-resistant than Adipoq-KO mice on DIO (Figure 40B).

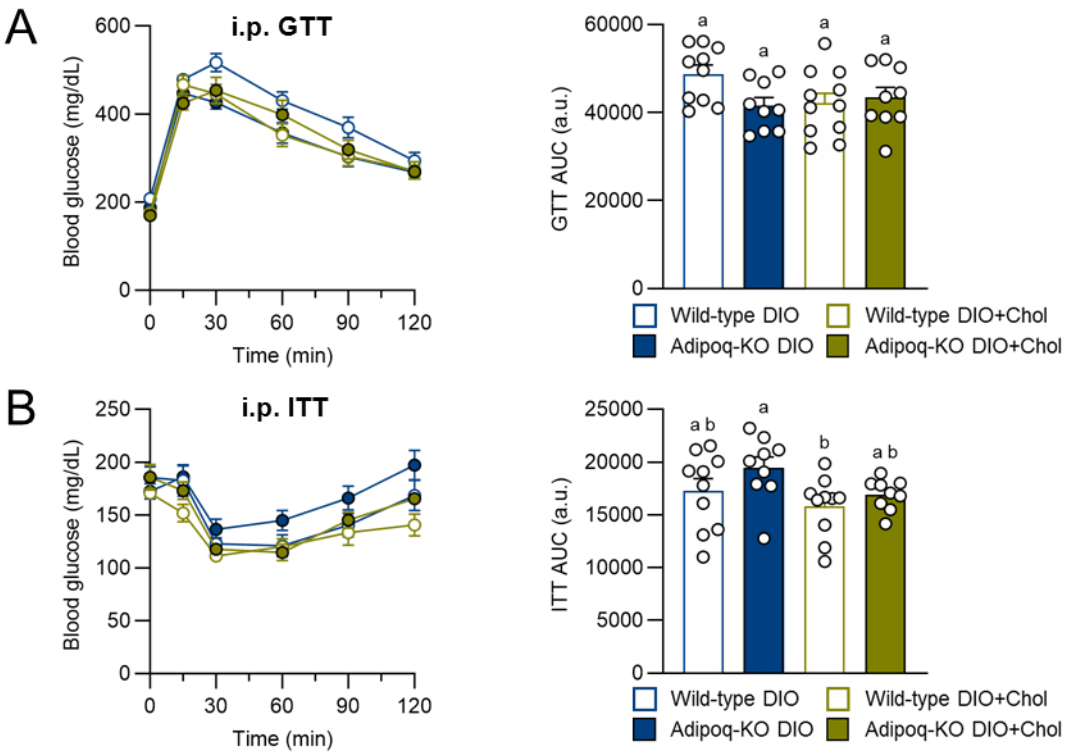

Figure 40 | Glucose and insulin tolerance of male Adipoq-Cre Nfe2l1$^{fl/fl}$ mice on DIO supplemented with cholesterol.

A i.p. GTT and **B** i.p. ITT of male wild-type and Adipoq-KO mice after 15 weeks on DIO with or without Chol. Throughout data are mean + s.e.m., n=9-12, distinct letters indicate significant differences (p_{adj}<0.05) between groups tested by one-way ANOVA with Tukey post-hoc test.

To investigate the impact of the cholesterol supplementation on lipid metabolism and adipocyte health, I also evaluated plasma parameter. Plasma cholesterol and triglycerides showed no significant differences among the four groups (Figure 41A,B). Plasma leptin and adiponectin levels were lower in Adipoq-KO mice, but this was independent of the cholesterol supplementation (Figure 41C,D). Insulin plasma levels were similar between the groups (Figure 41E).

In conclusion, the observed lipoatrophy and body weight disparity in male Adipoq-KO mice is independent of the ApoE$^{-/-}$ background, specific to white adipocytes, and manifests solely under the influence of an atherogenic WD, but not during DIO. However, the precise origin of the phenotype in terms of energy metabolism remains vague.

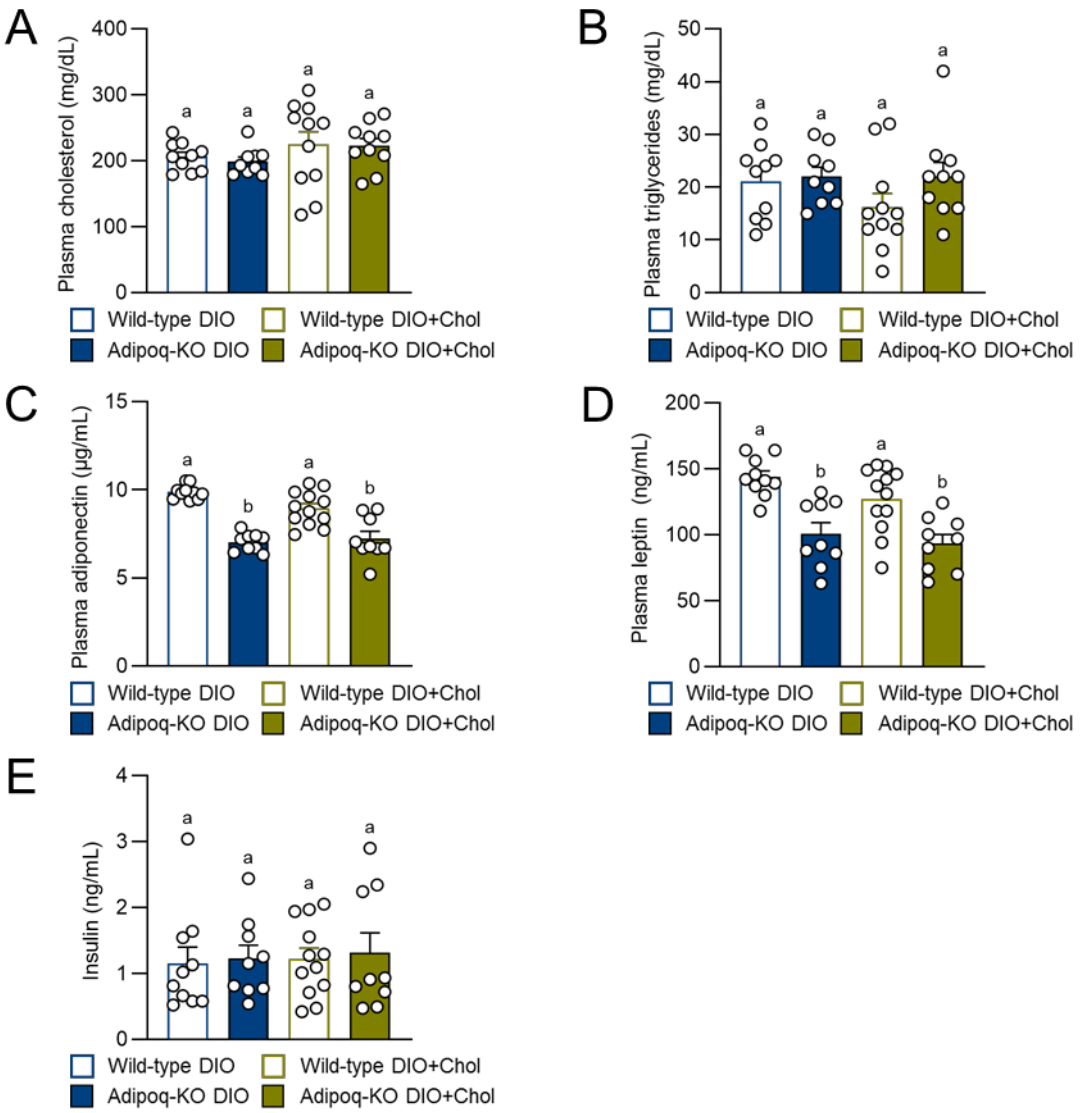

Figure 41 | Plasma parameter of male Adipoq-Cre Nfe2l1$^{fl/fl}$ mice on DIO supplemented with cholesterol.

A Cholesterol, **B**, triglyceride, **C** adiponectin, **D** leptin and **E** insulin plasma concentration of male wild-type and Adipoq-KO mice after 16 weeks on DIO with or without Chol. Throughout data are mean + s.e.m., n=9-12, distinct letters indicate significant differences (p_{adj}<0.05) between groups tested by one-way ANOVA with Tukey post-hoc test.

4.3 Overview of adipocyte Nfe2l1 phenotypes *in vivo*

The following table summarizes all phenotypes observed in mouse models in this study as well as additional studies performed in our lab (Supplementary Figure 3,4).

Table 6 | Overview of Nfe2l1 KO phenotypes in mice
Changes indicated in comparison to wild-type littermates. * study performed by Alexander Bartelt (LMU), m: male, f: female, n.a.: not available

Genotype	Gender	Diet	Body weight	SCAT weight	GWAT weight	Liver weight	Adipo-nectin	Leptin	Insulin resist.	Athero-sclerosis
Adipoq-Cre$^{wt/tg}$ Nfe2l1$^{fl/fl}$	*m	*chow	↔	↓	↔	↔	↓↓	↔	↔	n.a.
	f	chow	↔	↓	↑	↑	n.a.	n.a.	↑	n.a.
	m	DIO	↔	↓	↓	↑	↓	↓	↑	n.a.
	m	WD	↓	↓↓	↓↓	↔	↓↓	↓↓	↔	n.a.
	m	DIO + Chol	↔	↓	↓	↔	↓	↓	↔	n.a.
ApoE$^{-/-}$ Adipoq-Cre$^{wt/tg}$ Nfe2l1$^{fl/fl}$	f	Chow	↔	↓	↔	↑↑	↓↓	↔	↑	↔
	f	WD	↔	↓↓	↓↓	↑↑	↓↓	↓↓	↑	↑
	m	WD	↓	↓↓	↓↓	↔	↓↓	↓↓	n.a.	↔
Ucp1-Cre$^{wt/tg}$ Nfe2l1$^{fl/fl}$	m	WD	↔	↔	↓	↔	n.a.	n.a.	↔	n.a.

4.4 Cellular mechanisms of adipocyte Nfe2l1

Nfe2l1 is widely recognized for its pivotal role in coordinating adaptive proteostasis, primarily through the regulation of proteasome subunit genes in response to proteasome inhibition or overload, as outlined in the introduction. In brown adipocytes, this function becomes particularly crucial during cellular adaptation to cold exposure, facilitating non-shivering thermogenesis[112]. Additionally, in the liver, Nfe2l1 has been identified to interact with LXRα, contributing to the regulation of cholesterol homeostasis and inflammation[99,110]. Nevertheless, the specific role of Nfe2l1 in white adipocytes and its cellular mechanisms remain elusive. Thus, this study aimed to decipher cellular mechanisms of Nfe2l1 that link it to cholesterol homeostasis in white adipocytes.

4.4.1 Characterizing the inflammatory phenotype in Nfe2l1-KO adipose tissue

To investigate the cellular mechanisms governed by Nfe2l1, I first verified the model by analyzing tissues from Adipoq-Cre Nfe2l1$^{fl/fl}$ knock-out and wild-type mice. Notably, Cre-mediated recombination exclusively occurred in BAT, SCAT, and GWAT, sparing non-adipose tissue (Figure 42A). In the SCAT and GWAT, knockout of Nfe2l1 resulted in robustly lower *Nfe2l1* mRNA expression (0.5-fold and 0.3-fold, respectively) (Figure 42B,C). Loss of Nfe2l1 has been linked to ER stress and inflammation in other organs[109,110,112]. Thus, I also included marker genes of inflammation and stress response in my analysis to investigate if this was also the case in WAT. There was 11-fold higher expression of the inflammatory marker gene *Ccl2*, encoding MCP1, and a 1.5-fold induction of *Cd68,* encoding for a surface marker gene expressed on monocytes and tissue macrophages. In GWAT, however, *Ccl2* was 5.3-fold induced and *Cd68* expression was unchanged. Most prominently, there was a 25-fold induction of stress marker gene *Atf3* in SCAT and a 4.5-fold induction in GWAT. Other members of the Atf family, *Atf4* and *Atf6*, which belong to the unfolded protein response pathway, were only mildly higher in SCAT (2.2-fold and 1.3-fold, respectively) and unchanged in GWAT. Moreover, there was also higher expression of the apoptotic marker *Ddit3* in both SCAT (2.4-fold) and GWAT (2-fold) (Figure 42B,C). In summary, the recombination in the target tissues was successful, leading to a substantially lower in Nfe2l1 gene expression in both SCAT and GWAT, with effects on inflammation and stress marker gene expression.

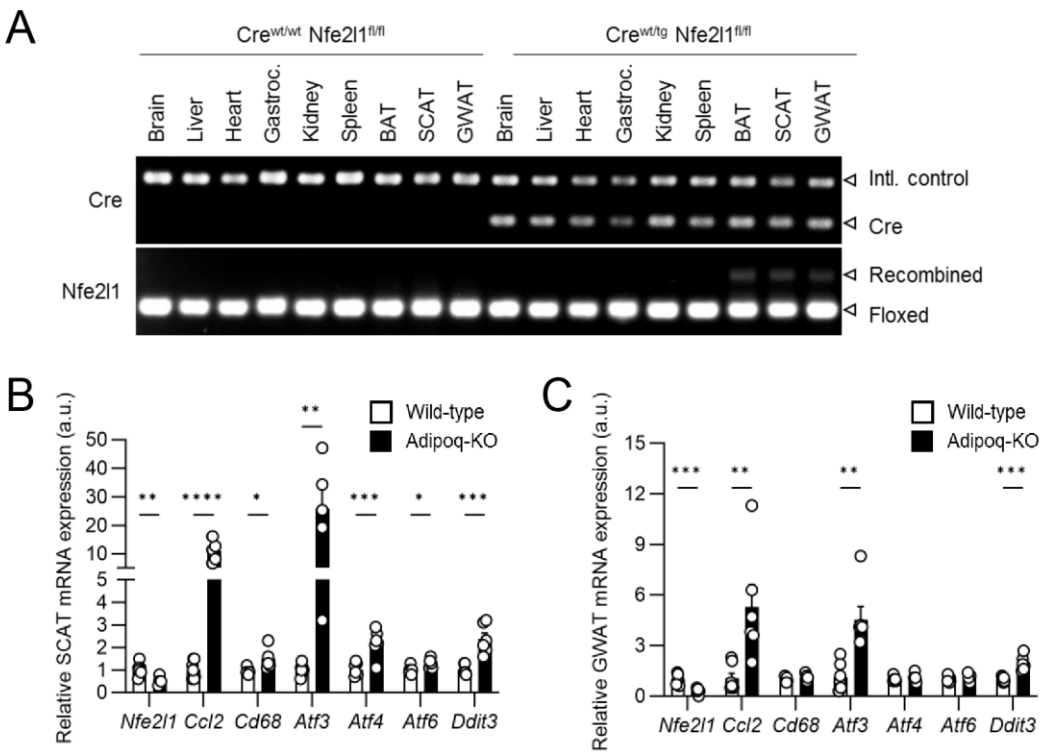

Figure 42 | Validation of the Adipoq-Cre Nfe2l1$^{fl/fl}$ model.

A Adipose tissue-specific Cre-mediated recombination of Nfe2l1, **B** relative mRNA expression of inflammation and stress associated genes in SCAT and **C** in GWAT. **B,C** qPCR measured by Janina Caesar (LMU Munich), analyzed by CJ**. B,C** Data are mean + s.e.m, n=5-7. * p<0.05, ** p<0.01, *** p<0.001, **** p<0.0001 tested by Student's t test. Gastroc.: *Musculus Gastrocnemius*.

Chronic low-grade inflammation of the adipose tissue is a hallmark of adipocyte dysfunction[55], which was observed in all Adipoq-Cre Nfe2l1$^{fl/fl}$ mouse models investigated in this study. To comprehensively explore the inflammatory phenotype of the KO WAT, I performed histological analysis, RNA sequencing and flow cytometry of WAT from chow-fed Adipoq-Cre Nfe2l1$^{-/-}$ mice. Notably, I observed distinctive histological differences in Adipoq-KO SCAT and GWAT compared to wild-type tissues, characterized by adipocyte hypertrophy and the presence of numerous crown-like structures - a condition typically associated with immune cell infiltration in DIO (Figure 43A). To achieve a broader understanding of the processes initiated by loss of Nfe2l1 in the WAT, RNA sequencing analysis of SCAT from Adipoq-KO mice was performed. The most up-regulated pathways according to gene ontology (GO) analysis were all associated with immune cell activation and infiltration (Figure 43B).

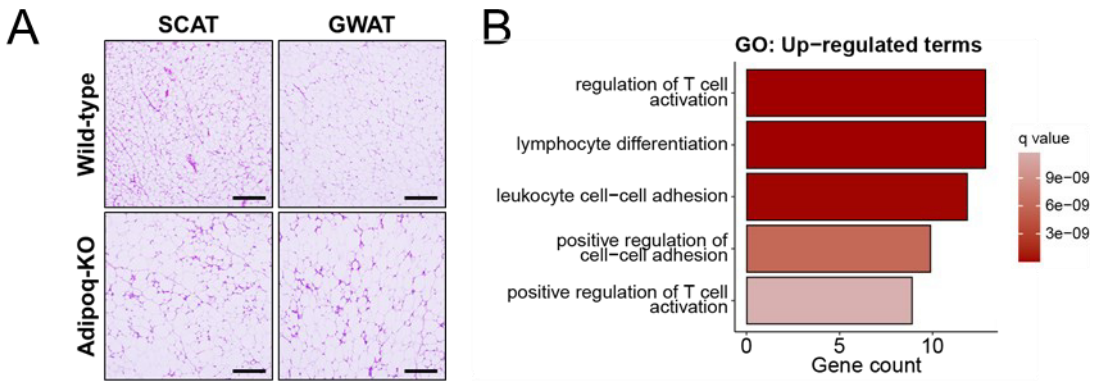

Figure 43 | Complex inflammation in Adipoq-KO WAT.

A Representative hematoxilin-eosin staining of SCAT and GWAT (scale bar = 200 µm), **B** up-regulated GO terms in Adipoq-KO SCAT vs wild-type SCAT, **A,B** Data provided by Alexander Bartelt (LMU Munich), analyzed by CJ.

To quantitatively validate the histological findings and RNA sequencing data, I performed flow cytometry analysis on selected immune cell populations within SCAT and GWAT. Adipose tissue inflammation is characterized by an overall increase in immune cells and a shift towards a more pro-inflammatory macrophage profile. Thus, this analysis aimed to detect F4/80+ cells, indicative of macrophages and more specifically F4/80+ Cd11c+ cells, indicative of pro-inflammatory macrophages. Significantly higher numbers of F4/80+ Cd11c+ cells were observed in both SCAT and GWAT of Adipoq-KO mice compared to their wild-type littermates (Figure 44A-C). Although increases in F4/80+ Cd11c- cells were noted in the WAT of Adipoq-KO mice, these differences were not statistically significant (Figure 44A-C). Furthermore, aligning with the GO analysis results pointing towards T cell activation, the distribution of lymphocytes in GWAT was assessed. There was a notable increase in both Cd3+Cd8a+ cells, indicative of T1 cells, and Cd3+Cd4+ cells, indicative of Th1 cells, in the Adipoq-KO GWAT compared to wild-type GWAT (Figure 44D,E). Collectively, these findings confirm that the WAT of Adipoq-KO mice on a standard chow diet is marked by significant immune cell infiltration and inflammation.

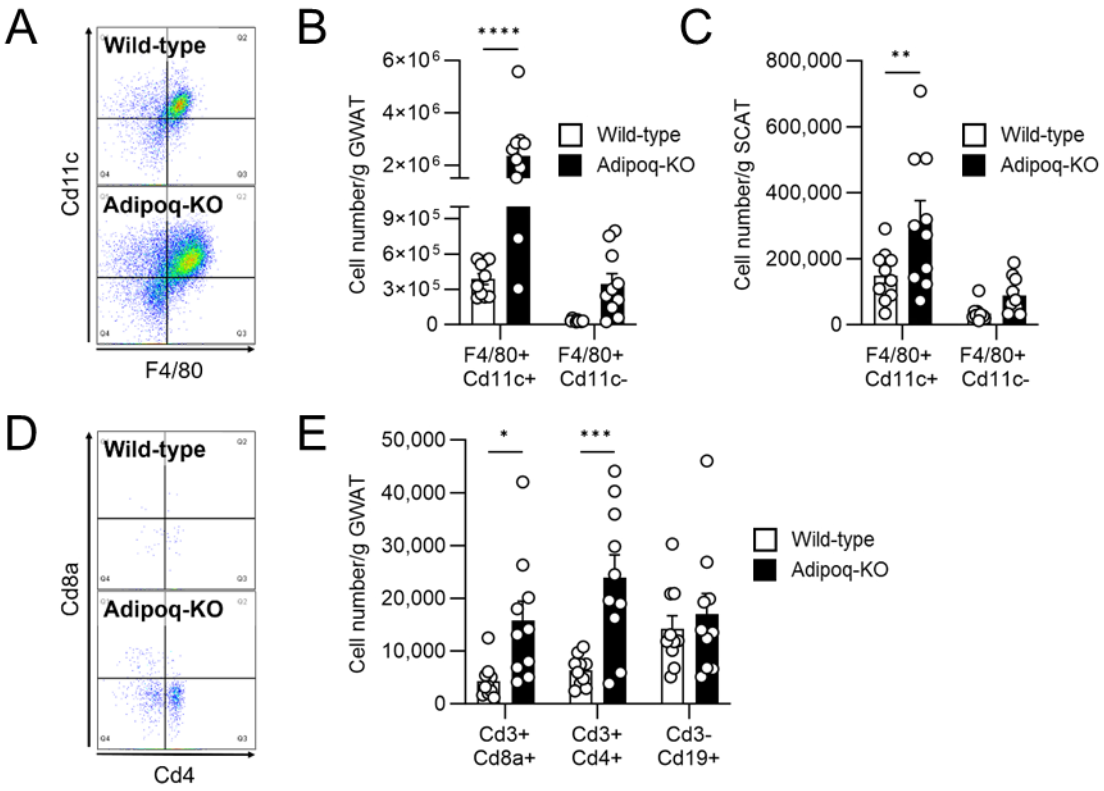

Figure 44 | Quantitative analysis of immune cell populations in Adipoq-KO WAT.

A Representative flow cytometry plot of adipose tissue SVF stained for F4/80 and Cd11c, **B** absolute cell number of F4/80+ cell in GWAT and **C** in SCAT, **D** representative flow cytometry plot of AT SVF stained for Cd4 and Cd8a, **E** absolute cell number of Cd3+ and Cd19+ cells in GWAT. **B,C,E** Data is mean + s.e.m., n=10, * p<0.05, ** p<0.01, *** p<0.001, **** p<0.001 by two-way ANOVA with Šidák post-hoc test (**B,C,E**).

To understand which mechanisms in the adipocytes promoted immune cell infiltration in the tissue, I also studied the activation of the most prominent inflammation and stress kinase signaling pathways in primary white adipocytes of Adipoq-Cre Nfe2l1$^{fl/fl}$ mice (Figure 45A). NF-κB and Jnk are major intracellular inducers of inflammatory cytokine production[55], whereas p38 coordinates cellular responses to a variety of stressors[56]. To check for activation of the UPR, I also assessed phosphorylation of eIF2α. KO adipocytes had stronger NF-κB and eIF2α phosphorylation, whereas Jnk phosphorylation was similar between KO and WT (Figure 45B). Interestingly, there was a strikingly robust p38 phosphorylation in the KO adipocytes compared to WT adipocytes (Figure 45C). Overall, loss of adipocyte Nfe2l1 promoted activation of major inflammation and stress signaling pathways.

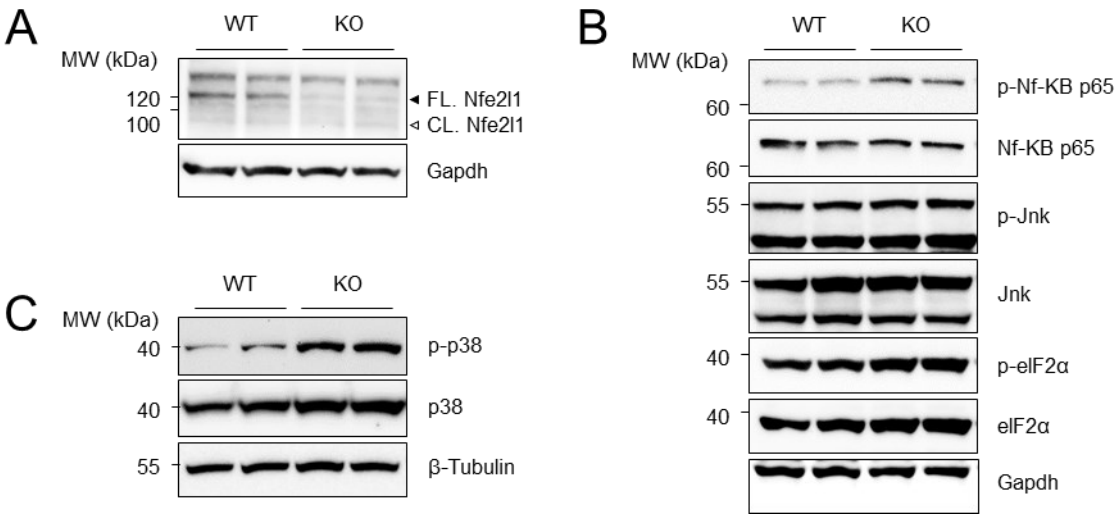

Figure 45 │ Stress kinase signaling in Nfe2l1 KO white adipocytes.

A-C immunoblots of primary white adipocytes of wild-type and Adipoq-KO Nfe2l1 mice. **A-C** n=2 (representative experiment). FL.: full-length, CL.: cleaved.

4.4.2 Analysis of intracellular Nfe2l1 mechanisms by genetic manipulation

In order to further investigate cellular mechanisms of adipocyte Nfe2l1 *in vitro*, I employed RNA interference (RNAi) to silence *Nfe2l1* in an immortalized murine white adipocyte cell line, 3T3-L1, which can be differentiated into mature white adipocytes. In addition, I also used primary white adipocytes. The siRNA-mediated knockdown in differentiated 3T3-L1 adipocytes resulted in notably lower Nfe2l1 mRNA expression (0.2-fold) (Figure 46A). However, this had no discernible impact on the baseline gene expression of downstream targets such as *proteasome subunit alpha 1* (Psma1) and *proteasome subunit beta 1* (*Psmb1*). When combined with the proteasome inhibitor epoxomicin, the knockdown of Nfe2l1 exhibited no effect on *Psma1* expression but led to lower expression of *Psmb1*. It is noteworthy that the expressions of both *Nfe2l1* and *Psma1* were already lower with epoxomicin treatment alone (Figure 46A). Epoxomicin treatment also led to more protein ubiquitination, albeit independently of Nfe2l1 (Figure 46B). The knockdown of *Nfe2l1* in 3T3-L1 adipocytes only had minimal impact on the expression of stress marker genes. In fact, the expressions of *Atf3* and *Hspa5* (encoding heat-shock protein 5 (Hsp5)) were even lower in *siNfe2l1*-treated adipocytes (Figure 46C).

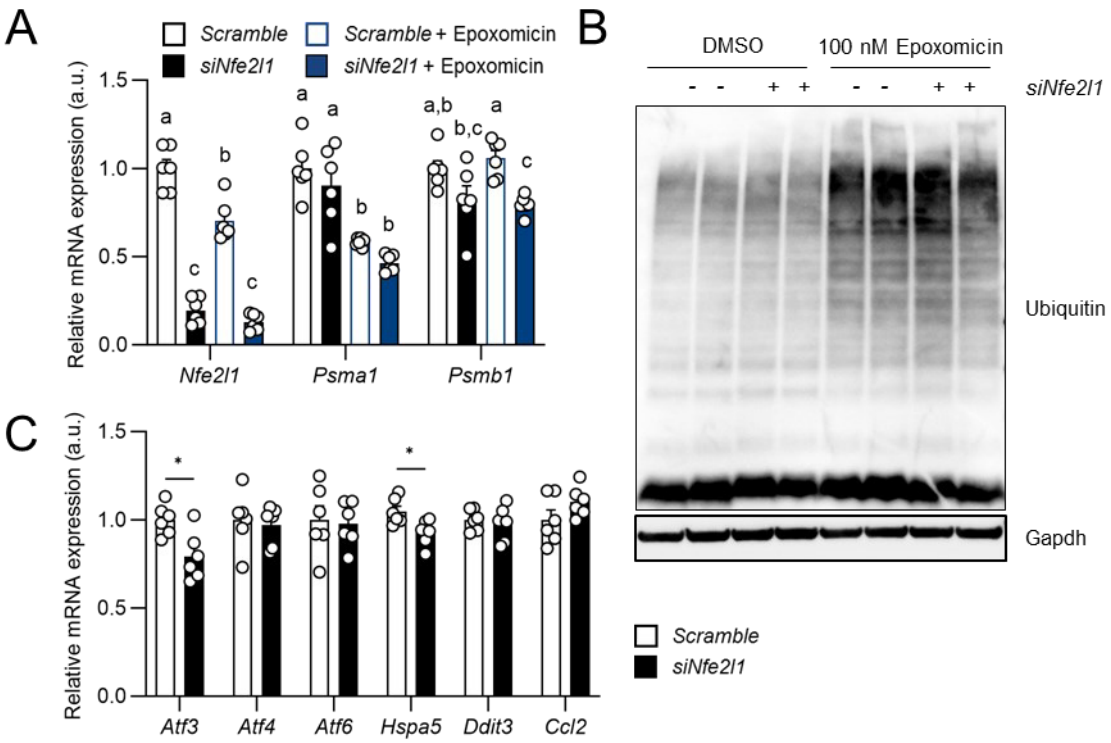

Figure 46 | RNAi-mediated knockdown of *Nfe2l1* in 3T3-L1 adipocytes.

A relative mRNA expression of *Nfe2l1* and downstream targets, **B** representative ubiquitin immunoblot and **C** relative mRNA expression of stress and inflammation associated genes in 3T3-L1 adipocytes. Data is mean + s.e.m., n=6 (from two independent experiments). Different letters indicate significant differences (p_{adj}<0.05) between groups tested by one-way ANOVA (**A**). * p<0.05, *** p<0.001, **** p<0.001 by Student's t test (**C**).

To rule out artificial effects of the immortalized cell line and to have a more physiological cell model, I also used primary white adipocytes from the SCAT and GWAT of 8-week-old wild-type mice. In addition, here *Nfe2l1* could successfully be silenced via siRNA-mediated knockdown (0.2-fold and 0.3-fold, respectively). However, similar to the findings in 3T3-L1 cells, the knockdown had little effect on the expression of *Ccl2* and *Atf3*, with only a mild induction of *Ccl2* observed in primary white adipocytes from SCAT (Figure 47A,B). Overall, despite successful silencing of *Nfe2l1* on the transcriptional level, this did not have an effect on the evaluated target genes or cause inflammation and stress in the cells.

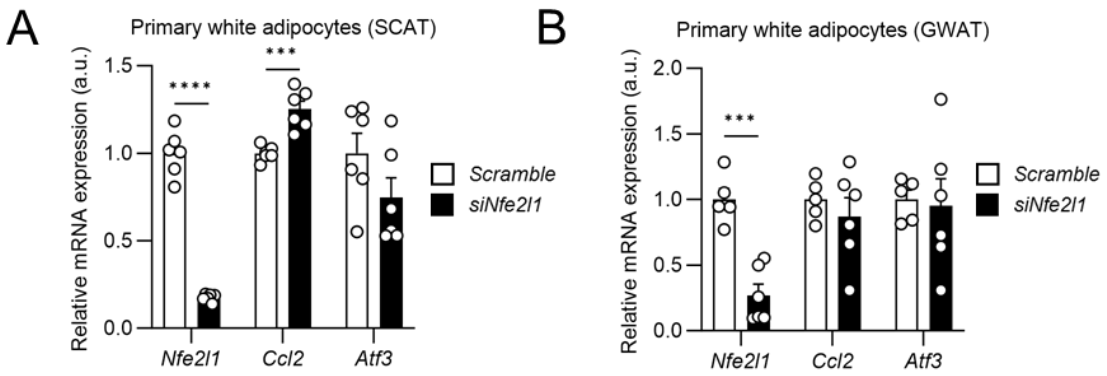

Figure 47 | RNAi-mediated knockdown of *Nfe2l1* in primary white adipocytes.
A Relative mRNA expression in primary white adipocytes from SCAT and **B** GWAT. Data is mean + s.e.m., n=6 (from two independent experiments). *** p<0.001, **** p<0.001 by Student's t test.

Since knockdown of *Nfe2l1* had minimal impact on the expression of its target genes and stress marker genes, I pursued an alternative approach to model the phenotype observed in the adipose tissue of the Adipoq-KO mice. Based on the protocol by Widenmaier et al.[110], I subjected 3T3-L1 adipocytes to cholesterol and epoxomicin treatment to induce cholesterol overload of the endoplasmic reticulum (ER) membrane and proteasome inhibition (Figure 48A). This is presumed to result in the retention of Nfe2l1 in the ER membrane, impeding its function as a transcription factor for proteasome subunit genes, consequently leading to ER stress[110]. Initially, I assessed the cellular toxicity of the cholesterol treatment. Cholesterol concentrations below 200 µM exhibited no effect on viability, while concentrations ranging from 400 µM to 1 mM led to a 20 % to 30 % decrease in viability (Figure 48B). The successful loading of cholesterol was confirmed by lower expression of Srebf2 target genes, namely *3-hydroxy-3- Hmgcr* and *Ldlr* (Figure 48C).

Next, I explored the impact of cholesterol and epoxomicin treatment on Nfe2l1 protein levels and cleavage. In 3T3-L1 pre-adipocytes, increasing cholesterol concentrations resulted in lower expression of full-length (FL.) Nfe2l1. However, this observation was not made in mature adipocytes, where Nfe2l1 protein levels remained unaffected by cholesterol. Notably, epoxomicin, employed as a positive control for Nfe2l1 activation, induced a robust level of the cleaved (CL.) transcriptionally active form of Nfe2l1, specifically in mature adipocytes (Figure 48D). In mature adipocytes treated with varying cholesterol concentrations in combination with epoxomicin, FL. Nfe2l1 decreased in a cholesterol-concentration dependent manner, while CL. Nfe2l1 remained unchanged (Figure 48E).

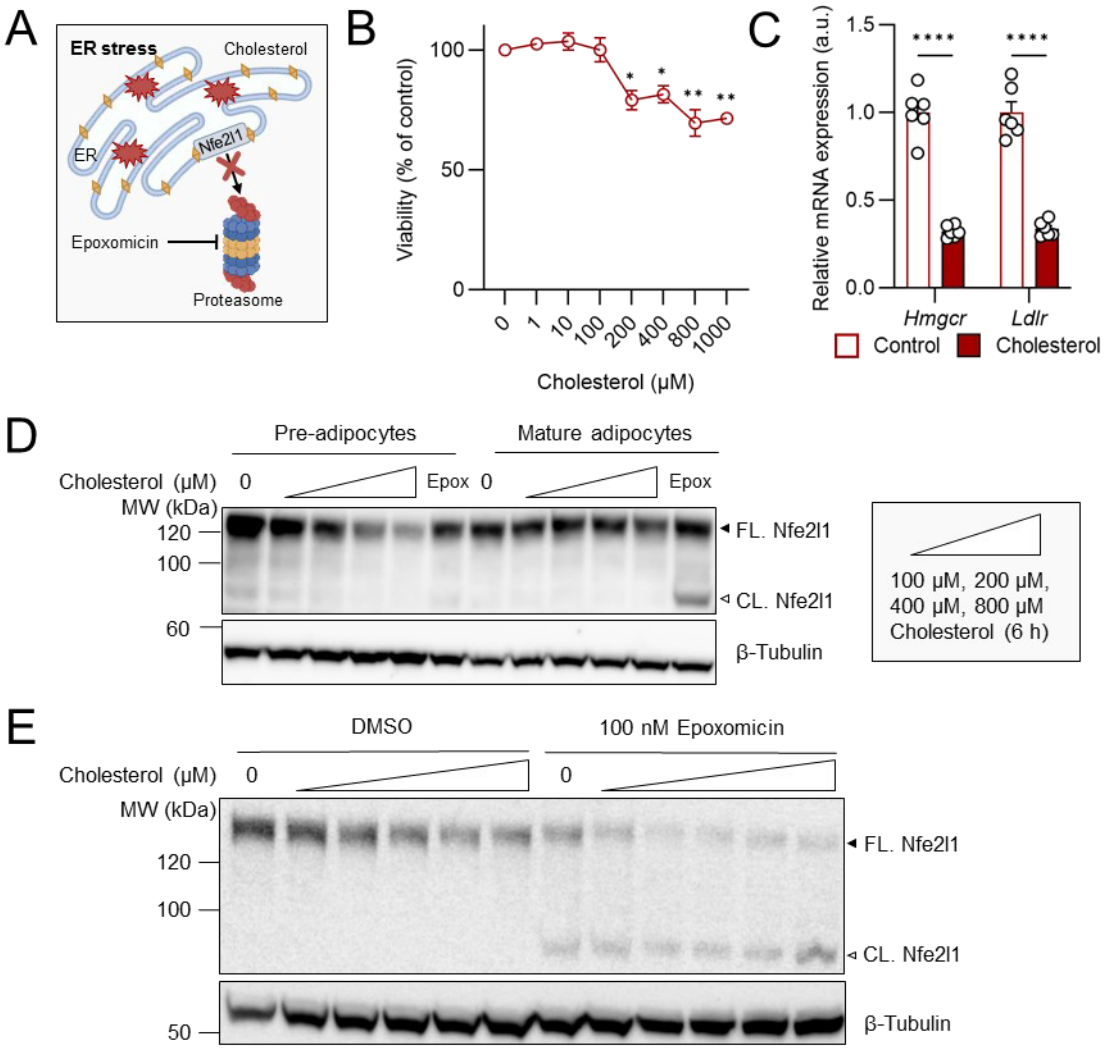

Figure 48 | Effect of cholesterol treatment on 3T3-L1 adipocytes.

A Effect of combined cholesterol and epoxomicin treatment[110], **B** viability in response to 24 h treatment with increasing concentrations of cholesterol, **C** mRNA expression of Srebp-2 target genes in differentiated 3T3-L1 treated with 400 µM cholesterol for 6 h, **D** representative immunoblot of 3T3-L1 pre-adipocytes and differentiated 3T3-L1 and **E** differentiated 3T3-L1 adipocytes treated with increasing concentrations of cholesterol or 100 nM epoxomicin or the combination of both for 6 h. **B,C** Data is mean + s.e.m., n=6 (from two independent experiments), * p_{adj}<0.05, ** p_{adj}<0.01 by one-way ANOVA with Dunnett's post hoc test vs. 0 µM/DMSO (**B**) and **** p<0.001 by Student's t test (**C**). FL.: full length, CL.: cleaved.

On gene expression level, the treatment of 3T3-L1 adipocytes with cholesterol and epoxomicin led to a significant induction of *Atf3*, *Ccl2*, and *Cxcl10*. Interestingly, while cholesterol alone induced the expression of inflammation marker genes, epoxomicin treatment had a more pronounced effect on *Atf3* and *Ccl2* induction. However, the combined treatment of cholesterol and epoxomicin resulted in an exponential induction of *Atf3*, *Ccl2*, and *Cxcl10*, suggesting a synergistic interaction between cholesterol and epoxomicin. Notably, canonical ER stress marker genes such as *Hspa5*, *Ddit3*, and spliced *Xbp1* (*sXbp1*) were unaffected by the treatment, except for cells treated with cholesterol, which

exhibited higher *sXbp1* levels. Similarly to the gene expression pattern observed in the adipose tissue, *Atf4* and *Atf6* remained largely unaltered (Figure 49A). Given the substantial induction of *Atf3*, I hypothesized that it could play a role in mediating the inflammatory response. To test this hypothesis, I also silenced *Atf3* using siRNA-mediated knockdown (Figure 49B). Indeed, knockdown of *Atf3* resulted in markedly lower *Ccl2* gene expression in both cholesterol and epoxomicin-treated adipocytes and epoxomicin-only treated adipocytes compared to *Scramble* (Figure 49C). However, knockdown of *Nfe2l1* had no effect on *Atf3* or *Ccl2* gene expression, even in combination with the different treatment regiments. Furthermore, the combination of *siNfe2l1* and *siAtf3* did not offset the effect of *Atf3* knockdown (Figure 49B,C).

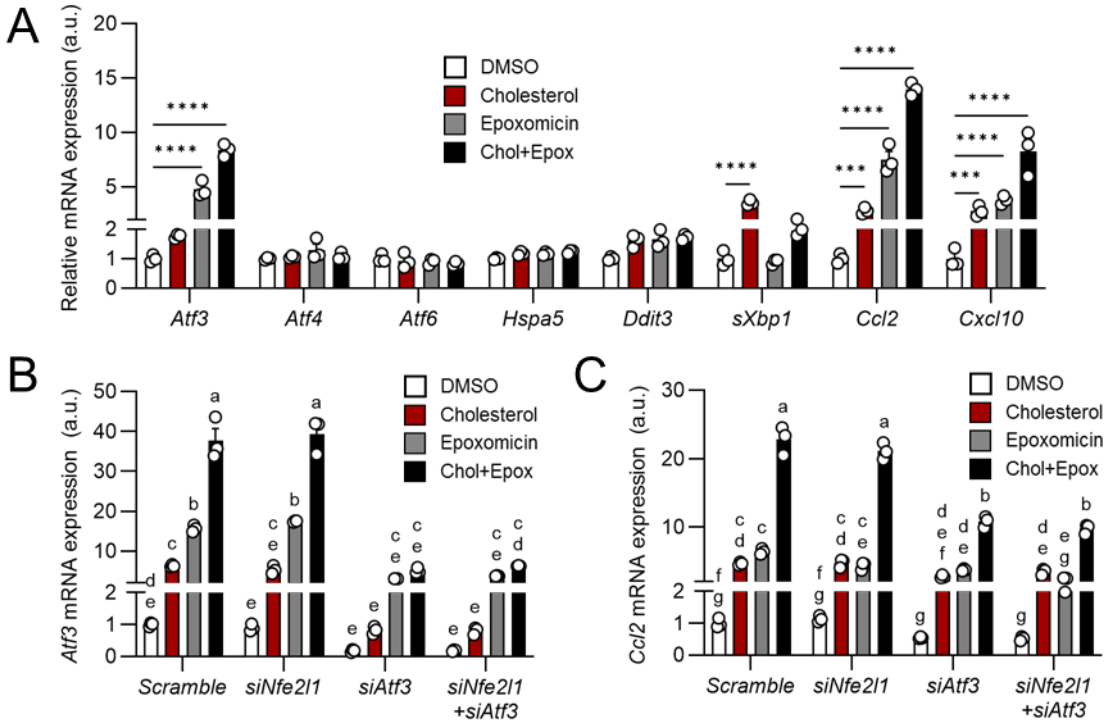

Figure 49 | Cholesterol treatment partially phenocopies loss of Nfe2l1 *in vitro*.

A Relative mRNA expression of stress and inflammation associated genes in 3T3-L1 adipocytes, **B** relative *Atf3* mRNA expression and **C** relative *Ccl2* mRNA expression in mature 3T3-L1 adipocytes. Cells where treated with 400 µM cholesterol, 100 nM epoxomicin or the combination of both for 6 h. Throughout data is mean + s.e.m., n=3 from representative experiment. ***p_{adj}<0.001, **** p<0.001 by one-way ANOVA with Dunnett's post hoc test vs. 0 µM/DMSO (**A**), different letters indicate significant differences (p_{adj}<0.05) between groups tested by two-way ANOVA with Tukey post-hoc test (**B,C**). Chol: cholesterol, Epox: epoxomicin.

In summary, these data suggest that cholesterol treatment partially phenocopies loss of Nfe2l1, at least on the transcriptional level, as indicated by induction of *Atf3*, *Ccl2* and *Cxcl10*. The inflammation induced by cholesterol treatment is likely mediated by Atf3. However, while this inflammatory component of the Nfe2l1 KO phenotype is replicated

by cholesterol and epoxomicin treatment, it did not affect expression of ER stress marker genes *Hspa5* and *Ddit3*.

4.4.3 Transcriptomic analysis of Nfe2l1-Atf3-cholesterol interaction

To gain a more comprehensive understanding of the intricate interplay among Nfe2l1, Atf3, and cholesterol, I conducted transcriptomics on primary white adipocytes in which I silenced *Nfe2l1*, *Atf3*, or both using RNAi, and treated them with cholesterol (Figure 50A). The principal component analysis (PCA) separated the groups based on cholesterol treatment and *Atf3* knockdown, indicating that cholesterol treatment significantly influenced the transcriptome, while genetic manipulation via siRNAs had less impact. Specifically, scramble and *siNfe2l1* samples clustered closely together, suggesting that *siNfe2l1* only exerted minor effects on the transcriptome (Figure 50B). This observation was further supported by the analysis of differentially expressed genes (DEGs), revealing that *siNfe2l1* had only 281 DEGs compared to *Scramble*, whereas *siAtf3* had 2,666 DEGs, and *siNfe2l1*+*siAtf3* had 1,751 DEGs for a total of 56,748 genes analyzed. In contrast, cholesterol had the most substantial impact among all conditions, resulting in 6,517 DEGs. (Figure 50C). While the double knockdown of *Nfe2l1* and *Atf3* shared some DEGs with *siNfe2l1*, the majority of DEGs were shared with *siAtf3*. However, there was a significant portion of DEGs regulated exclusively by *siAtf3* (Figure 50D).

In summary, transcriptomic analysis of the Nfe2l1-Atf3-cholesterol interaction revealed fundamental differences in the effects of siRNA-mediated genetic manipulation and cholesterol treatment. To further dissect these data, I opted to uncouple the effects of siRNAs from the treatment and evaluate them separately.

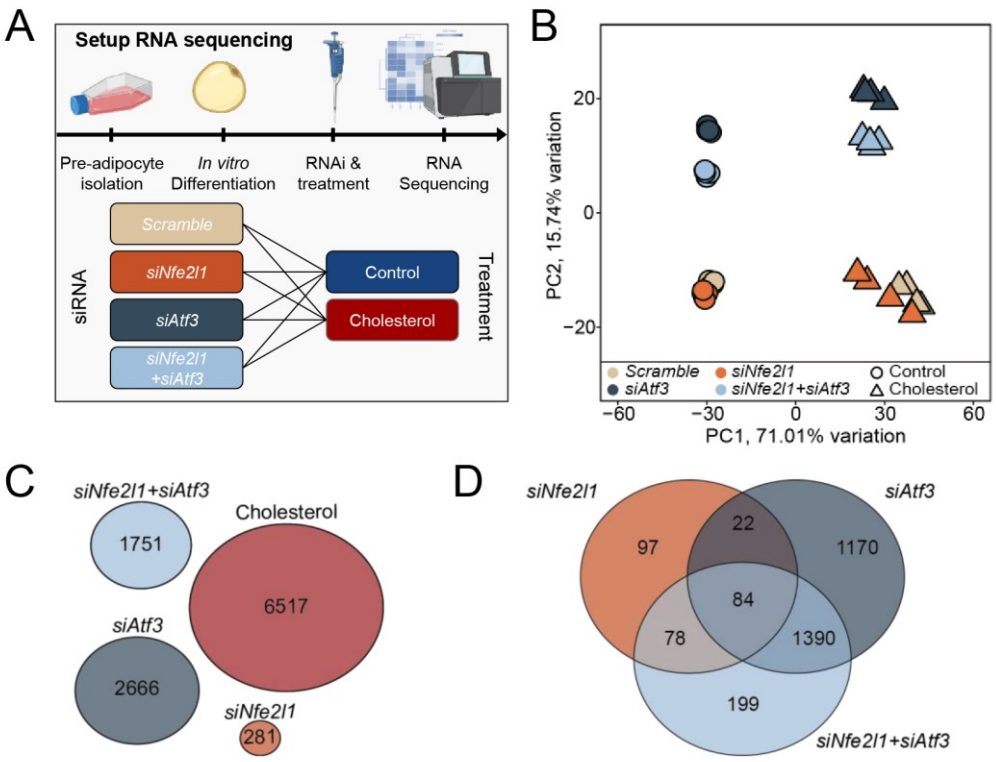

Figure 50 | Transcriptomic analysis of Nfe2l1-Atf3-cholesterol interaction

A workflow of the transcriptomic analysis, **B** PCA plot, **C** Euler diagram of differentially expressed genes (DEGs) and **D** Venn diagram of DEGs. n = 4, DEGs were filtered by p_{adj} <0.05 and absolute log_2 fold change >0.3 and base mean >50.

First, to assess the impact of knockdowns, I performed gene enrichment analysis using gene ontology (GO) for both up- and downregulated genes. Surprisingly, no enriched GO pathways were identified for genes upregulated by *siAtf3*. However, a substantial overlap of upregulated terms was observed between *siNfe2l1* and *siNfe2l1+siAtf3*, involving pathways associated with inflammation and immunity (Figure 51A). GO analysis of downregulated genes showed more enriched terms for *siAtf3*, with significant overlap with *siNfe2l1+siAtf3*. Specifically enriched GO terms for *siAtf3* included fat cell differentiation, metabolic, and biosynthetic processes. Shared GO terms by *siAtf3* and *siNfe2l1+siAtf3* were rather unspecific or not applicable for adipocytes, such as extracellular matrix organization, wound healing, and angiogenesis (Figure 51B). Knockdown of *Nfe2l1*, however, was linked to the regulation of lipid metabolism and the proteasomal catabolic process, leading to significantly lower expression of 20 proteasome subunit genes. Interestingly, double knockdown of *Atf3* and *Nfe2l1* exhibited a similar lower expression pattern for proteasome subunit genes, but the Z-Score was not as low as with *siNfe2l1* alone. *Scramble* and *siAtf3* samples, however, showed an opposite pattern with higher expression of proteasome subunit genes compared to knockdown of *Nfe2l1* (Figure 51C).

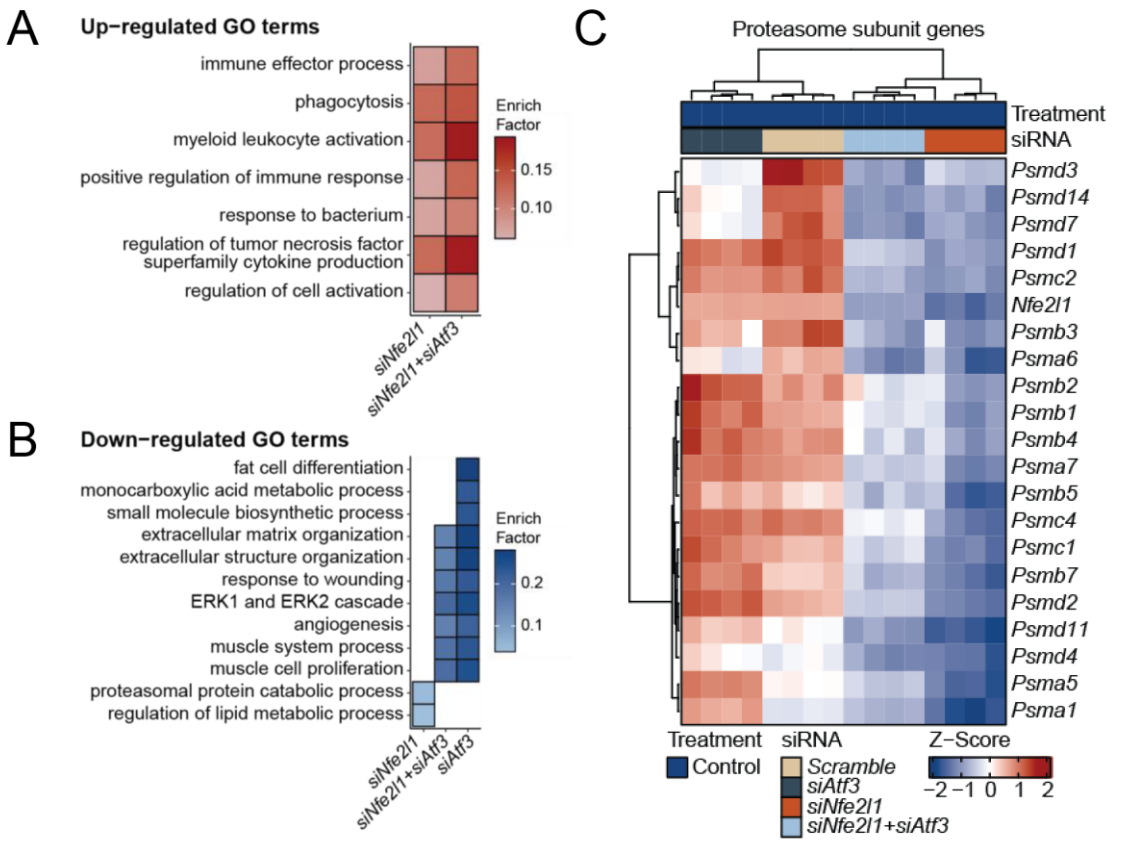

Figure 51 | *Nfe2l1* knockdown in primary white adipocytes is linked to inflammation and lower expression of proteasome subunit genes.

A GO enrichment analysis of up-regulated genes and **B** down-regulated genes, **C** expression pattern of proteasome subunit genes. **A,B** Data is Enrich Factor, **C** data is Z-Score, n=4.

Overall, siRNA-mediated manipulation of *Nfe2l1* primarily resulted in lower expression of proteasome subunit genes, while knockdown of *Atf3* did not show a clear effect at the baseline level. Similarly, the double knockdown of *Nfe2l1* and *Atf3* together showed a considerable overlap of both *siNfe2l1* and *siAtf3*, but no clear picture of the interaction between *Nfe2l1* and *Atf3* emerged.

One major goal of the transcriptomic analysis was to unravel how cholesterol treatment affects adipocytes, which pathways are activated and which factors regulated these. To start with, I conducted GO analysis of the significantly up-regulated genes. The five most significantly enriched terms were “Response to unfolded protein”, “Regulation of DNA-templated transcription in response to stress”, “Response to lipids”, “Negative regulation of cell population proliferation” and “Inflammatory response”. Notably, amongst the most up-regulated genes were inflammatory genes such as *Cxcl1*, *Cxcl2* and *Cxcl10*, as well as stress marker genes such as *Hspa1a*, *Hspa1b*, *Didt3* and *Atf3* (Figure 52).

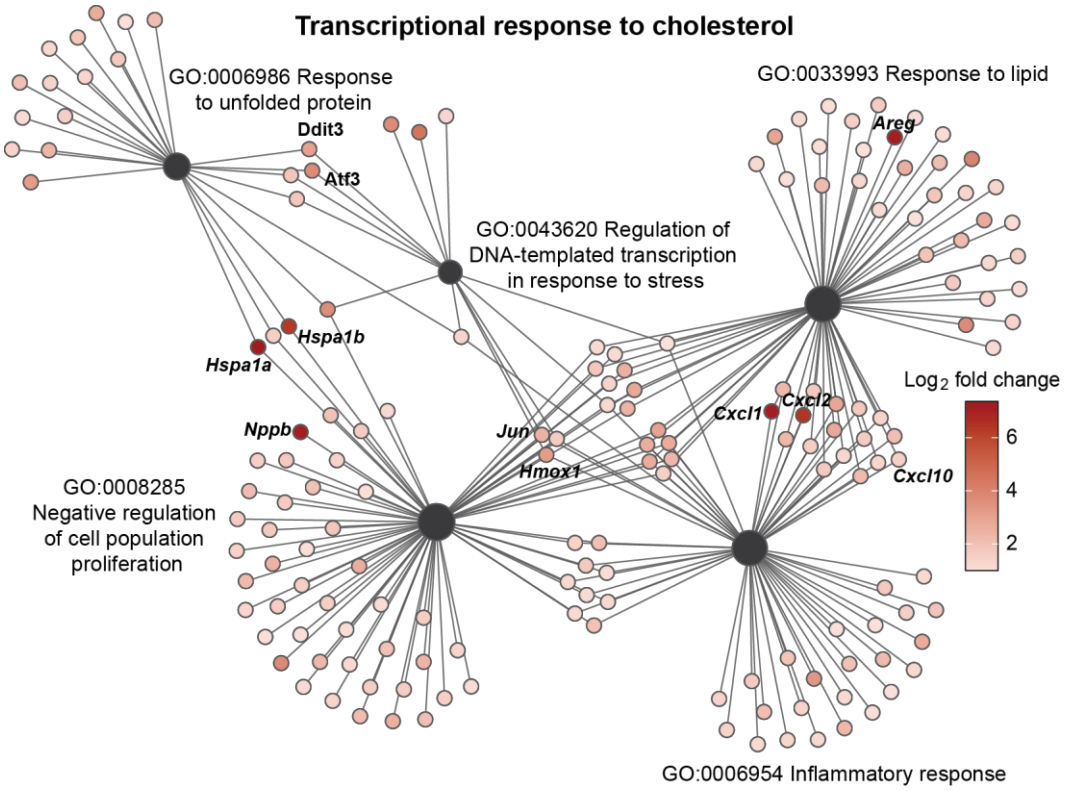

Figure 52 | Cholesterol induces a lipotoxic stress response in white adipocytes.
Top five up-regulated GO terms by cholesterol treatment (log_2 fold change >1). Data is mean log_2 fold change, n=4.

Indeed, under cholesterol stimulation, Atf3 emerged as the most upregulated among all transcription factors (Figure 53A) and silencing *Atf3* under cholesterol treatment robustly attenuated the upregulation of the top five GO terms (Figure 53B).

Since primary white adipocytes of Adipoq-KO mice displayed enhanced inflammatory and stress kinase signaling, I investigated if cholesterol treatment elicits a similar signaling response in 3T3-L1 adipocytes and whether this can be modulated by silencing of *Atf3*. Cholesterol treatment resulted in stronger phosphorylation of NF-κB, Jnk, and p38 compared to the control treatment (DMSO), and the combined treatment of cholesterol and epoxomicin exhibited the most robust phosphorylation signal. Knockdown of *Atf3* resulted in slightly higher Jnk phosphorylation in the DMSO condition and markedly higher NF-κB phosphorylation in the cholesterol condition. However, knockdown of *Atf3* led to lower p38 phosphorylation in both the cholesterol and cholesterol+epoxomicin conditions (Figure 53C). At the gene expression level, knockdown of *Atf3* led to decreased expression of *Ddit3* and *Cxcl1* (Figure 53D,E). Interestingly, the expression of *Cxcl10* was not affected by the knockdown of *Atf3* (Figure 53F).

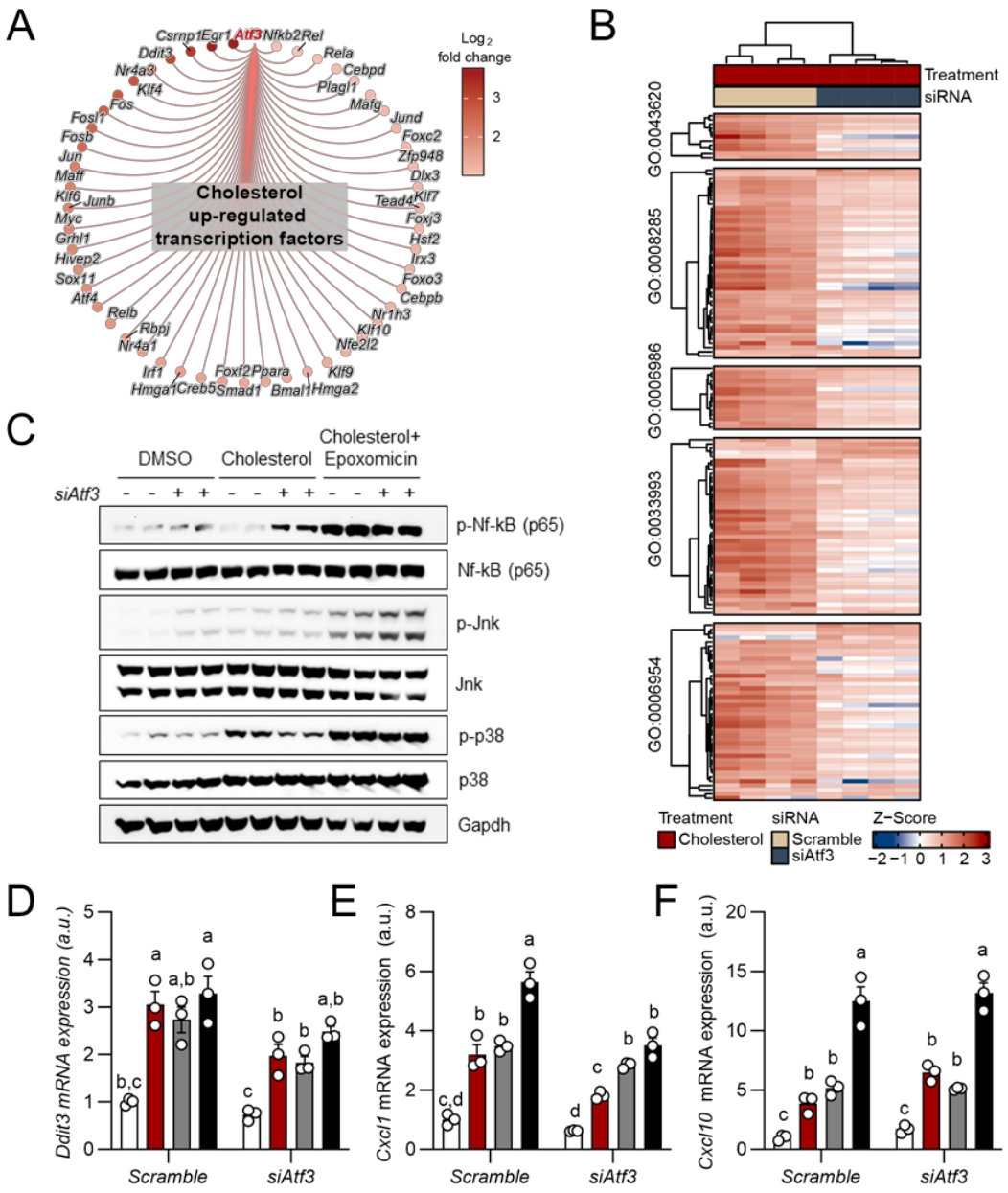

Figure 53 | Atf3 mediates cholesterol-induced inflammation in white adipocytes.

A Up-regulated transcription factors by cholesterol, **B** regulation of top five up-regulated GO terms by *siAtf3*, **C** immunoblot, **D** *Ddit3*, **E** *Cxcl1* and **F** *Cxl10* mRNA expression in 3T3-L1 adipocytes transfected with *siAtf3* and treated with cholesterol with and without epoxomicin for 6h. **A,B** n=4; **C** n=2 (representative immunoblot); **D-F** Data is mean + s.e.m., n=3, different letters indicate significant differences (p_{adj}<0.05) between groups tested by two-way ANOVA with Tukey post-hoc test.

In conclusion, loss of adipocyte Nfe2l1 resulted in severe inflammation of the adipose tissue, most likely as a consequence of proteasome maladaptation. *In vitro* loss of function experiments remained elusive and did not fully provide insight into the intricate interplay between Nfe2l1-mediated proteasomal function, Atf3 activation and the onset of inflammation. However, this study contributed to our understanding of cholesterol homeostasis in adipocytes as an underlying factor in metabolic diseases.

4.5 The NFE2L1-proteasome pathway in human adipose tissue

Finally, I investigated whether the NFE2L1-proteasome pathway in WAT is also relevant for obesity in humans. To start with, I analyzed publicly available RNA sequencing data of SCAT and VISAT of lean adult individuals to verify *NFE2L1* expression in human WAT (Figure 55). Intriguingly, *NFE2L1* was highly expressed in both SCAT and VISAT. Moreover, *NFE2L1* expression even exceeded that of its homologs *NFE2L2* and *NFE2L3* as well as known adipocyte transcription factors such as *PPARG* (Peroxisome Proliferator Activated Receptor Gamma), *CEBPA* (CCAAT Enhancer Binding Protein Alpha) or *SREBF1* (Sterol Regulatory Element Binding Transcription Factor 1) (Figure 54).

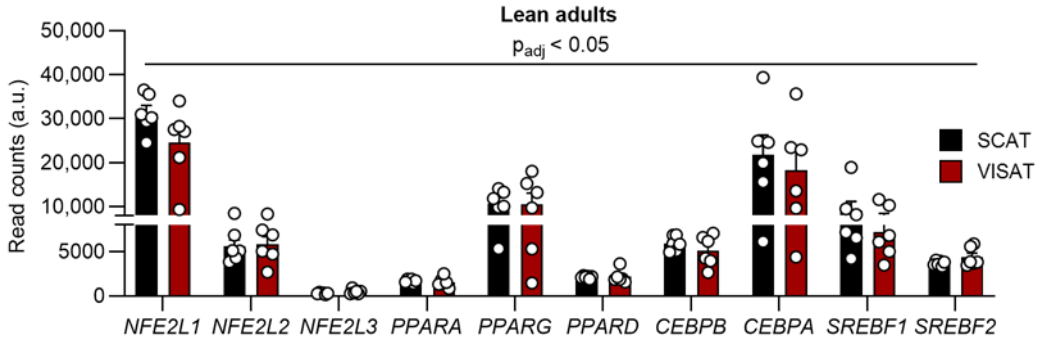

Figure 54 | Expression of selected transcription factors in human WAT.

Expression of selected transcription factors in SCAT and VISAT of lean adults (n=6, mean BMI 23.7±1.9 kg/m^2). Open access RNA sequencing data from Song et al. [129], data is mean + s.e.m, n=6. p_{adj}<0.5 by one-way ANOVA with Dunnett's post hoc test vs. *NFE2L1* for each tissue.

To investigate the relationship of NFE2L1 in WAT with human obesity, I correlated *NFE2L1* expression in SCAT and VISAT with BMI in a human cohort from the Leipzig Obesity Biobank (LOBB) comprising of 478 individuals with a broad range of BMI. *NFE2L1* expression was inversely correlated with BMI and average adipose tissue gene expression was significantly lower in obese individuals (BMI>30) compared to non-obese individuals (BMI<30) in both SCAT (Figure 55A,B) and VISAT (Figure 55C,D). Furthermore, correlation analysis in another cohort of the LOBB comprising of 1,479 individuals demonstrated a positive association between *NFE2L1* expression and the majority of proteasome subunit genes in SCAT and VISAT (Figure 55E).

Collectively, these data provided first evidence that *NFE2L1* and the entire proteasome-pathway are inversely correlated with obesity in humans. Specifically, lower expression of *NFE2L1* in WAT and a concomitant decrease in proteasome subunit expression are associated with higher BMI. These findings suggest that adipocyte NFE2L1 could play a crucial role in regulating obesity and maintaining adipocyte health in humans.

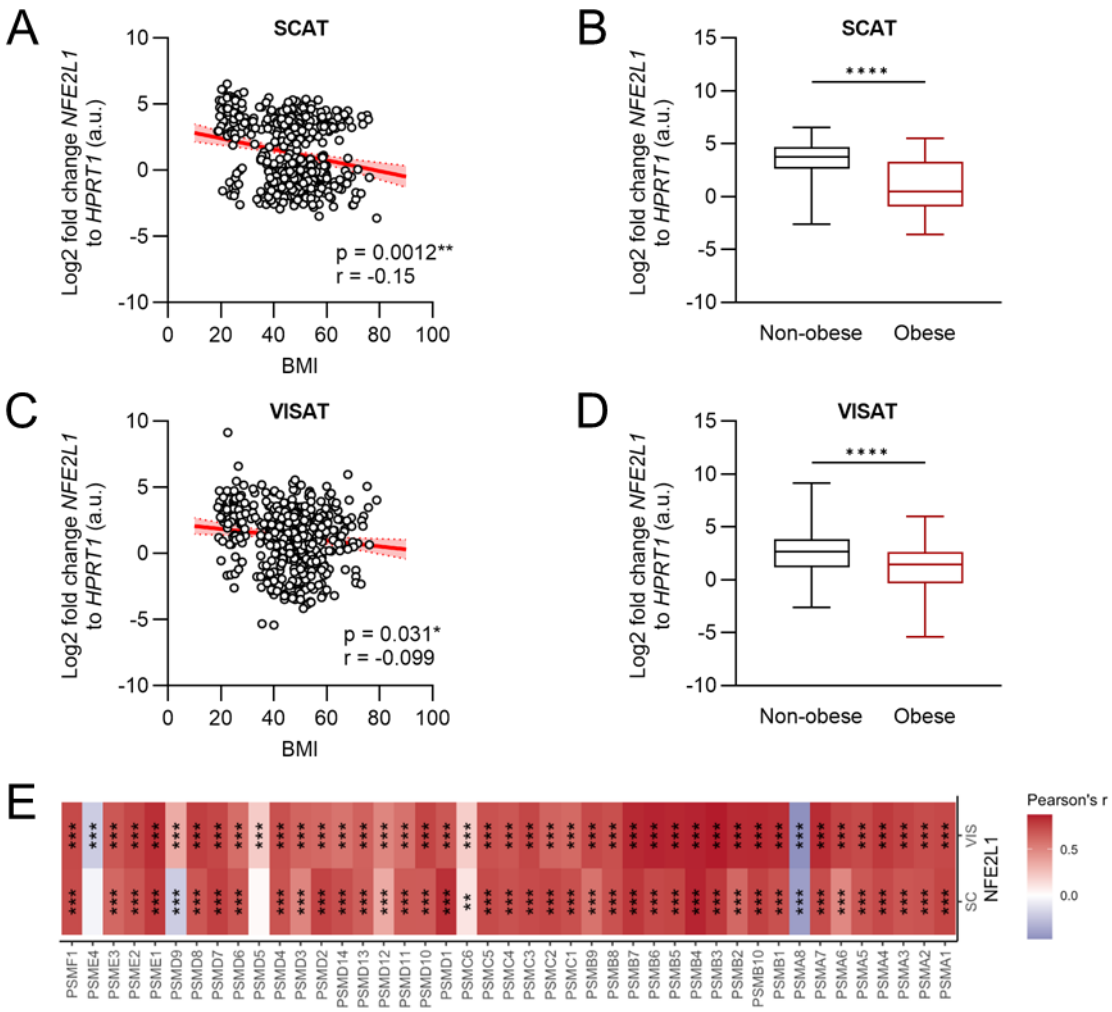

Figure 55 | The NFE2L1-proteasome pathway is inversely correlated with BMI in humans.

A Correlation of *NFE2L1* expression with BMI in SCAT, **B** average *NFE2L1* expression in SCAT, **C** correlation of *NFE2L1* expression with BMI in VISAT and **D** average *NFE2L1* expression in VISAT of non-obese (BMI <25) and obese (BMI ≥25) human individuals in the LOBB (n = 478), **E** correlation of *NFE2l1* expression in SCAT and VISAT with expression of proteasomal subunit genes in the LOBB (n = 1,479). **A-D** *NFE2L1* expression measured by qPCR, data is mean + s.e.m., provided by Matthias Blüher and Anne Hoffmann (LOBB, University of Leipzig) and analyzed by CJ. **E** *NFE2L1* and *PSM* gene expression measured by RNA sequencing. Data is Pearson's correlation coefficient (r), data and analysis provided by Matthias Blüher and Anne Hoffmann. * p<0.05, ** p<0.01, **** p<0.001 by linear regression with Spearman's correction (**A**,**C**), Mann-Whitney U-test (**B**,**C**) and multiple linear regression with Pearson's correction (**E**).

5. Discussion

The adaptation of adipocytes to an excess of nutrients, particularly lipids, is a pivotal process in obesity. It determines the onset of adipocyte dysfunction, potentially leading to the progression of cardiometabolic diseases. The ER plays an essential role in the metabolic adaptation of cells by sensing nutrient overload and regulating adaptive stress resistance pathways. Metabolic stress, manifested as proteotoxicity, lipotoxicity, or glucotoxicity depending on the stressor type, disrupts ER homeostasis. Unaddressed, this can escalate to ER stress, compromising critical ER functions such as proteostasis, lipid metabolism, and calcium signaling, and may ultimately result in cell death. The activation of stress-resistance pathways, notably the UPR, is well documented in obese, insulin-resistant tissues, especially adipose tissue, where ER stress is a significant contributor to adipocyte dysfunction[55,57,67]. However, little is known about the mechanisms that protect adipocyte health in obesity. Here, I show that the Nfe2l1-proteasome-pathway mediates adaptation to lipid-rich diets and guards metabolic health. In this way, Nfe2l1 protects adipocytes from lipotoxicity, in particular cholesterol-induced inflammation, which ultimately attenuates the progression of atherosclerosis.

Nfe2l1 is renowned for its role in activating the transcription of proteasome subunit genes adaptively when proteasomal activity is compromised[94,95,130]. Such precision in proteasome regulation is vital for survival, highlighted by the lethality of global Nfe2l1 deletion during embryonic development[96]. Tissue-specific deletion of Nfe2l1 underscores its necessity for maintaining normal tissue function by regulating metabolism and inflammation under metabolic stress conditions in BAT[112], liver[108–110] and the heart[111]. Notably, in the liver Nfe2l1 also acts as a cholesterol sensor which initiates cholesterol removal and limits inflammation once ER cholesterol becomes excessively high[110]. Recent findings have also associated the loss of Nfe2l1 in WAT with adipocyte hypertrophy, insulin resistance, and inflammation, further establishing Nfe2l1's connection to lipid homeostasis[113,114]. These effects are likely consequences of compromised proteasome function, as evidenced by lower basal proteasome subunit expression, lower proteasome activity, and the accumulation of ubiquitinated proteins following Nfe2l1's tissue-specific deletion in the liver and BAT[109,111,112]. However, the precise mechanisms by which adipocyte Nfe2l1 operates, its significance in the context of obesity and cardiometabolic diseases, and its applicability to human health, remain to be fully elucidated.

5.1 Nfe2l1 guards adipocyte health from the effects of excessive lipid exposure

To investigate the function of adipocyte Nfe2l1 in the context of obesity and cardiometabolic disorders, I utilized adipocyte-specific knockout mice on both a standard B6 and an ApoE-deficient genetic background, exposing them to lipid-rich diets. While DIO and an atherogenic WD resulted in distinct phenotypes, both diets led to lower SCAT and GWAT masses. Notably, WD also led to lower BAT mass, which was not observed with a standard chow diet (Supplementary Figure 3) or DIO. SCAT is the primary lipid storage in the body and only when its storage capacities exceed, lipids accumulate in the VISAT[131]. Thus, lower SCAT mass indicates a reduced ability to safely store lipids, which can lead to ectopic lipid deposition in the presence of excessive nutrient intake[27]. In fact, while WAT mass was diminished in the absence of Nfe2l1, liver mass was similar or even higher on DIO and WD, indicating ectopic lipid storage, which is associated with insulin resistance[27].

A consistent outcome of reduced WAT mass was the decreased levels of adiponectin and leptin, the predominant hormones produced by adipose tissue. While adiponectin has anti-inflammatory and insulin-sensitizing properties, leptin is required for appetite regulation and promotes energy expenditure[35]. Thus, secretion of these adipokines, in particular adiponectin, is an important function of adipocytes and a good marker for adipocyte health[36]. In both humans and rodents, adiponectin levels decrease with visceral obesity and correlate inversely with insulin resistance[35]. Adiponectin action is critical for systemic insulin sensitivity, since adiponectin-deficient mice develop insulin resistance, and overexpression of adiponectin in obese mice preserved insulin sensitivity[132]. In the present study, diminished circulating adiponectin and leptin in combination with lower adipose tissue mass indicate severe adipocyte dysfunction in Adipoq-KO animals. Interestingly, despite all Adipoq-KO models exhibiting low adiponectin levels, female mice on both B6 and ApoE$^{-/-}$ backgrounds showed higher insulin resistance, unlike their male counterparts, who only exhibited this condition under DIO. This suggests that female mice might be more sensitive to adipocyte dysfunction caused by loss of Nfe2l1. Moreover, since lipid-rich diets, especially cholesterol-rich WD, aggravated insulin resistance, this suggests that Nfe2l1 is required to regulate the effect of excessive lipids in adipocytes.

This is especially important in the context of atherosclerosis, in which circulating lipids, most notably LDL-Cholesterol, initiate the disease[18,19]. In this study, female ApoE$^{-/-}$ Adipoq-KO mice exhibited higher plasma cholesterol levels and dyslipidemia in comparison

to wild-type littermates. These are presumably attributed to insufficient buffering of cholesterol by the adipocytes, as WAT mass was severely diminished on WD. Moreover, insufficient cholesterol buffering manifested as steatosis, with higher cholesterol deposition in the liver. This was accompanied by elevated liver and plasma bile acid levels, possibly as a result of a compensatory mechanism to limit cholesterol accumulation by converting it to bile acids. Finally, lower circulating adiponectin level *per se* might also enhance atherosclerosis, since its anti-inflammatory and anti-fibrotic activities are absent[35] and it has been shown that overexpression of adiponectin is sufficient to lower atherosclerosis burden[133].

This raises a crucial question regarding the cause of lower adiponectin and leptin levels. While partially attributable to diminished WAT mass, as adipokine secretion in the lean state is typically proportional to adipose tissue mass[27], this does not explain the observed adipokine reductions in lean animals with comparable adipose tissue masses (Supplementary Figure 3,4). Leptin and adiponectin are peptide hormones synthesized from amino acids, which adipocytes absorb from the bloodstream or derive from the proteasomal recycling of proteins. Therefore, one possible explanation for the decreased hormone levels in Nfe2l1-deficient adipocytes could be reduced basal proteasomal activity[112], leading to diminished protein recycling and a subsequent shortage of amino acids for *de novo* adipokine synthesis. Alternatively, the ER stress experienced by obese adipocytes, driven by the higher demand for protein synthesis during expansion, adipokine secretion, and exposure to excessive nutrients and inflammation, could also play a role[67,134].

5.2 Adipocyte Nfe2l1 limits ER stress and inflammation in adipose tissue to protect insulin sensitivity

Obesity, insulin resistance and atherosclerosis are immunometabolic diseases, in which aberrant metabolism incites a chronic low-grade inflammatory response. This involves the activation of pro-inflammatory signaling pathways and the irregular production of cytokines and chemokines[25,42,64]. The absence of Nfe2l1 exacerbates inflammation within the WAT, evidenced by the marked infiltration of F4/80+ Cd11c+ macrophages and Cd4+ and Cd8+ T cells, in chow-fed mice. While Cd4+ T cells typically inhibit macrophage infiltration by secreting Il-4 and Il-10, Cd8+ T cells initiate and drive inflammation in obese adipose tissue by promoting macrophage activation and migration[52,135]. These contradictory roles usually lead to a reduction of Cd4+ T cells, as well as Treg cells in the later stages of inflammation, which possibly augments inflammation in advanced obesity[52]. Interestingly, Nfe2l1-deficient mice displayed higher numbers of both Cd4+ and Cd8+ T cells. This might be attributable to their lean state and the potential presence of anti-

inflammatory mechanisms in the lean adipose tissue. It is conceivable that DIO or WD-fed Adipoq-KO mice might exhibit lower number of Cd4+ T cell counts.

At the cellular level, white adipocytes lacking Nfe2l1 showed stronger activation of the pro-inflammatory and stress kinase signaling pathways NF-κB and p38, whereas Jnk activation was similar to wild-type adipocytes. NF-κB is the main signaling pathway that promotes inflammation in adipocytes in response to overnutrition through the induction of chemokines and cytokines[136,137]. Canonical NF-κB signaling can be activated by lipopolysaccharides, FFAs, pro-inflammatory cytokines, most notably TNF-a, as well as ER stress[138]. Stress kinase pathways p38 and Jnk are activated in obesity in many tissues including adipose tissue by glucose, FFAs and by pro-inflammatory signals[56]. While Jnk activation has been linked to aggravated ER stress[57], activation of p38 promotes nuclear Xbp1 accumulation and activity to restore ER homeostasis via the UPR[59]. Particularly in adipocytes, p38 has been reported to both induce and inhibit adipogenesis, as well as to regulate browning of WAT and thermogenesis in BAT[56,139]. Nfe2l1-deficient WAT displayed induction of ER stress marker genes, likely as a result of impaired proteasome activity[112], which contributed to stronger activation of NF-κB and p38 in the KO adipocytes. Ultimately, sustained stress signaling in adipocytes can be harmful and is associated with the progression of obesity-related diseases and insulin resistance[56,138,139]. Thus, unsurprisingly male Adipoq-KO mice on DIO as well as female Adipoq-KO mice irrespectively of the diet were more insulin-resistant compared to wild-type littermates. Overall, this suggests that adipocyte Nfe2l1 mediates insulin sensitivity by suppressing ER stress and inflammation, which is especially critical in conditions of excessive lipid intake.

5.3 Nfe2l1 in adipocytes protects against lipid-induced inflammation and atherosclerosis in a sex-specific manner

Inflammation is an essential component of atherosclerosis, which promotes the disease and its complications[19]. Inflammation in the PVAT is considered a risk factor for the development of atherosclerosis, as it is located in close proximity to the vessel wall and has paracrine effects there[16,17,26]. Although secretion of pro-inflammatory mediators such as TNFα and MCP-1 from adipocytes is well established, the contribution of adipocytes especially to circulating pro-inflammatory cytokines and chemokines remains unclear. In this study, loss of adipocyte Nfe2l1 was directly linked to enhanced athero-progression in female mice, potentially caused by dyslipidemia and higher level of circulating pro-

inflammatory cytokines Cxcl1, Ccl5 and Cxcl10 (also called IP-10). NF-κB mediated secretion of IP-10 from adipocytes has been linked to T cell migration[140] and might thus explain the substantial occurrence of Cd8+ and Cd4+ T cells in Nfe2l1-deficient WAT. *In vitro*, stimulation of adipocytes with cholesterol induced expression of *Cxcl1* and *Cxcl10* suggesting that inflamed Nfe2l1-deficient adipocytes indeed contribute to circulating cytokine level and with that to progression of atherosclerosis.

It should be noted that loss of Nfe2l1 promoted atherosclerotic plaque formation, dyslipidemia, and steatosis only in female ApoE$^{-/-}$ Adipoq-KO mice, whereas male mice did not display increased plaque area but showed more severe lipoatrophy and stagnating body weight gain. Consistent with this, female ApoE$^{-/-}$ Adipoq-KO mice had higher plasma cholesterol levels compared to wild-type littermates, while male mice had similar plasma cholesterol levels. Thus, it appears that female mice are more susceptible to disruption in cholesterol homeostasis caused by loss of adipocyte Nfe2l1. However, it has been frequently reported that female C57BL6/J ApoE$^{-/-}$ mice develop atherosclerosis faster and have larger aortic root lesions compared to male mice[141]. Consequently, the window for seeing an effect of adiocyte-Nfe2l1 deletion might just have been bigger in female ApoE$^{-/-}$ mice. Nevertheless, in contrast to the general notion that male mice exhibit more pronounced diet-induced phenotypes of insulin resistance and glucose intolerance[142], female ApoE$^{-/-}$ Adipoq-KO were profoundly insulin-resistant on both chow diet and WD. In fact, even female Adipoq-KO on chow diet displayed insulin resistance compared to their wild-type littermates (Supplementary Figure 4D), whereas male wild-type and Adipoq-KO mice showed no difference in insulin tolerance (Supplementary Figure 3D). Sex differences in insulin resistance on mouse models of obesity is linked to gonadal hormones and their influence on adipose tissue distribution. Although this is ill-defined, female mice generally display larger SCAT and smaller VISAT depots compared to male mice[143]. Thus, it could be hypothesized that female mice are more sensitive to lipoatrophy in SCAT caused by loss of Nfe2l1, consistent with the more pronounced liver lipid deposition.

5.4 Mechanisms of lipoatrophy by loss of adipocyte Nfe2l1

This study showed that lipoatrophy was primarily linked to the deletion of Nfe2l1 in white adipocytes, as targeting brown and beige adipocytes with Ucp1-Cre did not result in significant changes in adipose tissue weights and insulin sensitivity. Furthermore, the absence of Nfe2l1 had a more adverse effect on SCAT compared to GWAT, since Adipoq-KO mice on a chow diet displayed less SCAT but equivalent or more GWAT relative to wild-type littermates. However, under a lipid-rich DIO or WD, Adipoq-KO mice showed both lower SCAT and GWAT mass, specifically pronounced with WD. In addition, lower

body weights in male mice were only observed on WD, but not during DIO. These observations indicate that Nfe2l1 is required for the adaptation of adipocytes, most notably white adipocytes, to excessive lipid intake. Considering the role of Nfe2l1 in cholesterol homeostasis in the liver[99,110], I hypothesized that the more pronounced lipoatrophy and the body weight differences in male mice are a result of dietary cholesterol in the WD. Yet, adding the same amount of cholesterol to DIO did not replicate the lipoatrophy and body weight differences seen in Adipoq-KO mice, potentially because of the higher caloric content in DIO, which offsets the negative impact of dietary cholesterol. It is also conceivable that differences in amino acid and fatty acid compositions between HFD and WD contribute to the observed phenotype or issues may arise from the method of cholesterol supplementation in DIO. For this study, I dissolved cholesterol in ethanol and coated the HFD with this mixture. However, cholesterol precipitates quickly at room temperature, which could have led to an insufficient distribution of cholesterol.

The reasons behind lipoatrophy and reduced body weights in Adipoq-KO mice remain elusive despite an in-depth analysis of energy metabolism. In mouse models with constitutive activation of NF-κB, chronic inflammation in the adipose tissue is associated with higher energy expenditure and lower WAT mass[144,145]. Male Adipoq-KO mice on DIO displayed higher energy expenditure in dark and light phase. However, male Adipoq-KO mice on WD had similar energy expenditure compared to littermate controls. Only in the dark phase, they displayed a tendency for higher energy expenditure (p=0.123), similarly to female ApoE$^{-/-}$ Adipoq-KO mice on WD. Possibly, this trend would become significant in a larger cohort, however, yet higher energy expenditure does not explain the lipoatrophy. It is possible that Adipoq-KO mice also excrete more energy through the feces, an aspect not examined in this study. Additionally, all Nfe2l1 KO animals in this study did not respond to CL-induced BAT activation, as Nfe2l1-mediated proteasomal activity is required for BAT thermogenesis[112]. This aligns with the observed whiter BAT phenotype indicating that while BAT energy expenditure does not directly cause lipoatrophy, inactive BAT in Adipoq-KO models could exacerbate dyslipidemia and hypercholesterolemia due to diminished BAT lipid clearance[146,147]. Nonetheless, lower BAT lipid clearance alone does not explain enhanced dyslipidemia and atherosclerosis in ApoE$^{-/-}$ Adipoq-KO mice, since effective lipid reduction through BAT activation requires a functional ApoE-Ldlr axis[147]. While inflammation-induced higher energy expenditure cannot be ruled out as a causal factor for the observed lipoatrophy, persistent ER stress and inflammation could also lead to the death of adipocytes and thus to the loss of adipose tissue mass.

5.5 Atf3 mediates cholesterol-induced inflammation in Nfe2l1-deficient adipocytes

The loss of Nfe21 in WAT resulted in marked induction of inflammation and stress marker genes, specifically Atf3. Atf3 is family member of the ATF/cAMP response element-binding transcription factors[148] and a downstream target of Atf4 in the PERK pathway of the UPR[73]. The Atf3 promotor region contains multiple binding sites for other transcription factors, including NF-κB, indicating its induction by stress and inflammation signals[149].

In my research, I utilized 3T3-L1 adipocytes, genetically manipulated with RNAi to silence *Nfe2l1*, aiming to investigate the interplay between Nfe2l1 and Atf3 and the underlying cellular mechanisms of Nfe2l1 in adipocytes. However, silencing of *Nfe2l1* did not replicate the effects of KO in adipose tissue. This may be due to many reasons; firstly, low expression of Nfe2l1 may still be sufficient to achieve its effect on proteasome subunit expression. This is likely because its abundance and activity are mainly regulated at the post-transcriptional level[103–105]. Second, although Nfe2l1 mediates the bounce-back response of proteasomal activity under conditions of proteasomal inhibition[94,95], it is established that it only has modest effect on basal expression of proteasome subunits[95]. Moreover, Nfe2l1 is barely detectable under basal conditions as it is constantly degraded by the proteasome[103–105]. Only in situations where the proteasome cannot meet the activity demand, such as chemical proteasome inhibition[94,95] or under certain physiological conditions such as cold adaptation[112], active Nfe2l1 accumulates and promotes transcription in the nucleus.

Thus, I used cholesterol and epoxomicin treatment to mimic a situation of Nfe2l1 deficiency and increased demand for proteasome activity to stress the cells. Similar to the absence of Nfe2l1 in adipose tissue, cholesterol treatment induced *Atf3* and surrogate inflammation markers, which was highest in adipocytes treated with the combination of both cholesterol and epoxomicin. However, in contrast to hepatocytes[110], regulation of Nfe2l1 processing by cholesterol was not observed in 3T3-L1 adipocytes. Transcriptomic analysis of primary white adipocytes with knockdown of *Nfe2l1* and *Atf3* demonstrated lower expression of proteasome subunit genes with *Nfe2l1* knockdown, which was linked to inflammation. *Atf3* knockdown, however, was linked to down-regulation of adipogenesis and metabolism. This aligns with findings from other studies, including our lab, in which hypoxia[150], ER stress[151,152] or proteasome dysfunction[153] induced *Atf3* expression, which results in down-regulation of adipogenesis marker. Interestingly, silencing of *Atf3* is sufficient to allow lipid metabolism and adipogenesis[153]. While this requires further investigation, these findings indicate that Atf3-mediated inflammation contributes to

lipoatrophy observed in Nfe2l1-deficient adipose tissue, suggesting that blocking Atf3 activation *in vivo* might protect from lipoatrophy.

Cholesterol treatment significantly altered the adipocyte transcriptome towards a lipotoxic stress response characterized by inflammation, ER stress, and disrupted lipid metabolism. Remarkably, *Atf3* was the most highly induced transcription factor by cholesterol treatment. While silencing of *Nfe2l1* in combination with cholesterol treatment had only minor effects, the cholesterol-induced lipotoxic response was significantly attenuated by silencing of *Atf3*. In addition to that, I also investigated whether cholesterol activated stress kinase and inflammatory signaling pathways, a feature observed in Nfe2l1 KO adipocytes, and if silencing of *Atf3* would be able to diminish or even block it. Interestingly, while cholesterol treatment activated NF-κB, Jnk and p38 signaling, which was even exacerbated by the addition of epoxomicin, silencing of *Atf3* did not diminish Jnk and NF-κB signaling in 3T3-L1 adipocytes. Only p38 activation in response to cholesterol treatment was blunted by silencing of *Atf3*, which suggests p38 as an additional player between Atf3 and inflammatory gene transcription. However, more research in this direction is required. In conclusion, cholesterol induces an inflammatory stress response in adipocytes, which is substantially mediated by Atf3. Thus, Atf3 appeared as a lipotoxic stress marker, which can be modulated to limit inflammation.

5.6 Loss of adipocyte NFE2L1 is associated with human obesity

Lastly, the question remained regarding the relation of adipocyte NFE2L1 and obesity in humans. The NFE2L1 family is highly conserved in mammals and homologs are found in *Caenorhabditis elegans* (*skn-1*) and *Drosophila melanogaster* (CNC)[96]. The functional conservation of NFE2L1 in humans is highlighted by the fact that activation of the DDI2-NFE2L1-pathway in multiple myeloma contributes to treatment resistance with the proteasome inhibitor bortezomib[154,155]. Here, I showed that *NFE2L1* is highly expressed in SCAT and VISAT of lean adults and exceeds expression of classical adipogenic transcription factors. In a human cohort over a broad range of BMI, lower *NFE2L1* WAT expression was associated with higher BMI, and almost all proteasome subunit genes were positively correlated to *NFE2L1* gene expression. This suggests that the entire NFE2L1-proteasome pathway is downregulated in obese humans. In return, activating the NFE2L1-proteasome pathway in obese humans could thus be a promising strategy to improve adipocyte dysfunction and insulin resistance. However, this area requires further investigations into the molecular mechanisms governed by NFE2L1 in human adipocytes, as well as targeted approaches to restore NFE2L1 activity.

6. Conclusions

Given the escalating global obesity crisis, which significantly contributes to the prevalence of cardiometabolic diseases such as T2DM, CVDs, and certain cancers, understanding the mechanisms underlying adipocyte dysfunction is crucial.

Adipocytes, known for their remarkable plasticity to fluctuating nutrient availability, play a vital role in whole-body energy homeostasis and insulin sensitivity. However, chronic over-nutrition disrupts their metabolic adaptation mechanisms, which is linked to ectopic lipid accumulation, inflammation, and insulin resistance.

This study has provided comprehensive insights on the complex and specific roles of Nfe2l1 in adipocytes, particularly its impact on cardiometabolic disorders such as atherosclerosis. It highlights how the Nfe2l1-proteasome pathway is essential for allowing adipocytes to adjust to lipid-rich diets, safeguarding against metabolic disorders. Specifically, it points out that Nfe2l1 plays a critical role in preventing lipotoxicity, notably the inflammation caused by cholesterol, which in turn, slows down the progression of atherosclerosis.

My investigation revealed a crucial link between maintaining cellular balance in protein and cholesterol metabolism within white adipocytes and the broader aspect of cardiometabolic health. It demonstrated Nfe2l1 as a guardian of adipocyte health and systemic insulin sensitivity, by protecting against lipid-induced inflammation. Furthermore, it identified Atf3 as an important mediator in driving inflammation within fat tissue in response to lipid accumulation, particularly cholesterol. This suggests that promoting proteostasis in adipocytes might be a viable approach to counteracting the dysfunction that occurs in obesity and potentially avoids deleterious cardiometabolic effects.

In essence, this research enriches our understanding of adipocyte biology and its significance for metabolic health. The observed gender-specific responses, dietary interactions, and cellular reactions present a comprehensive view, laying the groundwork for future research in this domain. This study underscores the potential of targeting specific pathways, like those involving Nfe2l1 and Atf3, to develop strategies for combating cardiometabolic diseases linked to obesity and adipocyte stress.

Literature

1. World Health Organization. Obesity and overweight. Published 2021. https://www.who.int/en/news-room/fact-sheets/detail/obesity-and-overweight
2. Stefan N. SARS-CoV-2 fires up inflammation in adipose tissue. *Nat Rev Endocrinol*. 2022;19(January):8-9. doi:10.1038/s41574-022-00778-0
3. Blüher M. Obesity: global epidemiology and pathogenesis. *Nat Rev Endocrinol*. 2019;15(5):288-298. doi:10.1038/s41574-019-0176-8
4. Hagberg CE, Spalding KL. White adipocyte dysfunction and obesity-associated pathologies in humans. *Nat Rev Mol Cell Biol*. Published online 2023. doi:10.1038/s41580-023-00680-1
5. Tim Lobstein, Brinsden H, Neveux M. *World Obesity Atlas 2022*.; 2022. www.worldobesity.org#worldobesityatlas
6. Müller TD, Blüher M, Tschöp MH, DiMarchi RD. Anti-obesity drug discovery: advances and challenges. *Nat Rev Drug Discov*. 2022;21(3):201-223. doi:10.1038/s41573-021-00337-8
7. Abel ED. Next Chapter for Weight Control — Small-Molecule GLP-1 Receptor Agonists? *N Engl J Med*. 2023;389(10):949-950. doi:10.1056/NEJMe2307285
8. Jastreboff AM, Aronne LJ, Ahmad NN, et al. Tirzepatide Once Weekly for the Treatment of Obesity. *N Engl J Med*. 2022;387(3):205-216. doi:10.1056/nejmoa2206038
9. The GBD 2015 Obesity Collaborators. Health Effects of Overweight and Obesity in 195 Countries over 25 Years. *N Engl J Med*. 2017;377(1):13-27. doi:10.1056/NEJMoa1614362
10. Powell-Wiley TM, Poirier P, Burke LE, et al. Obesity and Cardiovascular Disease A Scientific Statement From the American Heart Association. *Circulation*. 2021;143(21):E984-E1010. doi:10.1161/CIR.0000000000000973
11. British Heart Foundation. Global Heart & Circulatory Diseases Factsheet. Published online 2023.
12. Global Cardiovascular Risk Consortium. Global Effect of Modifiable Risk Factors on Cardiovascular Disease and Mortality. *N Engl J Med*. Published online 2023:1-13. doi:10.1056/NEJMoa2206916
13. Sun YQ, Burgess S, Staley JR, et al. Body mass index and all cause mortality in HUNT and UK Biobank studies: Linear and non-linear mendelian randomisation analyses. *BMJ*. 2019;364:1-10. doi:10.1136/bmj.l1042
14. Larsson SC, Bäck M, Rees JMB, Mason AM, Burgess S. Body mass index and body composition in relation to 14 cardiovascular conditions in UK Biobank: A Mendelian randomization study. *Eur Heart J*. 2020;41(2):221-226. doi:10.1093/eurheartj/ehz388
15. Neeland IJ, Ross R, Després JP, et al. Visceral and ectopic fat, atherosclerosis, and cardiometabolic disease: a position statement. *Lancet Diabetes Endocrinol*. 2019;7(9):715-725. doi:10.1016/S2213-8587(19)30084-1
16. Oikonomou EK, Desai MY, Marwan M, et al. Perivascular Fat Attenuation Index Stratifies Cardiac Risk Associated With High-Risk Plaques in the CRISP-CT Study. *J Am Coll Cardiol*. 2020;76(6):755-757. doi:10.1016/j.jacc.2020.05.078
17. Mancio J, Oikonomou EK, Antoniades C. Perivascular adipose tissue and coronary atherosclerosis. *Heart*. 2018;104(20):1654-1662. doi:10.1136/heartjnl-2017-312324

18. Libby P, Buring JE, Badimon L, et al. Atherosclerosis. *Nat Rev Dis Prim*. 2019;5(1):56. doi:10.1038/s41572-019-0106-z

19. Soehnlein O, Libby P. Targeting inflammation in atherosclerosis — from experimental insights to the clinic. *Nat Rev Drug Discov*. 2021;0123456789. doi:10.1038/s41573-021-00198-1

20. Weber C, Noels H. Atherosclerosis: Current pathogenesis and therapeutic options. *Nat Med*. 2011;17(11):1410-1422. doi:10.1038/nm.2538

21. Libby P, Ridker PM, Hansson GK. Progress and challenges in translating the biology of atherosclerosis. *Nature*. 2011;473(7347):317-325. doi:10.1038/nature10146

22. Gisterå A, Hansson GK. The immunology of atherosclerosis. *Nat Rev Nephrol*. 2017;13(6):368-380. doi:10.1038/nrneph.2017.51

23. Rocha VZ, Libby P. Obesity, inflammation, and atherosclerosis. *Nat Rev Cardiol*. 2009;6(6):399-409. doi:10.1038/nrcardio.2009.55

24. Hotamisligil GS. Inflammation and metabolic disorders. *Nature*. 2006;444(7121):860-867. doi:10.1038/nature05485

25. Hotamisligil GS. Inflammation, metaflammation and immunometabolic disorders. *Nature*. 2017;542(7640):177-185. doi:10.1038/nature21363

26. Oikonomou EK, Antoniades C. The role of adipose tissue in cardiovascular health and disease. *Nat Rev Cardiol*. 2019;16(2):83-99. doi:10.1038/s41569-018-0097-6

27. Mann JP, Savage DB. What lipodystrophies teach us about the metabolic syndrome. *J Clin Invest*. 2019;129(10):4009-4021. doi:10.1172/JCI129190

28. Rosen ED, Spiegelman BM. What we talk about when we talk about fat. *Cell*. 2014;156(1-2):20-44. doi:10.1016/j.cell.2013.12.012

29. Sakers A, De Siqueira MK, Seale P, Villanueva CJ. Adipose-tissue plasticity in health and disease. *Cell*. 2022;185(3):419-446. doi:10.1016/j.cell.2021.12.016

30. Mazzotta C, Basu S, Gower AC, et al. Perivascular Adipose Tissue Inflammation in Ischemic Heart Disease. *Arterioscler Thromb Vasc Biol*. 2021;(March):1239-1250. doi:10.1161/ATVBAHA.120.315865

31. Trim W V., Lynch L. Immune and non-immune functions of adipose tissue leukocytes. *Nat Rev Immunol*. 2022;22(6):371-386. doi:10.1038/s41577-021-00635-7

32. Bartelt A, Heeren J. Adipose tissue browning and metabolic health. *Nat Rev Endocrinol*. 2014;10(1):24-36. doi:10.1038/nrendo.2013.204

33. Cannon B, Nedergaard J. Brown Adipose Tissue: Function and Physiological Significance. *Physiol Rev*. 2004;84(1):277-359. doi:10.1152/physrev.00015.2003

34. Ouchi N, Parker JL, Lugus JJ, Walsh K. Adipokines in inflammation and metabolic disease. *Nat Rev Immunol*. 2011;11(2):85-97. doi:10.1038/nri2921

35. Scheja L, Heeren J. The endocrine function of adipose tissues in health and cardiometabolic disease. *Nat Rev Endocrinol*. 2019;15(9):507-524. doi:10.1038/s41574-019-0230-6

36. Scherer PE. The many secret lives of adipocytes: implications for diabetes. *Diabetologia*. 2019;62(2):223-232. doi:10.1007/s00125-018-4777-x

37. Li N, Zhao S, Zhang Z, et al. Adiponectin preserves metabolic fitness during aging. *Elife*. 2021;10:1-21. doi:10.7554/ELIFE.65108

38. Ghaben AL, Scherer PE. Adipogenesis and metabolic health. *Nat Rev Mol Cell Biol*. 2019;20(4):242-258. doi:10.1038/s41580-018-0093-z

39. Vishvanath L, Gupta RK. Contribution of adipogenesis to healthy adipose tissue expansion in obesity. *J Clin Invest*. 2019;129(10):4022-4031. doi:10.1172/JCI129191

40. Kusminski CM, Bickel PE, Scherer PE. Targeting adipose tissue in the treatment of obesity-associated diabetes. *Nat Rev Drug Discov*. 2016;15(9):639-660. doi:10.1038/nrd.2016.75

41. Crewe C, An YA, Scherer PE. The ominous triad of adipose tissue dysfunction: inflammation, fibrosis, and impaired angiogenesis. *J Clin Invest*. 2017;127(1):74-82. doi:10.1172/JCI88883

42. Reilly SM, Saltiel AR. Adapting to obesity with adipose tissue inflammation. *Nat Rev Endocrinol*. 2017;13(11):633-643. doi:10.1038/nrendo.2017.90

43. Klein S, Gastaldelli A, Yki-Järvinen H, Scherer PE. Why does obesity cause diabetes? *Cell Metab*. 2022;34(1):11-20. doi:10.1016/j.cmet.2021.12.012

44. Lotta LA, Gulati P, Day FR, et al. Integrative genomic analysis implicates limited peripheral adipose storage capacity in the pathogenesis of human insulin resistance. *Nat Genet*. 2017;49(1):17-26. doi:10.1038/ng.3714

45. Vegiopoulos A, Rohm M, Herzig S. Adipose tissue: between the extremes. *EMBO J*. 2017;36(14):1999-2017. doi:10.15252/embj.201696206

46. Mclaughlin T, Ackerman SE, Shen L, Engleman E. Role of innate and adaptive immunity in obesity-associated metabolic disease. *J Clin Invest*. 2017;127(1):5-13. doi:10.1172/JCI88876

47. Halberg N, Khan T, Trujillo ME, et al. Hypoxia-Inducible Factor 1α Induces Fibrosis and Insulin Resistance in White Adipose Tissue. *Mol Cell Biol*. 2009;29(16):4467-4483. doi:10.1128/mcb.00192-09

48. Funcke J-BB, Scherer PE. Beyond adiponectin and leptin: Adipose tissue-derived mediators of inter-organ communication. *J Lipid Res*. 2019;60(10):1648-1697. doi:10.1194/jlr.R094060

49. Weisberg SP, McCann D, Desai M, Rosenbaum M, Leibel RL, Ferrante AW. Obesity is associated with macrophage accumulation in adipose tissue. *J Clin Invest*. 2003;112(12):1796-1808. doi:10.1172/JCI200319246

50. Xu H, Barnes GT, Yang Q, et al. Chronic inflammation in fat plays a crucial role in the development of obesity-related insulin resistance. *J Clin Invest*. 2003;112(12):1821-1830. doi:10.1172/JCI200319451

51. Lumeng CN, Bodzin JL, Saltiel AR, Lumeng CN, Bodzin JL, Saltiel AR. Obesity induces a phenotypic switch in adipose tissue macrophage polarization. *J Clin Invest*. 2007;117(1):175-184. doi:10.1172/JCI29881.both

52. Nishimura S, Manabe I, Nagasaki M, et al. CD8+ effector T cells contribute to macrophage recruitment and adipose tissue inflammation in obesity. *Nat Med*. 2009;15(8):914-920. doi:10.1038/nm.1964

53. Feuerer M, Herrero L, Cipolletta D, et al. Lean, but not obese, fat is enriched for a unique population of regulatory T cells that affect metabolic parameters. *Nat Med*. 2009;15(8):930-939. doi:10.1038/nm.2002

54. Deiuliis J, Shah Z, Shah N, et al. Visceral adipose inflammation in obesity is associated with critical alterations in tregulatory cell numbers. *PLoS One*. 2011;6(1). doi:10.1371/journal.pone.0016376

55. Gregor MF, Hotamisligil GS. Inflammatory mechanisms in obesity. *Annu Rev*

Immunol. 2011;29:415-445. doi:10.1146/annurev-immunol-031210-101322

56. Nikolic I, Leiva M, Sabio G. The role of stress kinases in metabolic disease. *Nat Rev Endocrinol*. 2020;16(12):697-716. doi:10.1038/s41574-020-00418-5

57. Özcan U, Cao Q, Yilmaz E, et al. Endoplasmic Reticulum Stress Links Obesity, Insulin Action, and Type 2 Diabetes. *Science*. 2004;306(5695):457-461. doi:10.1126/science.1103160

58. Gregor MF, Misch ES, Yang L, et al. The Role of Adipocyte XBP1 in Metabolic Regulation during Lactation. *Cell Rep*. 2013;3(5):1430-1439. doi:10.1016/j.celrep.2013.03.042

59. Lee J, Sun C, Zhou Y, et al. P38 MAPK-mediated regulation of Xbp1s is crucial for glucose homeostasis. *Nat Med*. 2011;17(10):1251-1260. doi:10.1038/nm.2449

60. Lemmer IL, Willemsen N, Hilal N, Bartelt A. A guide to understanding endoplasmic reticulum stress in metabolic disorders. *Mol Metab*. 2021;47(January):101169. doi:10.1016/j.molmet.2021.101169

61. Walter P, Ron D. The Unfolded Protein Response: From Stress Pathway to Homeostatic Regulation. *Science*. 2011;334(6059):1081-1086. doi:10.1126/science.1209038

62. Westrate LM, Lee JE, Prinz WA, Voeltz GK. Form follows function: The importance of endoplasmic reticulum shape. *Annu Rev Biochem*. 2015;84:791-811. doi:10.1146/annurev-biochem-072711-163501

63. Roberts MA, Olzmann JA. Protein Quality Control and Lipid Droplet Metabolism. Published online 2020.

64. Hotamisligil GS, Erbay E. Nutrient sensing and inflammation in metabolic diseases. *Nat Rev Immunol*. 2008;8(12):923-934. doi:10.1038/nri2449

65. Kharroubi I, Ladrière L, Cardozo AK, Dogusan Z, Cnop M, Eizirik DL. Free fatty acids and cytokines induce pancreatic β-cell apoptosis by different mechanisms: Role of nuclear factor-κB and endoplasmic reticulum stress. *Endocrinology*. 2004;145(11):5087-5096. doi:10.1210/en.2004-0478

66. Kaufman RJ, Scheuner D, Schröder M, et al. The unfolded protein response in nutrient sensing and differentiation. *Nat Rev Mol Cell Biol*. 2002;3(6):411-421. doi:10.1038/nrm829

67. Gregor MF, Hotamisligil GS. Adipocyte stress: The endoplasmic reticulum and metabolic disease. *J Lipid Res*. 2007;48(9):1905-1914. doi:10.1194/jlr.R700007-JLR200

68. Hetz C. The unfolded protein response: controlling cell fate decisions under ER stress and beyond. *Nat Rev Mol Cell Biol*. 2012;13(2):89-102. doi:10.1038/nrm3270

69. Hetz C, Kaufman RJ. Mechanisms, regulation and functions of the unfolded protein response. *Nat Rev Mol Cell Biol*. 2020;(Box 1):1-18. doi:10.1038/s41580-020-0250-z

70. Harding HP, Zhang Y, Ron D. Protein translation and folding are coupled by an endoplasmic- reticulum-resident kinase. *Nature*. 1999;397(6716):271-274. doi:10.1038/16729

71. Vattem KM, Wek RC. Reinitiation involving upstream ORFs regulates ATF4 mRNA translation in mammalian cells. *Proc Natl Acad Sci U S A*. 2004;101(31):11269-11274. doi:10.1073/pnas.0400541101

72. Lu PD, Harding HP, Ron D. Translation reinitiation at alternative open reading frames regulates gene expression in an integrated stress response. *J Cell Biol*.

2004;167(1):27-33. doi:10.1083/jcb.200408003

73. Harding HP, Zhang Y, Zeng H, et al. An integrated stress response regulates amino acid metabolism and resistance to oxidative stress. *Mol Cell*. 2003;11(3):619-633. doi:10.1016/S1097-2765(03)00105-9

74. Yoshida H, Matsui T, Yamamoto A, Okada T, Mori K. XBP1 mRNA Is Induced by ATF6 and Spliced by IRE1 in Response to ER Stress to Produce a Highly Active Transcription Factor phorylation, the activated Ire1p specifically cleaves HAC1 precursor mRNA to remove an intron of 252 nucle-otides. The cleaved 5 and . *Cell*. 2001;107:881-891.

75. Calfon M, Zeng H, Urano F, et al. IRE1 couples endoplasmic reticulum load to secretory capacity by processing the XBP-1 mRNA. *Nature*. 2002;415(6867):92-96. doi:10.1038/415092a

76. Hollien J, Weissman JS. Decay of Endoplasmic Reticulum-Localized mRNAs During the Unfolded Protein Response. *Science*. 2006;313(5783):104-107. doi:10.1126/science.1129631

77. Upton J-P, Wang L, Han D, et al. IRE1α Cleaves Select microRNAs During ER Stress to Derepress Translation of Proapoptotic Caspase-2. *Science*. 2012;338(6108):818-822. doi:10.1126/science.1226191

78. Haze K, Yoshida H, Yanagi H, Yura T, Mori K. Mammalian transcription factor ATF6 is synthesized as a transmembrane protein and activated by proteolysis in response to endoplasmic reticulum stress. *Mol Biol Cell*. 1999;10(11):3787-3799. doi:10.1091/mbc.10.11.3787

79. Wu J, Rutkowski DT, Dubois M, et al. ATF6α Optimizes Long-Term Endoplasmic Reticulum Function to Protect Cells from Chronic Stress. *Dev Cell*. 2007;13(3):351-364. doi:10.1016/j.devcel.2007.07.005

80. Tabas I, Ron D. Integrating the mechanisms of apoptosis induced by endoplasmic reticulum stress. *Nat Cell Biol*. 2011;13(3):184-190. doi:10.1038/ncb0311-184

81. Onodera J, Ohsumi Y. Autophagy is required for maintenance of amino acid levels and protein synthesis under nitrogen starvation. *J Biol Chem*. 2005;280(36):31582-31586. doi:10.1074/jbc.M506736200

82. Nakatogawa H, Suzuki K, Kamada Y, Ohsumi Y. Dynamics and diversity in autophagy mechanisms: Lessons from yeast. *Nat Rev Mol Cell Biol*. 2009;10(7):458-467. doi:10.1038/nrm2708

83. Kaushik S, Cuervo AM. The coming of age of chaperone-mediated autophagy. *Nat Rev Mol Cell Biol*. 2018;19(6):365-381. doi:10.1038/s41580-018-0001-6

84. Murata S, Yashiroda H, Tanaka K. Molecular mechanisms of proteasome assembly. *Nat Rev Mol Cell Biol*. 2009;10(2):104-115. doi:10.1038/nrm2630

85. Rousseau A, Bertolotti A. Regulation of proteasome assembly and activity in health and disease. *Nat Rev Mol Cell Biol*. 2018;19(11):697-712. doi:10.1038/s41580-018-0040-z

86. Vembar SS, Brodsky JL. One step at a time: Endoplasmic reticulum-associated degradation. *Nat Rev Mol Cell Biol*. 2008;9(12):944-957. doi:10.1038/nrm2546

87. Meusser B, Hirsch C, Jarosch E, Sommer T. ERAD: The long road to destruction. *Nat Cell Biol*. 2005;7(8):766-772. doi:10.1038/ncb0805-766

88. van den Boom J, Meyer H. VCP/p97-Mediated Unfolding as a Principle in Protein Homeostasis and Signaling. *Mol Cell*. 2018;69(2):182-194. doi:10.1016/j.molcel.2017.10.028

89. Schmidt M, Hanna J, Elsasser S, Finley D. Proteasome-associated proteins:

Regulation of a proteolytic machine. *Biol Chem*. 2005;386(8):725-737. doi:10.1515/BC.2005.085

90. Arendt CS, Hochstrasser M. Identification of the yeast 20S proteasome catalytic centers and subunit interactions required for active-site formation. *Proc Natl Acad Sci U S A*. 1997;94(14):7156-7161. doi:10.1073/pnas.94.14.7156

91. Heinemeyer W, Ramos PC, Dohmen RJ. Ubiquitin-proteasome system. *Cell Mol Life Sci*. 2004;61(13):1562-1578. doi:10.1007/s00018-004-4130-z

92. Finley D. Recognition and processing of ubiquitin-protein conjugates by the proteasome. *Annu Rev Biochem*. 2009;78:477-513. doi:10.1146/annurev.biochem.78.081507.101607

93. Ohsumi Y. Historical landmarks of autophagy research. *Cell Res*. 2014;24(1):9-23. doi:10.1038/cr.2013.169

94. Steffen J, Seeger M, Koch A, Krüger E. Proteasomal degradation is transcriptionally controlled by TCF11 via an ERAD-dependent feedback loop. *Mol Cell*. 2010;40(1):147-158. doi:10.1016/j.molcel.2010.09.012

95. Radhakrishnan SK, Lee CS, Young P, Beskow A, Chan JY, Deshaies RJ. Transcription Factor Nrf1 Mediates the Proteasome Recovery Pathway after Proteasome Inhibition in Mammalian Cells. *Mol Cell*. 2010;38(1):17-28. doi:10.1016/j.molcel.2010.02.029

96. Ruvkun G, Lehrbach N. Regulation and Functions of the ER-Associated Nrf1 Transcription Factor. *Cold Spring Harb Perspect Biol*. 2023;15(1). doi:10.1101/cshperspect.a041266

97. Sykiotis GP, Bohmann D. Stress-Activated Cap'n'collar Transcription Factors in Aging and Human Disease. *Sci Signal*. 2010;3(112). doi:10.1126/scisignal.3112re3

98. Liu P, Kerins MJ, Tian W, Neupane D, Zhang DD, Ooi A. Differential and overlapping targets of the transcriptional regulators NRF1, NRF2, and NRF3 in human cells. *J Biol Chem*. 2019;294(48):18131-18149. doi:10.1074/jbc.RA119.009591

99. Akl MG, Li L, Baccetto R, et al. Complementary gene regulation by NRF1 and NRF2 protects against hepatic cholesterol overload. *Cell Rep*. 2023;42(4):112399. doi:10.1016/j.celrep.2023.112399

100. Ma Q. Role of Nrf2 in Oxidative Stress and Toxicity. *Annu Rev Pharmacol Toxicol*. 2013;53(1):401-426. doi:10.1146/annurev-pharmtox-011112-140320

101. Kobayashi A. Roles of NRF3 in the Hallmarks of Cancer: Proteasomal Inactivation of Tumor Suppressors. *Cancers (Basel)*. 2020;12(9):2681. doi:10.3390/cancers12092681

102. Tsuchiya Y, Morita T, Kim M, et al. Dual Regulation of the Transcriptional Activity of Nrf1 by β-TrCP- and Hrd1-Dependent Degradation Mechanisms. *Mol Cell Biol*. 2011;31(22):4500-4512. doi:10.1128/mcb.05663-11

103. Radhakrishnan SK, den Besten W, Deshaies RJ. p97-dependent retrotranslocation and proteolytic processing govern formation of active Nrf1 upon proteasome inhibition. *Elife*. 2014;3:1-15. doi:10.7554/elife.01856

104. Tomlin FM, Gerling-Driessen UIM, Liu YC, et al. Inhibition of NGLY1 Inactivates the Transcription Factor Nrf1 and Potentiates Proteasome Inhibitor Cytotoxicity. *ACS Cent Sci*. 2017;3(11):1143-1155. doi:10.1021/acscentsci.7b00224

105. Koizumi S, Irie T, Hirayama S, et al. The aspartyl protease DDI2 activates Nrf1 to compensate for proteasome dysfunction. *Elife*. 2016;5(August):1-10.

doi:10.7554/eLife.18357

106. Katsuoka F, Yamamoto M. Small Maf proteins (MafF, MafG, MafK): History, structure and function. *Gene*. 2016;586(2):197-205. doi:10.1016/j.gene.2016.03.058

107. Toki T, Itoh J, Kitazawa J, et al. Human small Maf proteins form heterodimers with CNC family transcription factors and recognize the NF-E2 motif. *Oncogene*. 1997;14(16):1901-1910. doi:10.1038/sj.onc.1201024

108. Hirotsu Y, Hataya N, Katsuoka F, Yamamoto M. NF-E2-Related Factor 1 (Nrf1) Serves as a Novel Regulator of Hepatic Lipid Metabolism through Regulation of the Lipin1 and PGC-1 β Genes . *Mol Cell Biol*. 2012;32(14):2760-2770. doi:10.1128/mcb.06706-11

109. Lee CS, Ho D V., Chan JY. Nuclear factor-erythroid 2-related factor 1 regulates expression of proteasome genes in hepatocytes and protects against endoplasmic reticulum stress and steatosis in mice. *FEBS J*. 2013;280(15):3609-3620. doi:10.1111/febs.12350

110. Widenmaier SB, Snyder NA, Nguyen TB, et al. NRF1 Is an ER Membrane Sensor that Is Central to Cholesterol Homeostasis. *Cell*. 2017;171(5):1094.e15-1109.e15. doi:10.1016/j.cell.2017.10.003

111. Cui M, Atmanli A, Morales MG, et al. Nrf1 promotes heart regeneration and repair by regulating proteostasis and redox balance. *Nat Commun*. 2021;12(1):1-15. doi:10.1038/s41467-021-25653-w

112. Bartelt A, Widenmaier SB, Schlein C, et al. Brown adipose tissue thermogenic adaptation requires Nrf1-mediated proteasomal activity. *Nat Med*. 2018;24(3):292-303. doi:10.1038/nm.4481

113. Ren S, Hou Y, Zuo Z, et al. Protracted rosiglitazone treatment exacerbates inflammation in white adipose tissues of adipocyte-specific Nfe2l1 knockout mice. *Food Chem Toxicol*. 2020;146(September):111836. doi:10.1016/j.fct.2020.111836

114. Hou Y, Liu Z, Zuo Z, et al. Adipocyte-specific deficiency of Nfe2l1 disrupts plasticity of white adipose tissues and metabolic homeostasis in mice. *Biochem Biophys Res Commun*. 2018;503(1):264-270. doi:10.1016/j.bbrc.2018.06.013

115. Tabas I. Cholesterol in health and disease. *J Clin Invest*. 2002;110(5):583-590. doi:10.1172/JCI200216381

116. Song Y, Liu J, Zhao K, Gao L, Zhao J. Cholesterol-induced toxicity: An integrated view of the role of cholesterol in multiple diseases. *Cell Metab*. 2021;33(10):1911-1925. doi:10.1016/j.cmet.2021.09.001

117. Feng B, Yaol PM, Li Y, et al. The endoplasmic reticulum is the site of cholesterol-induced cytotoxicity in macrophages. *Nat Cell Biol*. 2003;5(9):781-792. doi:10.1038/ncb1035

118. Chang TY, Chang CCY, Ohgami N, Yamauchi Y. Cholesterol sensing, trafficking, and esterification. *Annu Rev Cell Dev Biol*. 2006;22:129-157. doi:10.1146/annurev.cellbio.22.010305.104656

119. DeBose-Boyd RA, Ye J. SREBPs in Lipid Metabolism, Insulin Signaling, and Beyond. *Trends Biochem Sci*. 2018;43(5):358-368. doi:10.1016/j.tibs.2018.01.005

120. Goldstein JL, DeBose-Boyd RA, Brown MS. Protein sensors for membrane sterols. *Cell*. 2006;124(1):35-46. doi:10.1016/j.cell.2005.12.022

121. Kovanen PT, Nikkila EA, Miettinen TA. Regulation of cholesterol synthesis and

storage in fat cells. *J Lipid Res*. 1975;16(3):211-223. doi:10.1016/s0022-2275(20)36728-6

122. Yu BL, Zhao SP, Hu JR. Cholesterol imbalance in adipocytes: A possible mechanism of adipocytes dysfunction in obesity. *Obes Rev*. 2010;11(8):560-567. doi:10.1111/j.1467-789X.2009.00699.x

123. Le Lay S, Ferré P, Dugail I. Adipocyte cholesterol balance in obesity. *Biochem Soc Trans*. 2004;32(1):103-106. doi:10.1042/BST0320103

124. Love MI, Huber W, Anders S. Moderated estimation of fold change and dispersion for RNA-seq data with DESeq2. *Genome Biol*. 2014;15(12):1-21. doi:10.1186/s13059-014-0550-8

125. Stephens M. False discovery rates: A new deal. *Biostatistics*. 2017;18(2):275-294. doi:10.1093/biostatistics/kxw041

126. Tilg H, Moschen AR. Adipocytokines: Mediators linking adipose tissue, inflammation and immunity. *Nat Rev Immunol*. 2006;6(10):772-783. doi:10.1038/nri1937

127. Giroud M, Jodeleit H, Prentice KJ, Bartelt A. Adipocyte function and the development of cardiometabolic disease. *J Physiol*. 2021;0:1-20. doi:10.1113/jp281979

128. Watanabe M, Houten SM, Mataki C, et al. Bile acids induce energy expenditure by promoting intracellular thyroid hormone activation. *Nature*. 2006;439(7075):484-489. doi:10.1038/nature04330

129. Song MK, Kim JE, Kim JT, et al. GDF10 is related to obesity as an adipokine derived from subcutaneous adipose tissue. *Front Endocrinol (Lausanne)*. 2023;14(July):1-8. doi:10.3389/fendo.2023.1159515

130. Hirotsu Y, Higashi C, Fukutomi T, et al. Transcription factor NF-E2-related factor 1 impairs glucose metabolism in mice. *Genes to Cells*. 2014;19(8):650-665. doi:10.1111/gtc.12165

131. Börgeson E, Boucher J, Hagberg CE. Of mice and men: Pinpointing species differences in adipose tissue biology. *Front Cell Dev Biol*. 2022;10(September):1-8. doi:10.3389/fcell.2022.1003118

132. Kim JY, Van De Wall E, Laplante M, et al. Obesity-associated improvements in metabolic profile through expansion of adipose tissue. *J Clin Invest*. 2007;117(9):2621-2637. doi:10.1172/JCI31021

133. Okamoto Y, Kihara S, Ouchi N, et al. Adiponectin reduces atherosclerosis in apolipoprotein E-deficient mice. *Circulation*. 2002;106(22):2767-2770. doi:10.1161/01.CIR.0000042707.50032.19

134. Fasshauer M, Blüher M. Adipokines in health and disease. *Trends Pharmacol Sci*. 2015;36(7):461-470. doi:10.1016/j.tips.2015.04.014

135. Kintscher U, Hartge M, Hess K, et al. T-lymphocyte infiltration in visceral adipose tissue: A primary event in adipose tissue inflammation and the development of obesity-mediated insulin resistance. *Arterioscler Thromb Vasc Biol*. 2008;28(7):1304-1310. doi:10.1161/ATVBAHA.108.165100

136. Harte AL, Tripathi G, Piya MK, et al. NFκB as a potent regulator of inflammation in human adipose tissue, influenced by depot, adiposity, T2DM status, and TNFα. *Obesity*. 2013;21(11):2322-2330. doi:10.1002/oby.20336

137. Tourniaire F, Romier-Crouzet B, Lee JH, et al. Chemokine Expression in Inflamed Adipose Tissue Is Mainly Mediated by NF-κB. Xu H, ed. *PLoS One*. 2013;8(6):e66515. doi:10.1371/journal.pone.0066515

138. Griffin MJ. On the Immunometabolic Role of NF-κB in Adipocytes. *Immunometabolism*. 2022;4(1). doi:10.20900/immunometab20220003

139. Gehart H, Kumpf S, Ittner A, Ricci R. MAPK signalling in cellular metabolism: Stress or wellness? *EMBO Rep*. 2010;11(11):834-840. doi:10.1038/embor.2010.160

140. Krinninger P, Brunner C, Ruiz PA, et al. Role of the adipocyte-specific NF-κB activity in the regulation of IP-10 and T cell migration. *Am J Physiol - Endocrinol Metab*. 2011;300(2):304-311. doi:10.1152/ajpendo.00143.2010

141. Robinet P, Milewicz DM, Cassis LA, Leeper NJ, Lu HS, Smith JD. Consideration of Sex Differences in Design and Reporting of Experimental Arterial Pathology Studies-Statement from ATVB Council. *Arterioscler Thromb Vasc Biol*. 2018;38(2):292-303. doi:10.1161/ATVBAHA.117.309524

142. Kleinert M, Clemmensen C, Hofmann SM, et al. Animal models of obesity and diabetes mellitus. *Nat Rev Endocrinol*. 2018;14(3):140-162. doi:10.1038/nrendo.2017.161

143. Macotela Y, Boucher J, Tran TT, Kahn CR. Sex and depot differences in adipocyte insulin sensitivity and glucose. *Diabetes*. 2009;58(4):803-812. doi:10.2337/db08-1054

144. Jiao P, Feng B, Ma J, et al. Constitutive activation of IKKβ in adipose tissue prevents diet-induced obesity in mice. *Endocrinology*. 2012;153(1):154-165. doi:10.1210/en.2011-1346

145. Tang T, Zhang J, Yin J, et al. Uncoupling of inflammation and insulin resistance by NF-κB in transgenic mice through elevated energy expenditure. *J Biol Chem*. 2010;285(7):4637-4644. doi:10.1074/jbc.M109.068007

146. Bartelt A, Bruns OT, Reimer R, et al. Brown adipose tissue activity controls triglyceride clearance. *Nat Med*. 2011;17(2):200-206. doi:10.1038/nm.2297

147. Berbeé JFP, Boon MR, Khedoe PPSJ, et al. Brown fat activation reduces hypercholesterolaemia and protects from atherosclerosis development. *Nat Commun*. 2015;6. doi:10.1038/ncomms7356

148. Ku HC, Cheng CF. Master Regulator Activating Transcription Factor 3 (ATF3) in Metabolic Homeostasis and Cancer. *Front Endocrinol (Lausanne)*. 2020;11(August):1-16. doi:10.3389/fendo.2020.00556

149. Hai T, Wolford CC, Chang YS. ATF3, a hub of the cellular adaptive-response network, in the pathogenesis of diseases: Is modulation of inflammation a unifying component? *Gene Expr*. 2010;15(1):1-11. doi:10.3727/105221610X12819686555015

150. Jang MK, Son Y, Jung MH. ATF3 plays a role in adipocyte hypoxia-mediated mitochondria dysfunction in obesity. *Biochem Biophys Res Commun*. 2013;431(3):421-427. doi:10.1016/j.bbrc.2012.12.154

151. Jang MK, Jung MH. ATF3 represses PPARγ expression and inhibits adipocyte differentiation. *Biochem Biophys Res Commun*. 2014;454(1):58-64. doi:10.1016/j.bbrc.2014.10.028

152. Jang MK, Kim CH, Seong JK, Jung MH. ATF3 inhibits adipocyte differentiation of 3T3-L1 cells. *Biochem Biophys Res Commun*. 2012;421(1):38-43. doi:10.1016/j.bbrc.2012.03.104

153. Willemsen N, Arigoni I, Studencka-Turski M, Krüger E, Bartelt A. Proteasome dysfunction disrupts adipogenesis and induces inflammation via ATF3. *Mol Metab*. 2022;62(May):101518. doi:10.1016/j.molmet.2022.101518

154. Sha Z, Goldberg AL. Proteasome-Mediated Processing of Nrf1 Is Essential for Coordinate Induction of All Proteasome Subunits and p97. *Curr Biol*. 2014;24(14):1573-1583. doi:10.1016/j.cub.2014.06.004

155. Op M, Ribeiro ST, Chavarria C, De Gassart A, Zaffalon L, Martinon F. The aspartyl protease DDI2 drives adaptation to proteasome inhibition in multiple myeloma. *Cell Death Dis*. 2022;13(5). doi:10.1038/s41419-022-04925-3

Supplementary data

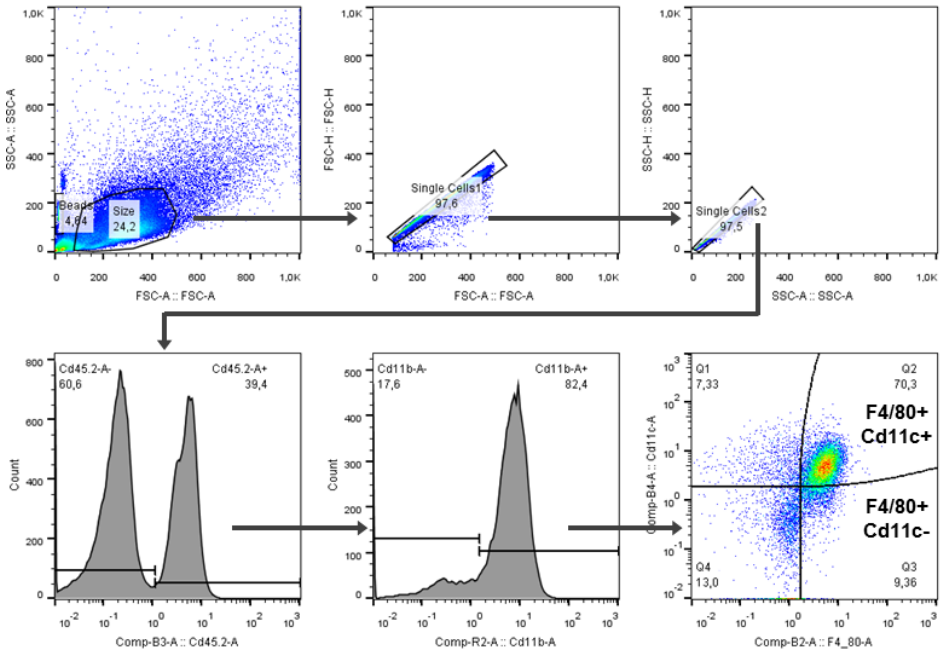

Supplementary Figure 1 | Flow cytometry gating strategy for F4/80+ cells

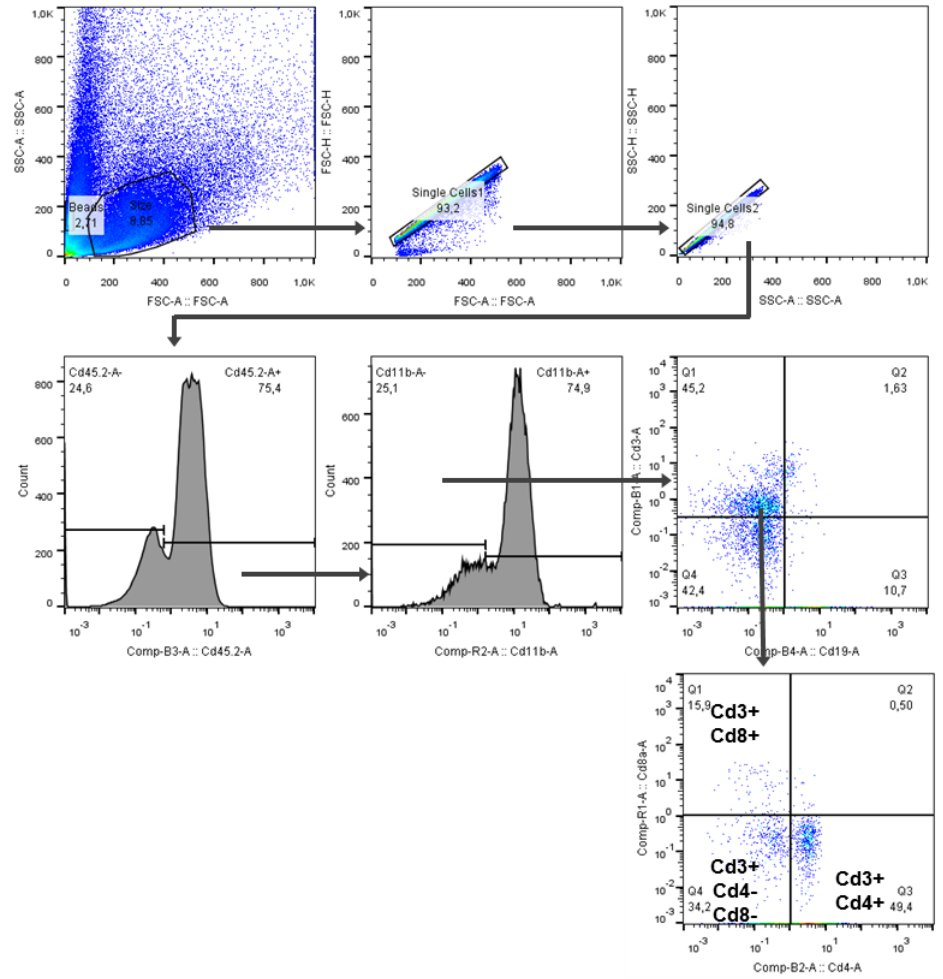

Supplementary Figure 2 | Flow cytometry gating strategy for Cd3+ cells

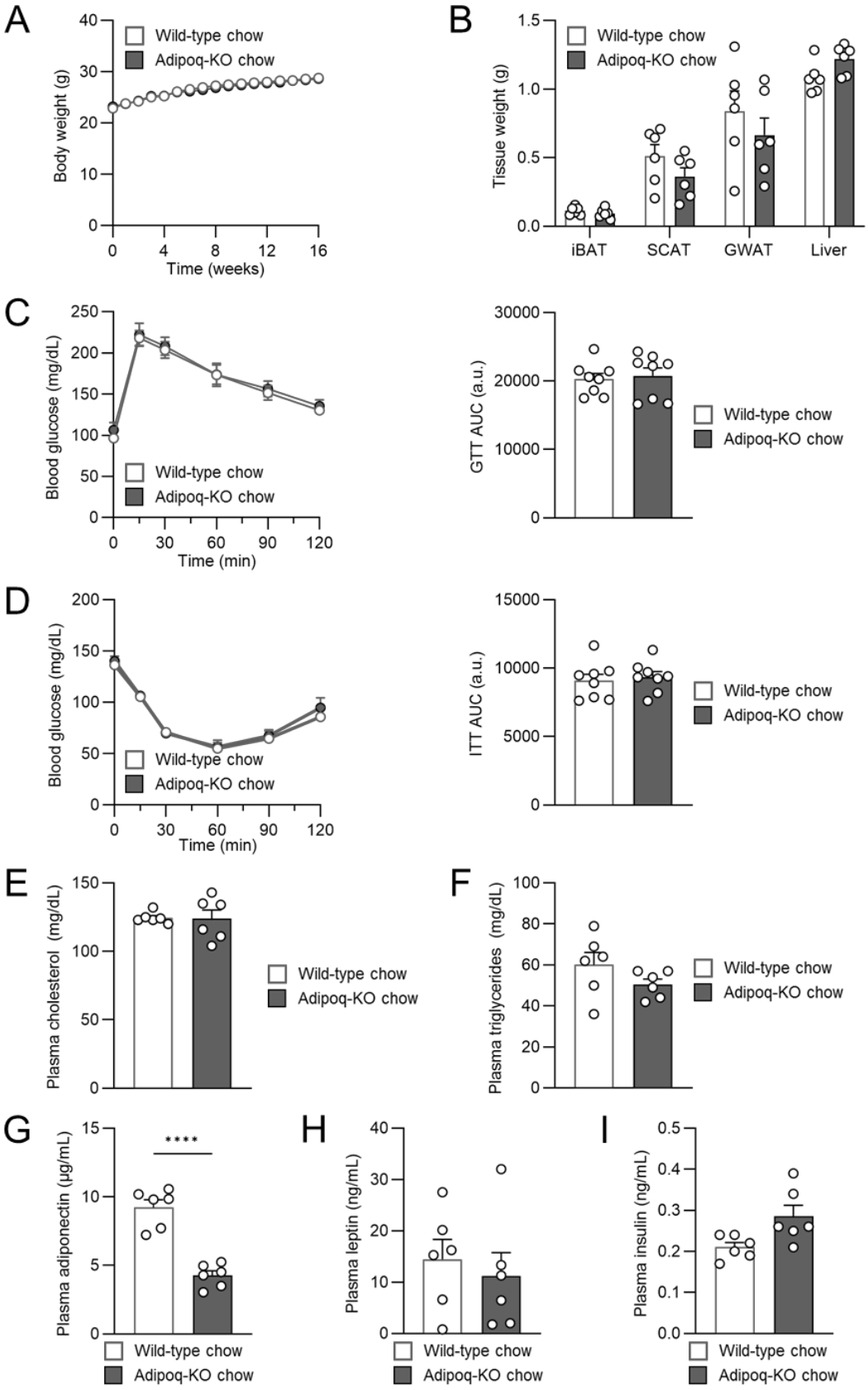

Supplementary Figure 3 | Male Adipoq-Cre Nfe2l1 mice on chow diet

A Body weight, **B** tissue weights, **C** i.p. GTT, **D** i.p. ITT, **E** cholesterol, **F** triglyceride, **G** adiponectin **H** leptin and **I** insulin plasma level of male wild-type and Adipoq-KO mice after 16 weeks of chow diet. Data provided by Alexander Bartelt (LMU Munich). Throughout data are mean + s.e.m, n=8 (**A**,**C**,**D**) and n=6 (**B**,**E-I**).**** p<0.001 by Student‘s t test (**G**).

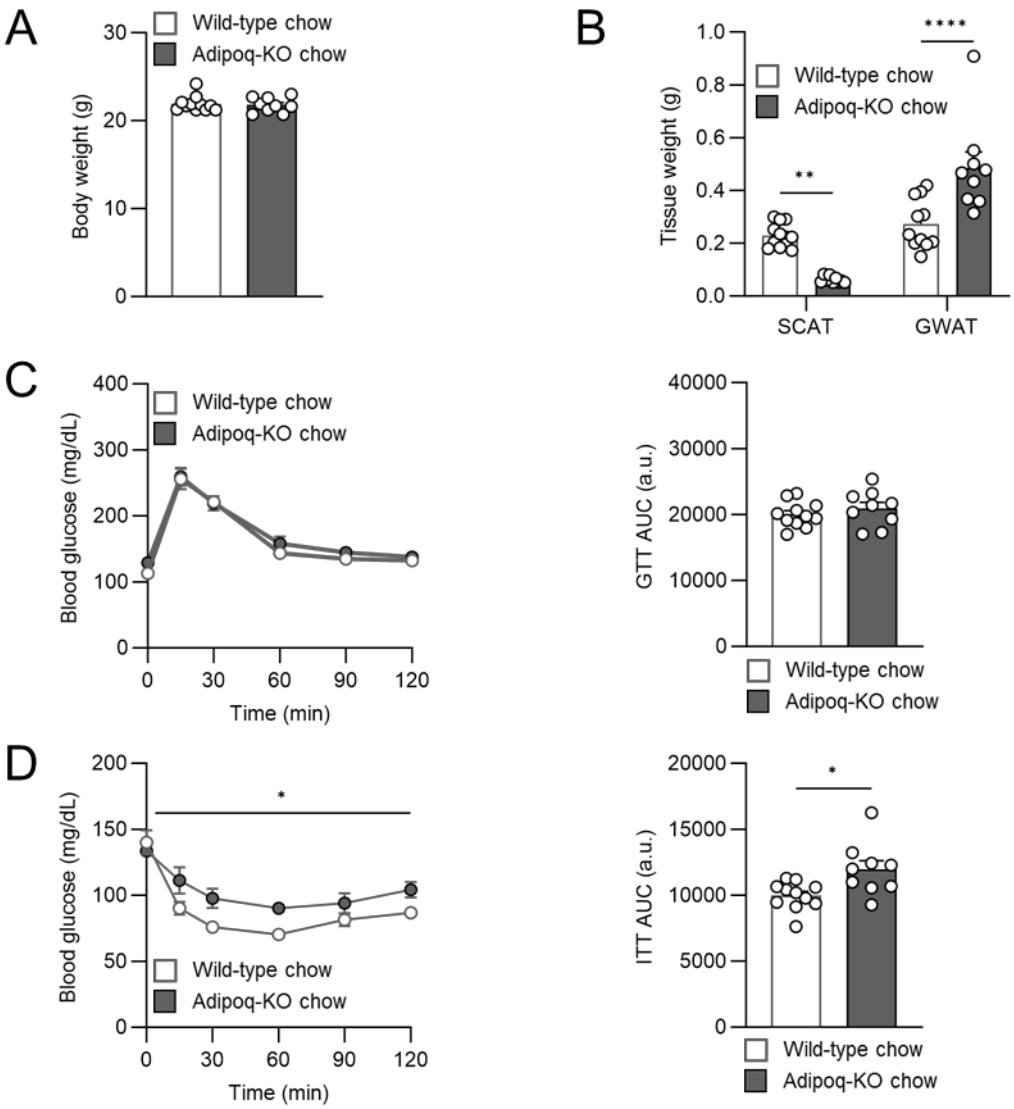

Supplementary Figure 4 | Female Adipoq-Cre Nfe2l1 mice on chow diet

A Body weight, **B** tissue weights, **C** i.p. GTT, **D** i.p. ITT female wild-type and Adipoq-KO mice after 16 weeks of chow diet. Throughout data are mean + s.e.m, n=9-11. * p<0.05, ** p<0.01, **** p<0.001 by Student's t test (**G**).

Acknowledgements

First and foremost, I would like to thank my supervisor and mentor Prof. Alexander Bartelt for giving me the opportunity to work on such an exciting and relevant topic for my PhD. Dear Alex, thank you very much for your continuous support, trainings from grant writing to hiring, and for enabling all the collaborations and publications. Thank you for allowing me to visit so many exciting conferences and of course for the numerous beers over the last four years. I have learned a lot from you and I am very grateful for everything.

Next, I would like to thank all my current and former colleagues from the Bartelt lab and the Ries lab for the best working environment I could have wished for during my PhD. Thank you for the support, especially with the *in vivo* experiments, the scientific exchange, your friendship and the many happy hours in the lab, in the mountains and in the beer garden.

A special thank you goes to my PhD colleagues Alba, Anna, Imke and Nienke for proofreading this thesis, as well as to our alumna Janina for the excellent preliminary work on this project and Stefan for teaching me proper murine anatomy.

A big thank you also goes to my collaboration partners, who supported me and my thesis with measurements, analyses and data. These include Prof. Matthias Blüher (University of Leipzig, HI-MAG), Dr. Anne Hoffmann (University of Leipzig, HI-MAG) and Dr. Anna Worthmann (UKE Hamburg). I would also like to thank Yvonne Jansen for her patient instruction and technical support with the histology.

Last but not least, I am extremely grateful to my parents, who always have supported me in every decision. Thank you for your love and trust in me. My deepest gratitude goes to my husband, for always believing in me and supporting me all the way. Thank you for picking me up from the lab late at night, proof reading this thesis on weekends and making the best coffee. I would never have never gotten this far without you – at least not in such a good mental state. I love you.

Figures 4, 5, 6, 48A and 50A were created with BioRender.com.

Publications

Article

Y. Wang et al., “Myeloid cannabinoid CB1 receptor deletion confers atheroprotection in male mice by reducing macrophage proliferation in a sex-dependent manner”, accepted in *Cardiovascular Research*, May 2024

N. Li et al., “Dicer prevents activation of the type I interferon pathway in lipid-loaded macrophages”, *European Heart Journal*, Volume 43, Issue Supplement_2, October, 2022, ehac544.3083, doi:10.1093/eurheartj/ehac544.3083

C. Muley, J. Caesar and A. Bartelt, “Nfe2l1 protects white adipocytes from cholesterol-induced inflammation”, *Atherosclerosis*, vol. 355, P42, August, 2022, doi:10.1016/j.atherosclerosis.2022.06.207

F.-F. Tsokanos and C. Muley* et al., “Methylglyoxal Drives a Distinct, Nonclassical Macrophage Activation Status,” *Thromb. Haemost.*, vol. 121, no. 11, pp. 1464–1475, November, 2021, doi: 10.1055/s-0041-1726346. *shared first-author

C. Muley, S. Kotschi, and A. Bartelt, “Role of Ubiquilins for Brown Adipocyte Proteostasis and Thermogenesis,” *Front. Endocrinol.* (Lausanne)., vol. 12, no. September, pp. 1–9, 2021, doi: 10.3389/fendo.2021.739021.

C. Muley, J. Caesar, S. Kotschi, and A. Bartelt, “NFE2L1 protects adipocytes from cholesterol-induced inflammation”, *Atherosclerosis*, vol. 331, E145, August, 2021, doi:10.1016/j.atherosclerosis.2021.06.434

C. Muley and A. Bartelt, “Fuse your mitochondria, lose appetite: an anorexic, anti-obesity sphingolipid,” *EMBO Mol. Med.*, vol. 13, no. 8, pp. 2–4, 2021, doi: 10.15252/emmm.202114618.

M. Lukas et al., “Survey of ex vivo drug combination effects in chronic lymphocytic leukemia reveals synergistic drug effects and genetic dependencies,” Leukemia, May 2020, doi: 10.1038/s41375-020-0846-5.

C. Silaidos, J. Grube, C. Muley, and G. P. Eckert, “Time-dependent melatonin secretion is associated with mitochondrial function in peripheral blood mononuclear cells (PBMC) of male volunteers,” *Mitochondrion*, vol. 53, no. March, pp. 21–29, 2020, doi: 10.1016/j.mito.2020.04.006.

Oral and poster presentations

“Adipocyte-Nfe2l1 guards cardiometabolic health in diet-induced obesity and atherosclerosis”, poster presentation, 23rd Lipid Meeting, Leipzig (Germany), 2023

“Adipocyte-Nfe2l1 protects from cholesterol-induced lipoatrophy and atherosclerosis”, short-talk, 29th Annual Scandinavian Atherosclerosis conference, Humlebæk (Denmark), 2023

“Adipocyte-Nfe2l1 protects from cholesterol-induced lipoatrophy and atherosclerosis”, poster presentation, Atherosclerosis - Mechanisms and novel therapeutic targets, International Symposium, Munich (Germany), 2022

“Adipocyte-Nfe2l1 protects from cholesterol-induced lipoatrophy and atherosclerosis”, short-talk, 45th European Lipoprotein Club (ELC) Meeting, Tutzing (Germany), 2022

“Nfe2l1 protects adipocytes from cholesterol-induced lipotoxicity in obesity”, poster presentation, Adipose Tissue and Metabolic Health Keystone Symposium, Whistler (Canada), 2022

“Nfe2l1 protects white adipocytes from cholesterol-induced inflammation”, poster presentation, 90th European Atherosclerosis Society (EAS) Congress, Milan (Italy), 2021

“Adipocyte-Nfe2l1 protects from cholesterol-induced lipodystrophy and atherosclerosis”, short-talk, 28th Annual Scandinavian Atherosclerosis conference, Humlebæk (Denmark), 2022

“Adipocyte-Nfe2l1 protects from cholesterol-induced lipodystrophy and atherosclerosis”, short-talk, Deutsche Zentrum für Herz-Kreislauf-Forschung e. V. Metabolism Workshop, virtual, 2022

“Nfe2l1 protects adipocytes from cholesterol-induced inflammation during obesity”, poster presentation, 22nd Lipid Meeting, Leipzig (virtual), 2021

“Nfe2l1 protects white adipocytes from cholesterol-induced inflammation”, short-talk, 44th ELC Meeting, Tutzing (Germany), 2021

“Nfe2l1 protects adipocytes from cholesterol-induced inflammation”, poster presentation, 89th EAS Congress, Helsinki (virtual), 2021

LMU LUDWIG-MAXIMILIANS-UNIVERSITÄT MÜNCHEN

Dekanat Medizinische Fakultät
Promotionsbüro

Eidesstattliche Versicherung

Jethwa, Carolin

Name, Vorname

Ich erkläre hiermit an Eides statt, dass ich die vorliegende Dissertation mit dem Titel:

The role of adipocyte Nfe2l1 in cholesterol homeostasis and atherogenesis

selbständig verfasst, mich außer der angegebenen keiner weiteren Hilfsmittel bedient und alle Erkenntnisse, die aus dem Schrifttum ganz oder annähernd übernommen sind, als solche kenntlich gemacht und nach ihrer Herkunft unter Bezeichnung der Fundstelle einzeln nachgewiesen habe.

Ich erkläre des Weiteren, dass die hier vorgelegte Dissertation nicht in gleicher oder in ähnlicher Form bei einer anderen Stelle zur Erlangung eines akademischen Grades eingereicht wurde.

Penzberg, 01.03.2025
Ort, Datum

Carolin Jethwa
Unterschrift Doktorandin/Doktorand

LMU LUDWIG-MAXIMILIANS-UNIVERSITÄT MÜNCHEN

Dekanat Medizinische Fakultät
Promotionsbüro

Erklärung zur Übereinstimmung der gebundenen Ausgabe der Dissertation mit der elektronischen Fassung

Jethwa, Carolin

Name, Vorname

Hiermit erkläre ich, dass die elektronische Version der eingereichten Dissertation mit dem Titel:

The role of adipocyte Nfe2l1 in cholesterol homeostasis and atherogenesis

in Inhalt und Formatierung mit den gedruckten und gebundenen Exemplaren übereinstimmt.

Penzberg, 01.03.2025

Ort, Datum

Carolin Jethwa

Unterschrift Doktorandin/Doktorand